

Quantum state engineering and reconstruction in cavity QED: An analytical approach

Dissertation der Fakultät für Physik
der Ludwig-Maximilians-Universität München

vorgelegt von
Pavel Lougovski
aus Minsk (Weißrussland)

München, den 25.09.2004

1. Gutachter: Prof. Dr. H. Walther
2. Gutachter: Prof. Dr. A. Schenzle

Tag der mündlichen Prüfung: 23.09.2004

Zusammenfassung

In dieser Arbeit werden Modelle für den stark getriebenen Micromaser und den Einatomlaser entwickelt. Die analytischen Lösungen dieser Probleme werden unter Verwendung von Phasenraumtechniken erarbeitet. Es wird gezeigt, wie das Modell des Einatomlasers für gleichzeitige Erzeugung der ‘Schrödinger Katze’ Zustände von Atom und Feld und zur Überwachung ihrer Dekohärenz verwendet werden kann. Der gleiche Formalismus erlaubt in einer leichten Abwandlung eine analytische Lösung für das Problem der Erzeugung von maximal-verschränkten Zuständen zweier Atome in einem optischen Resonator. Die stationäre Lösung des Problems zeigt eine Struktur, in der der gemeinsame Zustand der beiden maximal-verschränkten Atome mit dem Vakuum im Resonator korreliert. Als eine Folgerung hieraus wird gezeigt, daß in Abhängigkeit der Kopplungsstärke dieser Zustand durch eine einzeln oder eine Folge von Null-Photonen-Messungen erzeugt werden kann. Es wird die Frage nach der Implementierung eines Quantenspeichers behandelt, der durch die dispersive Wechselwirkung zwischen dem kollektiven internen Grundzustand eines atomaren Ensembles und zwei zueinander senkrechten Resonatormoden realisiert wird. Die Fragestellung der Rekonstruktion eines quantenmechanischen Zustandes im Rahmen der Resonator-Quantenelektrodynamik wird betrachtet. Die optimale Definition der Wignerverteilung zur Beschreibung von Resonatormoden wird herausgearbeitet: sie basiert auf der Fresnel-Transformation der atomaren Inversion eines Abfrageatoms. Ferner wird die allgemeine Integral-Transformation der Rekonstruktion der Wignerverteilung für ein Teilchen in einem symmetrischen Potential hergeleitet.

Abstract

The models of a strongly-driven micromaser and a one-atom laser are developed. Their analytical solutions are obtained by means of phase space techniques. It is shown how to exploit the model of a one-atom laser for simultaneous generation and monitoring of the decoherence of the atom-field ‘Schrödinger cat’ states. The similar machinery applied to the problem of the generation of the maximally-entangled states of two atoms placed inside an optical cavity permits its analytical solution. The steady-state solution of the problem exhibits a structure in which the two-atom maximally-entangled state correlates with the vacuum state of the cavity. As a consequence it is demonstrated that the atomic maximally-entangled state, depending on a coupling regime, can be produced via a single or a sequence of no-photon measurements. The question of the implementation of a quantum memory device using a dispersive interaction between the collective internal ground state of an atomic ensemble and two orthogonal modes of a cavity is addressed. The problem of quantum state reconstruction in the context of cavity quantum electrodynamics is considered. The optimal operational definition of the Wigner function of a cavity field is worked out. It is based on the Fresnel transform of the atomic inversion of a probe atom. The general integral transformation for the Wigner function reconstruction of a particle in an arbitrary symmetric potential is derived.

Contents

1	Introduction	1
2	Phase space concept in quantum theory	5
2.1	Classical vs. quantum description	5
2.2	Quantum phase space and Wigner function	10
2.3	Quantum quasidistributions and their properties	14
2.3.1	Wigner representation	15
2.3.2	The P representation	16
2.3.3	The Q representation	18
3	Models in Cavity QED	21
3.1	Jaynes-Cummings model	22
3.2	Jaynes-Cummings model in the presence of a strong classical field	28
3.3	Micromaser	31
3.3.1	Model of the Micromaser	32
3.3.2	Dynamics of the Micromaser	33
3.4	Strongly-driven micromaser	36
3.4.1	Hamiltonian and coherent dynamics	37
3.4.2	SDM master equation and analytical solutions	45
3.4.3	SDM field statistics	47
3.4.4	Atomic correlations	48
3.4.5	Numerical simulations	51
3.5	One-atom laser	54
3.5.1	Model	55
3.5.2	Monitoring the cavity field decoherence using a one-atom laser	57

4	Quantum state engineering in Cavity QED	65
4.1	Generation of Fock states using the micromaser	65
4.2	Generation of maximally-entangled atomic states in optical cavities . .	67
4.3	Multipartite entanglement using atomic coherences	74
4.3.1	Model	75
4.3.2	Mesoscopic superposition of atomic states	77
4.3.3	Generation of the multiatom entangled states	79
5	Quantum state reconstruction in Cavity QED	81
5.1	Operational definition of the quantum quasidistribution functions . . .	82
5.2	Fresnel representation of the Wigner function	83
5.3	Integral representation of the Wigner function: General case	90
6	Outlook	93

Chapter 1

Introduction

The starting point in the history of cavity quantum electrodynamics (CQED) can be regarded to Purcell who has suggested one of its principle ideas - the modification of spontaneous emission rate of an atom coupled to a resonant electrical circuit. The main reason for that is alteration of the structure of the free-space radiation modes seen by the atom induced by the circuit or, more generally, a cavity. The next big step forward in the field of CQED has been done when the theory of a two-level atom interacting with a single quantized mode of the radiation field, which is at the heart of any CQED problem, has been worked out by Jaynes and Cummings and seems to have opened a floodgate to enormous number of theoretical articles in the field. However the experimental advances proceeded at noticeably slower rate. The main reason for that was a technical limitation on fabricating of the high quality resonators which provide the strong coupling regime of the atom-field interaction. The strong coupling regime, otherwise irrelevant for conventional lasers¹, plays an important role for the observation of coherent single-atom-field dynamics.

The break-through in manufacturing of high-Q resonators in microwave domain in the eighties opened an avenue for the experimental studies of the atom-field systems described by the Jaynes-Cummings model. Inspired by a conventional maser the group of H. Walther in Garching has experimentally realized a one-atom maser or micromaser. At about the same time the group of S. Haroche in Paris has achieved superradiance and a vacuum-field controlled modification of the lifetime of Rydberg atoms in cavities. In contrast to the conventional maser the micromaser operates in the regime where there is on average only one atom interacting with the cavity at a time. This fact implies that the atom-cavity coupling must be strong in order to reach the strong coupling limit of matter-field interaction and consequently achieve an amplification of the cavity field. The latter condition has been fulfilled by sending highly-excited Rydberg atoms, possessing a large dipole moment, through the cavity. The micromaser became the first cavity QED experiment which allowed detailed study of the Jaynes-Cummings

¹In the laser each individual atom of a lasing medium couples to the cavity field in the weak coupling regime however due to macroscopic number of atoms the generation of the cavity field is achieved

model. It has permitted to observe resonant single-atom-cavity energy exchange, Rabi oscillation and collapses and revivals of atomic population, non-classical states of the cavity field as well as entangled atom-field states.

On the other hand, experimental accomplishment of the micromaser had triggered the achievement of the strong coupling regime in the domain of optical cavity QED. The main advantage of cavity QED with the optical resonators over the microwave regime is a possibility to measure the cavity field directly by means of counting of the photons leaking through the cavity mirrors. However the price for this is noticeably shorter lifetime of the optical photons and stronger decoherence of the cavity field when compared to a microwave cavity. In the last decade the experiments in the domain of optical QED became a routine mainly due to two groups of researchers, one led by J. Kimble at Caltech and another by G. Rempe in Garching. They have reached a trapping of an atom by the field of a cavity, realized a one-atom laser and a single photon source, demonstrated basics of quantum information processing employing atomic qubits. At the same time the progress achieved recently, by researchers in the group of H. Walther in Garching, in the deterministic coupling of trapped ions to an optical cavity has allowed to realize today the most stable single photon source.

Nowadays the rapid development of the quantum information theory gave a new impulse to both experimental and theoretical research on implementation of quantum computation in the framework of cavity QED. It turned out that the Jaynes-Cumming model describes a situation when a two-level atom(qubit) gets entangled with the cavity field. By letting several atoms to interact with the same cavity field one can entangle the atoms what can be interpreted, depending on the states of atoms, as a quantum logic operation. Experimental advances in controlling and manipulating of atoms and cavity fields have allowed to make proof-of-principles demonstration of two-qubits quantum gates using the micromaser and optical resonators. Despite the achieved success there are still challenges to overcome. One of them is to answer the question whether a scalable quantum computation can be realized in principle by means of cavity QED.

This thesis is an attempt to look at cavity QED from the point of view of practical realization of quantum information processing taking into account the main experimental limitations and imperfections. The striking feature of this work is that we do not stick here to a standard approach developed over years in the literature and which can be formulated as follows. The atom-cavity interaction is described by the Jaynes-Cumming model and is a unitary process when the atom-cavity system is perfectly isolated from its environment. However any model, which pretends to give a realistic description of an experiment, ought to include effects of decoherence. This leads to a description of an entire atom-cavity system in terms of a master equation, which can be further evaluated numerically. This approach obviously has an important drawback. If one wants now to describe a dynamics of a quantum register consisting out of dozens of atoms the numerical calculations fail pretty fast giving no definite prediction about the system. On the other hand the number of atoms in the register is still small to use thermodynamical methods of description. Consequently, we conclude that the standard method suitable for several atoms does not give a satisfactory analysis for the

case of the mesoscopic systems. In contrast here we introduce two novel cavity QED models, namely the model of the strongly-driven micromaser (SDM) and the one-atom laser model which are indeed analytical soluble and cover the whole spectrum of current experiments from microwave to optical.

The solubility of the models guaranties us an access to the solutions at any moment of time at any initial conditions and allows to solve also the scaled problems. So that for example using the model of a one-atom laser as a basis we are able to solve analytically the model of N -atom laser. For the case of $N = 2$ atoms we show that each time when the steady state output field is measured to be in vacuum state the atoms are prepared in the maximally-entangled state. It is remarkable that this approach allows to overcome the problem of the low detection efficiency of the conventional schemes based on detection of a single photon. To our knowledge our scheme is the first which completely solves the problem of low detection efficiency and makes atomic entanglement insensitive to photon detection. Moreover our model of a one-atom laser opens a new perspective for studies of the decoherence properties of an optical cavity field as well as an evolution from an atom-field entangled state towards a complete mixture. This question has been studied experimentally in the case of the micromaser, but we are the first who propose a possible experimental scheme in the optical domain.

It is worth to notice that there are only few examples of the quantum open systems described by solvable master equations. With this work we contribute to the matured field of cavity QED with two new solvable models. The key point here is to add to conventional models of the micromaser and one-atom laser a strong external classical driving field. It seems, at the first glance, that the external driving will complicate the dynamics even more, however, on the contrary, it makes the new models soluble.

Another important question we are concerned about in this thesis is a quantum state reconstruction. This subject, due to its significant importance for experimental needs, has been already extensively studied in the context of cavity QED over the last twenty years. Here however we come out with an idea of an optimal operational definition of the Wigner function of a cavity field in terms of the Fresnel transform of the measured atomic inversion. It turned out that this scheme is also applicable to the state reconstruction of a particle in an arbitrary symmetrical potential.

We are finishing the introduction by giving an overview of this thesis:

- The second chapter is an introductory overview of the phase space concept in quantum mechanics. The P-, Q-, and Wigner quasidistributions of a quantum state are discussed and the main mathematical phase-space tools are introduced.
- In the third chapter the well-known Jaynes-Cummings model as well as the model of the micromaser are considered. Moreover the analytically soluble models of the strongly-driven micromaser and a one-atom laser are presented. Their general solutions are found by means of the phase space techniques introduced in the second chapter.
- The questions of application of the models of the micromaser and a one-atom

laser to the generation of nonclassical states of the radiation as well as maximally-entangled states of two atoms are studied in the fourth chapter. The utilization of the ground state atomic coherences for a quantum memory and also generation of multi-atom entangled states are discussed.

- The fifth chapter examines the questions of the cavity field state reconstruction. It is shown how an optimal operational scheme for the reconstruction of the Wigner function of a cavity field can be built using the Fresnel transform of the atomic inversion. The generalization of this approach to the case of a particle in an arbitrary symmetrical potential is considered.

Chapter 2

Phase space concept in quantum theory

The concept of phase space or configurational space stems from classical mechanics. It gives a vivid description of a dynamical behaviour of a classical system in terms of geometrical trajectories in corresponding phase space. In contrast, quantum mechanics describes a system by a density operator acting on Hilbert space of the system. The Hilbert space consists of all possible dynamical states of the system. This is quite obscure description, since we are used to deal with number and geometry rather than with operators. Fortunately, there exist representations of quantum mechanics which map a density operator to a quasidistribution function which is defined on corresponding quantum phase space, in such a way opening an opportunity to visualize quantum dynamics. The concept of quantum phase space as well as the first quasidistribution function has been introduced by Wigner [1]. Later Cahill and Glauber have shown [2, 3] that there exist a class of quasidistributions, with different mathematical properties, defined in phase space. Nowadays, the quantum quasidistribution functions are widely employed in different branches from nuclear physics to quantum optics. Particularly useful in quantum optics, quasidistribution methods give a plain description of quantum states of radiation and their interference in phase space [4].

In this chapter we introduce a notation of quantum phase space, define different quantum quasidistribution functions and study their properties. We draw an analogy between classical statistical mechanics and a phase space description of quantum mechanics. The formalism of characteristic functions developed in this chapter will serve as a key ingredient for an integration of a master equations for different open quantum systems.

2.1 Classical vs. quantum description

In classical mechanics, a dynamical state of a system with N degrees of freedom is described by a point $(q, p) = (q_1, \dots, q_N, p_1, \dots, p_N)$ in $2N$ -dimensional space consisting

of N generalized coordinates (q_1, \dots, q_N) and N conjugated momenta (p_1, \dots, p_N) often called the phase space. The time evolution of the dynamical state is then given by a trajectory $(q(t), p(t))$ in the phase space, where the dynamical variables $q_i(t)$ and $p_i(t)$ obey the Hamilton equations

$$\frac{dq_i(t)}{dt} = \frac{\partial H(q, p, t)}{\partial p_i}; \quad \frac{dp_i(t)}{dt} = -\frac{\partial H(q, p, t)}{\partial q_i}; \quad i = \overline{1, N}. \quad (2.1)$$

Here $H(q, p, t)$ is the Hamiltonian *function* of the system. In a case of N identical particles system it has the form

$$H(q, p, t) = \sum_{j=1}^N \frac{p_j^2}{2m} + V(q_1, \dots, q_N). \quad (2.2)$$

In the last equation the first term represents an overall kinetic energy of N particles, whereas $V(q_1, \dots, q_N)$ corresponds to a potential energy of the system including the contributions from an interparticle interaction and external fields.

In order to determine the dynamical state $(q(t), p(t))$ of a system with a given Hamiltonian H at any moment of time t , one has to integrate the equations of motion (2.1) with given initial conditions $(q(t_0), p(t_0))$. The equivalent approach to the problem of determination of the dynamical state is to find integrals of motion $C_i(p, q)$ of the system. Then each trajectory of the system in the phase space is characterized by a certain value c_i of the integrals $C_i(p, q)$, which constrains the subspace $\Gamma(p, q; c_i)$ of the whole phase space of the system accessible to the trajectories. If for a N -particle system, N integrals of motion can be found then the system is said to be integrable. Trivial example of an integrable mechanical system is a system of N noninteracting particles.

Such a trajectory description is widely employed for a study of dynamical instabilities in both linear and nonlinear mechanical systems. We mention it briefly here. Let us consider two close initial conditions $(q(t_0), p(t_0))$ and $(q(t_0) + \Delta q(t_0), p(t_0) + \Delta p(t_0))$. Their distance $(\Delta q(t), \Delta p(t))$ can grow exponentially with time, depending on the dynamical properties of the system. Thus, even a small initial deviation $(\Delta q(t_0), \Delta p(t_0))$ can exceed a given value at a sufficient long time interval, so that the state of the system becomes unpredictable¹.

Although, the dynamical description is completely reliable in a case of systems with few degrees of freedom, there are several reasons why it is non applicable to the complex systems with a large number degrees of freedom. First of all, it is impossible to determine the exact initial state of a many-body system. As a consequence, one automatically faces a problem of integration of the equations of motion (2.1). On the other hand, even though one can determine the initial conditions with a finite accuracy it does not warrant that these uncertainties will not blow up exponentially with the course of time leading to the dynamical chaos. The second reason follows from the

¹This situation is regarded as a dynamical chaos

first one and states that any limited accuracy solution of the Hamilton equations does not allow one to specify a single trajectory on a long times scale. Summarizing, we come to a conclusion that it is not possible to describe exactly the evolution of a macroscopic system from one point to another point of the phase space, because of the uncertainties mentioned above. In other words, we can not specify a microscopic state of a macroscopic system in a deterministic manner, i.e. we can determine the dynamical state of the system only with a certain probability.

The above introduced physical arguments clearly show that the probabilistic description of the dynamical processes in many-particle systems is a natural language. Therefore, following Gibbs, instead of the given macroscopic system we consider a collection of an infinitely large number of its copies, all are placed in identical external conditions, i.e. we introduce a statistical ensemble representing the macroscopic state of the system. Each system from the ensemble has its own trajectory in phase space. Hence, we can associate a certain probability, that M systems from the ensemble, during their evolution, pass through the point (q, p) , with each point (q, p) of phase space. Consequently, the ensemble can be specified by the distribution function $\rho(q, p, t)$ which is proportional to the probability density of the distribution of systems in phase space. The phase space distribution function has to be normalized with respect to integration over the whole phase space. So that

$$\int_{\Gamma} \rho(q, p, t) d\Gamma = 1, \quad (2.3)$$

where $d\Gamma$ denotes an infinitely small volume of the phase space Γ . The quantity $\rho(q, p, t)d\Gamma$ has a meaning of the probability of finding a system of ensemble in the volume $d\Gamma$ close to the phase space point (q, p) at time t .

Having at our disposal basic ideas of statistical mechanics, we can answer the following important practical question: Given the distribution function $\rho(q, p, t)$, how to calculate a result of measurement of a physical quantity A described by a mean value of the corresponding dynamical variable $A(q, p, t)$? It is assumed, in statistical mechanics, that the observed physical quantities, which are the time averages over the history of a single system, can be obtained from the averaging over the statistical ensemble. This assumption is known as the ergodic hypothesis. According to it we write the desirable quantity as

$$\langle A \rangle = \int_{\Gamma} A(q, p, t) \rho(q, p, t) d\Gamma. \quad (2.4)$$

The dynamical behaviour of each single system of ensemble is given by Hamilton equations (2.1). Hence a question arises: Which equation of motion obeys the distribution function $\rho(q, p, t)$? In order to answer this question, we formulate first the Liouville theorem:

Suppose that at the initial moment of time t_0 a certain volume $\Delta\Gamma_0$ with the center at (q_0, p_0) was selected in phase space. Then at later time t the selected points occupy

the region $\Delta\Gamma_t$ with the center at (q_t, p_t) , where q_t , and p_t are corresponding solutions of the equations of motion (2.1). Then the following statement takes place

$$\int_{\Delta\Gamma_0} dq_0 dp_0 = \int_{\Delta\Gamma_t} dq_t dp_t, \quad (2.5)$$

i.e. the phase volume occupied by the points remains constant during the motion of the system.

As a consequence of Liouville's theorem the distribution function remains constant along the phase trajectories. In other words, $\rho(q(t), p(t), t) = \rho(q(t'), p(t'), t')$. If times t and t' are infinitesimally close, i.e. $t' = t + dt$, then

$$\rho(q(t), p(t), t) = \rho(q(t) + \dot{q}dt, p(t) + \dot{p}dt, t + dt). \quad (2.6)$$

Assuming that the function $\rho(q, p, t)$ is differentiable, we arrive at

$$\frac{\partial \rho}{\partial t} + \sum_{j=1}^N \left[\frac{\partial \rho}{\partial q_j} \dot{q}_j + \frac{\partial \rho}{\partial p_j} \dot{p}_j \right] = 0. \quad (2.7)$$

Taking into account the Hamilton equations (2.1), we obtain Liouville equation for the distribution function:

$$\frac{\partial \rho}{\partial t} = \{H, \rho\}, \quad (2.8)$$

where

$$\{H, \rho\} = \sum_{j=1}^N \left[\frac{\partial \rho}{\partial p_j} \frac{\partial H}{\partial q_j} + \frac{\partial \rho}{\partial q_j} \frac{\partial H}{\partial p_j} \right] \quad (2.9)$$

is the Poisson bracket for the Hamiltonian function H and ρ .

In contrast to classical description, quantum mechanics characterizes a dynamical state of a system by a state vector $|\Psi(t)\rangle$ in a Hilbert space \mathcal{H} . The state vector is normalized to one, i.e. its scalar product with itself $\langle \Psi(t) | \Psi(t) \rangle = 1$. Depending on a system this linear complex vector space can have different dimension. All dynamical variables(observables), which can be measured in an experiment, are described by self-adjoint operators acting on the Hilbert space of a system. According to the eigenvalues, all observables can be divided into two classes: (i) Observables with discrete spectrum. (ii) Observables with continuous spectrum. Typical representatives of the first group are angular momentum and spin operators, whereas the second class is presented by position and momentum operators.

Choosing in a Hilbert space of a system, a basis of orthogonal states $|x_1, \dots, x_N\rangle$ defined by a complete set of compatible observables $\{X_1, \dots, X_N\}$ one can represent any state $|\Psi(t)\rangle$ of the system by a complex function, which is defined as

$$\Psi(x_1, \dots, x_N, t) = \langle x_1, \dots, x_N | \Psi(t) \rangle. \quad (2.10)$$

The function $\Psi(x_1, \dots, x_N, t)$ is called the wave function of the system in the X -representation. Another possibility to represent a quantum state of a system is to write it in a basis of eigenvectors of an observable A . For the sake of simplicity, we assume that the A has a nondegenerate spectrum. Hence,

$$|\Psi(t)\rangle = \sum_a C_a(t)|a\rangle, \quad (2.11)$$

$$|\Psi(t)\rangle = \int_b^a C(a, t)|a\rangle da, \quad (2.12)$$

where $C_a(t) = \langle a|\Psi(t)\rangle = C(a, t)$ and the first expression corresponds to a discrete case, whereas the second one is valid for a continuous case.

The mean value of an observable A in an arbitrary state $|\Psi(t)\rangle$ is given by

$$\langle A \rangle = \langle \Psi(t)|A|\Psi(t)\rangle = \sum_a a |\langle a|\Psi(t)\rangle|^2. \quad (2.13)$$

We note here that the quantity $|\langle a|\Psi(t)\rangle|^2 = |C_a(t)|^2$ plays a role of the probability to find the system at time t in the quantum state $|a\rangle$. Probabilistic interpretation is the inherent feature of quantum description. All information about possible outcomes of a measurement on a quantum system is hidden in a quantum state description and reveals when an appropriate measurement is performed.

The time evolution of an arbitrary quantum state $|\Psi(t)\rangle$ is governed by the Schrödinger equation

$$i\hbar \frac{\partial |\Psi(t)\rangle}{\partial t} = \mathcal{H}|\Psi(t)\rangle, \quad (2.14)$$

where \mathcal{H} is the Hamiltonian operator of the system of interest. The standard procedure to obtain the Hamiltonian operator is to change to quantum position and momentum operators in the correspondent classical Hamiltonian function, except the cases when a quantum system has no classical analog (e.g. quantum spin Hamiltonian).

The state of a quantum system is then completely defined, if it is possible to determine a complete set of compatible observables and to state the results of their measurement. In this case, it can be described by a certain state vector $|\Psi\rangle$ which is called pure. It can also happen that our knowledge about the system is incomplete, so that it is possible to ascribe to the system only a set of probabilities $\{p_1, \dots, p_m\}$ for the system to be found in one of the states $\{|1\rangle, \dots, |m\rangle\}$. In contrast to the pure state, such a state is described by a positive defined hermitian density operator ρ with unitary trace, and regarded as mixed state. The density operator for mixed states can be expressed as

$$\rho = \sum_m p_m |m\rangle \langle m|; \quad \sum_m p_m = 1. \quad (2.15)$$

It follows from the last equation, that the crucial difference between the pure and mixed states is contained in the presence of quantum interference terms. Obviously, the

mixed state Eq.(2.15) is diagonal in $\{|m\rangle\}$ basis and does not comprise any interference, therefore it describes a statistical mixture of quantum states with well-defined weights, whereas a pure state $|\Psi\rangle = \sum_m c_m |m\rangle$, indeed, is a superposition of quantum states. The corresponding density operator for the pure quantum state $|\Psi\rangle$ can be written as

$$\rho = \sum_{n,m} p_{n,m} |n\rangle\langle m|; \sum_m p_{m,m} = 1. \quad (2.16)$$

Unlike the density operator for a mixed state Eq.(2.15), pure state density operator Eq.(2.16) has off-diagonal elements which contribute to quantum coherences.

Lack of knowledge about a quantum system forces us to describe it in term of an ensemble of quantum states with a probability attached to each state from the ensemble. We have applied a similar approach to the correspondent classical problem, where lack of precise initial conditions in many-body problem led to the probabilistic description by means of classical distribution function.

The description of a quantum many-body system in terms of a state vector whose evolution is governed by the Schrödinger equation is somewhat hopeless approach. Likewise in the classical mechanics, one faces the problem of initial conditions which makes it impossible to solve the Schrödinger equation. Therefore, it is reasonable to employ the density operator formalism for the solution of such problems. The equation of motion for the density operator ρ can be obtained directly from the Schrödinger equation and reads

$$\frac{\partial \rho}{\partial t} = -\frac{i}{\hbar} [\mathcal{H}, \rho]. \quad (2.17)$$

The last equation is similar to the classical Liouville equation (2.8). However, in quantum case, the classical Poisson bracket is changed to a commutator of the correspondent quantum operators.

The outcome of a measurement of an observable A is given by a mean value of the self-adjoint operator A and can be expressed as

$$\langle A \rangle = \text{Tr}(A\rho). \quad (2.18)$$

Calculating the trace in an arbitrary basis $|x\rangle = |x_1, \dots, x_N\rangle$ we obtain

$$\langle A \rangle = \int A(x, x') \rho(x, x', t) d^N x d^N x', \quad (2.19)$$

where $A(x, x') = \langle x_1, \dots, x_N | A | x'_1, \dots, x'_N \rangle$ and the density operator matrix representation is given by the two variables function $\rho(x, x', t) = \langle x_1, \dots, x_N | \rho(t) | x'_1, \dots, x'_N \rangle$.

2.2 Quantum phase space and Wigner function

As we have seen above quantum and classical descriptions are more different than similar. However, one would like to have an analogy to classical phase space in quantum

mechanics. The reason for that is quite simple. Our classical being is used to deal rather with number and simple geometrical constructions than with operators and infinite-dimensional Hilbert spaces. One of the possible way to construct the quantum phase space of a quantum mechanical system of N particles, fully described by a set of N position and N momentum operators², is to introduce a $2N$ -dimensional space, N axes of which correspond to the eigenvalues of N position operators and the other N attribute eigenvalues of momentum operators. In other words, for each operator there is an axis in the constructed space such that it contains all eigenvalues of this operator. It seems, *prima facie*, that the constructed quantum phase space does not differ from the corresponding classical one and one can again, as in classical mechanics, introduce now quantum trajectories in order to describe dynamics of a quantum system. Nevertheless, this is incorrect. One of the fundamental principles of quantum mechanics - the uncertainty principle prohibits the use of the concept of a trajectory. It states that it is impossible to measure two non-commuting observables instantaneously with infinite precision. It is known that the position and momentum operators do not commute and therefore for them the uncertainty relation reads $\Delta q \Delta p \geq \frac{\hbar}{2}$. As a consequence, any attempt to determine a position or momentum of a particle leads to an uncertainty in a conjugated variable.

Besides trajectories, another important object from the classical phase space is distribution function $\rho_{cl.}(p, q)$. It describes the probability to find a classical system in the point (p, q) . From the above reasoning it is clear that such a kind of joint distribution for the coordinate and momentum cannot be introduced in the quantum case due to the uncertainty relation. We recall that the quantum analog of the classical distribution function $\rho_{cl.}(p, q)$ is the density operator ρ . Its matrix elements, say in coordinate representation, $\langle \mathbf{r} | \rho | \mathbf{r}' \rangle = \rho(\mathbf{r}, \mathbf{r}')$ describes the probability density to find a particle at position \mathbf{r} (diagonal elements $\rho(\mathbf{r}, \mathbf{r})$) and quantum coherence (off-diagonal elements). On the other hand, one can write the density operator in other representation. For instance, in the momentum representation $\rho(\mathbf{p}, \mathbf{p})$ plays a role of the probability density to find a particle with momentum \mathbf{p} . Hence there is a principal question, whether it is possible to find a representation of the density operator which combines both coordinate and momentum representations? In other words, it should be possible to extract density matrixes $\rho(\mathbf{r}, \mathbf{r})$ and $\rho(\mathbf{p}, \mathbf{p})$ from the desired mixed representation.

In order to answer this question, consider, at first, a system consisting of one particle. The eigenvectors $\{|\mathbf{r}\rangle\}$ of a position operator \hat{q} of the particle constitute an orthonormal basis, i.e.

$$\langle \mathbf{r}' | \mathbf{r}'' \rangle = \delta(\mathbf{r}' - \mathbf{r}''), \quad \int_{-\infty}^{+\infty} d\mathbf{r} |\mathbf{r}\rangle \langle \mathbf{r}| = \mathbb{1}, \quad (2.20)$$

here $\delta(\mathbf{r}' - \mathbf{r}'')$ is Dirac's delta function. On the other hand, the eigenvectors $\{|\mathbf{p}\rangle\}$ of

²We assume here that the particle has no internal structure. Otherwise such a description is incomplete.

a momentum operator \hat{p} of the particle form another orthonormal basis

$$\langle \mathbf{p}' | \mathbf{p}'' \rangle = \delta(\mathbf{p}' - \mathbf{p}''), \quad \int_{-\infty}^{+\infty} d\mathbf{p} |\mathbf{p}\rangle \langle \mathbf{p}| = \mathbb{1}. \quad (2.21)$$

The scalar product of any two vectors from the position and momentum representations reads

$$\langle \mathbf{r} | \mathbf{p} \rangle = \frac{1}{\sqrt{V}} e^{(i/\hbar)\mathbf{p}\cdot\mathbf{r}}, \quad (2.22)$$

where V is a normalization volume. Using a completeness relation for the coordinate representation one can write a density operator of the system in the momentum basis as follows

$$\langle \mathbf{p}' | \rho | \mathbf{p}'' \rangle = \int_{-\infty}^{+\infty} d\mathbf{r}' \int_{-\infty}^{+\infty} d\mathbf{r}'' \langle \mathbf{p}' | \mathbf{r}' \rangle \langle \mathbf{r}' | \rho | \mathbf{r}'' \rangle \langle \mathbf{r}'' | \mathbf{p}'' \rangle. \quad (2.23)$$

By substituting scalar product Eq.(2.22) into Eq.(2.23) we arrive at

$$\langle \mathbf{p}' | \rho | \mathbf{p}'' \rangle = \frac{1}{V} \int_{-\infty}^{+\infty} d\mathbf{r}' \int_{-\infty}^{+\infty} d\mathbf{r}'' \exp \left\{ \frac{i}{\hbar} (\mathbf{p}'' \mathbf{r}'' - \mathbf{p}' \mathbf{r}') \right\} \langle \mathbf{r}' | \rho | \mathbf{r}'' \rangle. \quad (2.24)$$

Changing in the last equation to the new variables

$$\begin{aligned} \mathbf{r} &= \frac{1}{2}(\mathbf{r}' + \mathbf{r}''), \quad \mathbf{x} = \mathbf{r}' - \mathbf{r}'' \\ \mathbf{p} &= \frac{1}{2}(\mathbf{p}' + \mathbf{p}''), \quad \mathbf{q} = \mathbf{p}' - \mathbf{p}'' \end{aligned}$$

we obtain

$$\langle \mathbf{p} + \frac{1}{2}\mathbf{q} | \rho | \mathbf{p} - \frac{1}{2}\mathbf{q} \rangle = \frac{1}{V} \int_{-\infty}^{+\infty} d\mathbf{r} e^{(-i/\hbar)\mathbf{q}\cdot\mathbf{r}} f^W(\mathbf{r}, \mathbf{p}), \quad (2.25)$$

where

$$f^W(\mathbf{r}, \mathbf{p}) = \int_{-\infty}^{+\infty} d\mathbf{x} e^{(-i/\hbar)\mathbf{p}\cdot\mathbf{x}} \langle \mathbf{r} + \frac{1}{2}\mathbf{x} | \rho | \mathbf{r} - \frac{1}{2}\mathbf{x} \rangle \quad (2.26)$$

is the Wigner function. It was introduced by Wigner [1] to study quantum corrections to classical statistical mechanics. The Wigner function Eq.(2.26) depends both on the coordinate and momentum of a particle and is a desirable mixed representation of the density operator. The generalization of the Wigner function to a case of N particles is straightforward and gives

$$f^W(\mathbf{r}_1, \dots, \mathbf{r}_N; \mathbf{p}_1, \dots, \mathbf{p}_N) =$$

$$\int_{-\infty}^{+\infty} d\mathbf{x}_1 \cdots \int_{-\infty}^{+\infty} d\mathbf{x}_N e^{(-i/\hbar) \sum_{i=1}^N \mathbf{p}_i \cdot \mathbf{x}_i} \langle \mathbf{r}_1 + \frac{1}{2}\mathbf{x}_1 \cdots \mathbf{r}_N + \frac{1}{2}\mathbf{x}_N | \rho | \mathbf{r}_1 - \frac{1}{2}\mathbf{x}_1 \cdots \mathbf{r}_N - \frac{1}{2}\mathbf{x}_N \rangle. \quad (2.27)$$

The properties of the Wigner function are:

1. The Wigner function is real, i.e. $(f^W)^* = f^W$. This follows from the definition Eq.(2.26) and from the hermicity of the density operator ρ .
2. The probability distributions of the coordinate and momentum read

$$w(\mathbf{r}) = \rho(\mathbf{r}, \mathbf{r}) = \frac{1}{(2\pi\hbar)^3} \int_{-\infty}^{+\infty} d\mathbf{p} f^W(\mathbf{r}, \mathbf{p}), \quad (2.28)$$

$$w(\mathbf{p}) = \rho(\mathbf{p}, \mathbf{p}) = \frac{1}{V} \int_{-\infty}^{+\infty} d\mathbf{r} f^W(\mathbf{r}, \mathbf{p}). \quad (2.29)$$

3. The Wigner function is normalized to one:

$$\int_{-\infty}^{+\infty} d\mathbf{r} \int_{-\infty}^{+\infty} d\mathbf{p} f^W(\mathbf{r}, \mathbf{p}) = \text{Tr}(\rho) = 1. \quad (2.30)$$

4. If \hat{A} is an arbitrary hermitian operator and $f^W(p, q)$ is the Wigner function corresponding to a state ρ , then the mean value of \hat{A} in the state ρ reads

$$\langle \hat{A} \rangle = \text{Tr}(\hat{A}\rho) = \int_{-\infty}^{+\infty} d\mathbf{r} \int_{-\infty}^{+\infty} d\mathbf{p} A(\mathbf{r}, \mathbf{p}) f^W(\mathbf{r}, \mathbf{p}), \quad (2.31)$$

where $A(\mathbf{r}, \mathbf{p}) = \int_{-\infty}^{+\infty} d\mathbf{x} e^{(-i/\hbar)\mathbf{p}\cdot\mathbf{x}} \langle \mathbf{r} + \frac{1}{2}\mathbf{x} | \hat{A} | \mathbf{r} - \frac{1}{2}\mathbf{x} \rangle$ is a phase space representation of the operator \hat{A} .

It is instructive to compare the features of the Wigner function to the properties of the classical distribution function. The Wigner function and classical distribution function are both real and normalized to one. Moreover, the expression for the mean value of a hermitian operator \hat{A} Eq.(2.31) can be obtained formally, from the corresponding classical expression Eq.(2.4) by substituting $f^W(p, q, t)$ instead of $\rho(q, p, t)$ into it. This shows that the constructed Wigner function representation of the quantum mechanics, nominally, is close to classical description. However, they are not equivalent! Otherwise, classical and quantum description would not give different predictions. Therefore, there must be a peculiar feature of the Wigner function which makes it inherent in only

quantum formalism. Indeed, in contrast to classical distribution function, the Wigner function is not positive defined, i.e. it can take on negative values. Hence, even though, the Wigner function contains an information about distribution functions of momentum and coordinate it cannot be considered as a quantum analog of classical distribution function. It is therefore customary to call it quasidistribution function in quantum phase space.

The Wigner function is not only a quasidistribution which can be defined on quantum phase space³. As we will see in the next section, it is certainly possible to introduce a family of quasidistributions with different properties. Depending on a physical problem, it is convenient to use one or another phase space representation of the density operator.

2.3 Quantum quasidistributions and their properties

Let us consider a quantum mechanical system consisting of a particle in an arbitrary one-dimensional potential V . It is described by a pair of non-commuting Hermitian observables p and q . Instead of dealing with the momentum and coordinate operators we introduce a linear superposition of them

$$a = \frac{1}{\sqrt{2\hbar}}\left(\lambda q + \frac{i}{\lambda}p\right), \quad (2.32)$$

$$a^\dagger = \frac{1}{\sqrt{2\hbar}}\left(\lambda q - \frac{i}{\lambda}p\right), \quad (2.33)$$

where λ is a real parameter different from zero. Operators a and a^\dagger obey $[a, a^\dagger] = 1$ and therefore have the same algebraic properties as the photon creation and annihilation operators of quantum electromagnetic field.

For each complex number α we define the following displacement operator [5]

$$D(\alpha) = \exp(\alpha a^\dagger - \alpha^* a), \quad (2.34)$$

which is unitary, i.e. $D^\dagger(\alpha) = D^{-1}(\alpha) = D(-\alpha)$ and for $\alpha = \frac{1}{\sqrt{2}}(\lambda q' + \frac{i}{\lambda}p')$ can be rewritten as

$$D(\alpha) \equiv D(q', p') = \exp(iqp' - ipq'), \quad (2.35)$$

with q' and p' being eigenvalues of the coordinate and momentum operators q and p . The product of two displacement operators $D(\alpha)$ and $D(\beta)$ reads

$$D(\alpha)D(\beta) = D(\alpha + \beta) \exp\left(\frac{1}{2}\alpha\beta^* - \frac{1}{2}\alpha^*\beta\right), \quad (2.36)$$

³Hereafter, we say simply phase space, unless the opposite is stated

and therefore the displacement operators form an Abelian group with respect to multiplication. Furthermore, the displacement operator possesses the following properties

$$-\frac{\partial D(\alpha)}{\partial \alpha^*} = D(\alpha)\left(a + \frac{\alpha}{2}\right) = \left(a - \frac{\alpha}{2}\right)D(\alpha), \quad (2.37)$$

$$a + \alpha = D^{-1}(\alpha)aD(\alpha), \quad (2.38)$$

$$a^\dagger + \alpha^* = D^{-1}(\alpha)a^\dagger D(\alpha). \quad (2.39)$$

We denote an eigenstate of the operator a which corresponds to the eigenvalue zero by $|0\rangle$. Hence, by definition $a|0\rangle = 0$. Moreover, for each complex number α we define the coherent state $|\alpha\rangle$ [5] as $|\alpha\rangle = D(\alpha)|0\rangle$. It is clear from the definition of the coherent state $|\alpha\rangle$ that it is an eigenstate of the operator a with an eigenvalue α , i.e. $a|\alpha\rangle = \alpha|\alpha\rangle$. It is worth to notice that the set of coherent states $\{|\alpha\rangle\}$ is complete. In other words $\frac{1}{\pi} \int d^2\alpha |\alpha\rangle\langle\alpha| = \mathbb{1}$.

Having at our disposal a set of displacement operators $\{D(\alpha)\}$ and a correspondent set of coherent states $\{|\alpha\rangle\}$ we are ready to introduce the main quantum quasidistribution functions. To set the stage, we define the phase space of the system as a plane each point of which is given by a complex number α . Such a definition of the phase space, at the first sight, is different from the definition introduced in the preceding section, where the phase space plane has been specified by a pair of eigenvalues of the coordinate and momentum operators - (p, q) . However, taking into account that the complex number α is defined as a linear combination of the eigenvalues p and q we conclude that the both definition of the phase space are equivalent. It is more convenient for our future consideration to use a description of the phase space in terms of α .

2.3.1 Wigner representation

It was shown in [2] that the displacement operators form the complete set, so that any bounded operator⁴, which is a combination of coordinate and momentum operators, can be expanded as

$$F = \frac{1}{\pi} \int d^2\xi f(\xi) D^{-1}(\xi), \quad (2.40)$$

where the weight function $f(\xi) = \text{Tr}(FD(\xi))$ is unique and square-integrable and the integration is performed over the whole phase space. Thus since every density operator is bounded, we may write an arbitrary density operator in the form

$$\rho = \frac{1}{\pi} \int d^2\xi \chi(\xi) D^{-1}(\xi), \quad (2.41)$$

where the weight function $\chi(\xi) = \text{Tr}(\rho D(\xi))$ is the expectation value of the displacement operator $D(\xi)$ and is often called symmetrically ordered characteristic function

⁴We call an operator bounded if its Hilbert-Schmidt norm is finite, i.e. A is bounded if $\|A\| = (\text{Tr}A^\dagger A)^{\frac{1}{2}} < \infty$

or simply characteristic function. Since the displacement operator is unitary, the characteristic function $\chi(\xi)$ must be bounded. Indeed, the following conditions are satisfied $|\chi(\xi)| \leq 1$ and $\chi(0) = 1$. Moreover, it is square-integrable and hence, we can define its complex Fourier transform as

$$W(\alpha) = \frac{1}{\pi} \int d^2\xi e^{\alpha\xi^* - \alpha^*\xi} \chi(\xi), \quad (2.42)$$

which is up to a normalization factor equivalent to the definition of the Wigner function $W(r, p)$ in Eq.(2.26). In order to see that, one should change the variables $\xi \rightarrow \frac{1}{\sqrt{2}}(x + iq)$ and $\alpha \rightarrow \frac{1}{\sqrt{2}}(r + ip)$ in Eq.(2.42) and make use of the equivalent definition of the characteristic function $\chi(\xi) = \chi(x, q) = \int dt \exp(itx) \langle t - \frac{q}{2} | \rho | t + \frac{q}{2} \rangle$. Hence, by using the inverse Fourier transform applied to Eq.(2.42) we arrive at a definition of the characteristic function in terms of the Wigner function

$$\chi(\xi) = \frac{1}{\pi} \int d^2\alpha e^{-(\alpha\xi^* - \alpha^*\xi)} W(\alpha). \quad (2.43)$$

By substituting the expression for the characteristic function Eq.(2.43) into the expansion for the density operator Eq.(2.41) we obtain

$$\rho = \frac{1}{\pi} \int d^2\alpha W(\alpha) T(\alpha, 0), \quad (2.44)$$

where the operator $T(\alpha, 0) = 2D(\alpha)(-1)^{a^\dagger a} D^{-1}(\alpha)$ has been introduced. In other words, we have shown in the last equation that the Wigner function $W(\alpha)$ plays a role of a weight function for the expansion of the density operator ρ in the basis of operators $T(\alpha, 0)$.

There are three important direct consequences from Eq.(2.44). First of all, it allows us to express the Wigner function in a compact way as an expectation value of the operator $T(\alpha, 0)$, so that $W(\alpha) = \text{Tr}(\rho T(\alpha, 0))$. Secondly, since the eigenvalues of the Hermitian operator $T(\alpha, 0)$ are $2(-1)^n$, where n is integer, the Wigner function is naturally bounded according to the inequalities $-2 \leq W(\alpha) \leq 2$. Finally, evaluating the trace in the Fock basis we obtain that

$$W(\alpha) = \frac{2}{\pi} \sum_{n=0}^{\infty} (-1)^n \langle n | D^{-1}(\alpha) \rho D(\alpha) | n \rangle. \quad (2.45)$$

2.3.2 The P representation

As we have seen the Wigner function is a well-behaved square-integrable representation of an arbitrary density operator. But, is the representation Eq.(2.44) unique? One might formally write the following expansion [3]

$$\rho = \int d^2\alpha P(\alpha) T(\alpha, -1), \quad (2.46)$$

where $P(\alpha)$ is a weight function and $T(\alpha, -1)$ is a set of operators defined as

$$T(\alpha, s) = \frac{1}{\pi} \int d^2\xi D(\xi, s) e^{\alpha\xi^* - \alpha^*\xi}; \quad s = -1, \quad (2.47)$$

with $D(\xi, s) = D(\xi) e^{s|\alpha|^2/2}$. The function $P(\alpha)$ can be defined as in the case of the Wigner representation, namely $P(\alpha) = \pi^{-1} \text{Tr}(\rho T(\alpha, 1))$. However, this definition is not correct from the mathematical point of view, due to the following reason. The eigenvalues of the Hermitian operator $T(\alpha, s)$ are given by $c_n(s) = \frac{2}{1-s} \left(\frac{s+1}{s-1}\right)^n$ and consequently, they are all infinite for $s = 1$. Furthermore, the P function $P(\alpha)$, which is an expectation value of the operator $T(\alpha, 1)$, for certain classes of density operators, is extremely singular. Therefore, it is better to define a P function as a limit when $s \rightarrow 1$, so that $P(\alpha) = \pi^{-1} \lim_{s \rightarrow 1} \text{Tr}(\rho T(\alpha, s))$.

It is worth to notice, that the operator $T(\alpha, -1)$ can be alternatively presented as a projection operator onto a coherent state $|\alpha\rangle$. As the result we may write according to Eq.(2.46)

$$\rho = \int d^2\alpha P(\alpha) |\alpha\rangle \langle \alpha|. \quad (2.48)$$

Then, an expectation value of an arbitrary operator A , by virtue of Eq.(2.48) can be written as

$$\text{Tr}(\rho A) = \int d^2\alpha P(\alpha) \langle \alpha | A | \alpha \rangle. \quad (2.49)$$

The direct consequence of the last equation is a normalization condition for the P function. Calculating an expectation value of the unity operator we obtain

$$\text{Tr}(\rho \mathbb{1}) = 1 = \int d^2\alpha P(\alpha). \quad (2.50)$$

Hence, the P function can be also interpreted as a quantum quasidistribution function. Nevertheless, in contrast to the Wigner function, as we have seen above, it is not always well-behaved. The limiting process typically leads to a generalized function that is too singular to be used as a weight function for the P representation. For example, for the case of pure states, the P function is always singular. This, of course, reduces its applicability.

There is one more thing should be said about the P function. By substituting Eq.(2.47) into a definition of $P(\alpha)$ one obtains

$$P(\alpha) = \frac{1}{\pi^2} \int d^2\xi \chi_N(\xi) e^{\alpha\xi^* - \alpha^*\xi}, \quad (2.51)$$

where $\chi_N(\xi) = \lim_{s \rightarrow 1} \text{Tr}(\rho D(\xi, s)) = \text{Tr}(\rho e^{\xi a^\dagger} e^{\xi^* a})$ is the normally ordered characteristic function. If the inverse Fourier transform exists, i.e. if $P(\alpha)$ is square-integrable then

$$\chi_N(\xi) = \int d^2\alpha P(\alpha) e^{-(\alpha\xi^* - \alpha^*\xi)}. \quad (2.52)$$

The singular behaviour of the P function finds its reflection in properties of the characteristic function $\chi_N(\xi)$. For instance, a growth condition for the normally ordered characteristic function is given by the inequality $|\chi_N(\xi)| \leq e^{|\xi|^2/2}$ and therefore it does not always possess a Fourier transform.

2.3.3 The Q representation

We have studied two different representations of a density operator. Both of them were realized as an expansion of the density operator over a set of non-singular Hermitian operators, namely $T(\alpha, 0)$ for the Wigner representation and $T(\alpha, -1)$ for the P representation. Nevertheless, the properties of the weight functions, which play a role of quasidistribution functions, differ drastically from the bounded, square-integrable Wigner function to the unbounded, singular P function.

However, we would like to construct a quasidistribution function which is non-negative, bounded, differentiable, and normalized to one. Such a quasidistribution corresponds at most to a classical probability distribution function. Intuitively, we anticipate that such a well-behaved weight function is not necessary accompanied a non-singular set of operators.

To start with, we formally express a density operator as the integral

$$\rho = \frac{1}{\pi} \int d^2\alpha T(\alpha, 1) \langle \alpha | \rho | \alpha \rangle, \quad (2.53)$$

where the operator $T(\alpha, 1)$ is given by Eq.(2.47) for $s = 1$ and the function $\langle \alpha | \rho | \alpha \rangle$ is called the Q function. We recognize immediately that the expansion (2.53) is made over a set of singular operators⁵, but the question about the properties of the weight functions $\langle \alpha | \rho | \alpha \rangle$ is still open. Inverting Eq.(2.53) we may write by analogy to the $W(\alpha)$ and $P(\alpha)$

$$\langle \alpha | \rho | \alpha \rangle = \text{Tr}(\rho T(\alpha, -1)). \quad (2.54)$$

It is clear that, since the density operator ρ is a positive defined, bounded, Hermitian operator, the Q function, which is an average value of the density operator in the coherent state $|\alpha\rangle$, is non-negative and bounded according to the inequalities $0 \leq \langle \alpha | \rho | \alpha \rangle \leq 1$. Moreover, calculating a trace of the density operator in the basis of coherent states we obtain that a normalization condition for the Q function reads

$$1 = \text{Tr}(\rho) = \frac{1}{\pi} \int d^2\alpha \langle \alpha | \rho | \alpha \rangle. \quad (2.55)$$

Therefore, among the introduced quasidistribution functions, the Q function has the most classical properties.

The expectation value of an arbitrary operator A can be written using the definition (2.53) as

$$\text{Tr}(\rho A) = \frac{1}{\pi} \int d^2\alpha \text{Tr}(AT(\alpha, 1)) \text{Tr}(\rho T(\alpha, -1)), \quad (2.56)$$

⁵All eigenvalues of the operators $T(\alpha, 1)$ are infinite

and as in the case of the P function, it contains the singular operator $T(\alpha, 1)$. For this reason averages of the bounded operators in P and Q representations do not, in general, converge. The only representation which supports their convergence is thus the Wigner representation.

Let us introduce, by analogy, the antinormally ordered characteristic function $\chi_A(\xi)$ as the expectation value

$$\chi_A(\xi) = \text{Tr}(\rho D(\xi, -1)) = \text{Tr}(\rho e^{-\xi^* a} e^{\xi a^\dagger}). \quad (2.57)$$

The connection between the characteristic functions $\chi_N(\xi)$, $\chi(\xi)$ and $\chi_A(\xi)$ is then given by

$$\chi_N(\xi) = e^{|\xi|^2/2} \chi(\xi) = e^{|\xi|^2} \chi_A(\xi). \quad (2.58)$$

From the last relationship we obtain a boundary condition for the antinormally ordered characteristic function $|\chi_A(\xi)| \leq e^{-|\xi|^2/2}$. Consequently, it is bounded and possesses a Fourier transform so that

$$\chi_A(\xi) = \frac{1}{\pi} \int d^2\alpha \langle \alpha | \rho | \alpha \rangle e^{-(\alpha \xi^* - \alpha^* \xi)}. \quad (2.59)$$

The inverse transform gives the Q function as the following integral

$$\langle \alpha | \rho | \alpha \rangle = \frac{1}{\pi} \int d^2\xi \chi_A(\xi) e^{\alpha \xi^* - \alpha^* \xi}. \quad (2.60)$$

Chapter 3

Models in Cavity QED

Article by Purcell [6] can be apparently considered as the first proposal in the field which nowadays regarded as cavity quantum electrodynamics (CQED). In that work, it was suggested a possibility to increase the spontaneous emission rate of an atomic radio-frequency transition, when compared with the free space rate, by coupling an atom on resonance to an electric circuit. Later, a rigorous CQED calculation considering the force between an atom and a conducting plate was made by Casimir and Polder [7]. A numerous number of theoretical papers concerning the emission rates and levels shifts of atoms in the presence of conductors followed.

When an excited atom couples to the electromagnetic field in presence of a conducting structure (hereafter we regard this structure as a cavity), the free-space field modes distribution is modified by the cavity. In this case one can distinguish two possibilities. The spontaneous decay of excited state probability can be either exponential, as in free space, or oscillatory. However, both processes have rates different from the free-space case. The oscillatory case takes place when an atom interacts with a high-Q cavity, whereas the exponential case deals with low-Q cavities. Until recently the high-Q situation was not experimentally feasible. Nevertheless, demonstrations of modified radiation rates were done in the case of low-Q cavities in [8] (in the microwave domain) and [9] (for the visible domain).

Discovery of microwave high-Q cavities has opened an avenue for studies of single atom-cavity resonant interaction which allowed later to develop an one-atom maser, or micromaser [10, 11]. The micromaser became a fundamental model in CQED and allows one to prepare nonclassical field states, such as Fock states [12, 13], to test the complementarity in quantum mechanics [14] and the quantum information processing [15, 16, 17]. In the optical domain high-Q regime has been recently achieved [18] what gave a rise to a development of single photon sources [19] as well as a development of a one-atom laser [20]. Even more fascinating perspectives for building a quantum networks [21] aimed at quantum information storage and processing are opened by a possibility to trap a single atom with the help of a cavity field [22, 23].

In this chapter a basic model of an atom-cavity interaction is introduced and the effects of an external driving field are studied. The theoretical model of the micromaser

and its generalization to a strong-external-driving case are considered. Apart from the micromaser we introduce a soluble model of a one-atom laser and exploit it for an observation of the decoherence of the cavity field.

3.1 Jaynes-Cummings model

Jaynes-Cummings model [24, 25] deals with a case when a single mode of a quantized electromagnetic field couples to a two-level system. In this section, as well as in the next one, we confine our attention to unitary processes in such systems, leaving more general cases, which include the nonunitary dissipation effects due to an interaction with an environment, to the last three sections of this chapter. Any two relevant electronic states of an atom can be considered as a physical realization of such a system. To start with we will consider a semiclassical problem in which an atom consisted out of one electron interacts with a classical electromagnetic field. This interaction can be described by a minimal-coupling Hamiltonian [26]

$$\mathcal{H} = \frac{1}{2m}(\vec{p} - e\vec{A}(\vec{r}, t))^2 + e\Phi(\vec{r}, t) + V(r), \quad (3.1)$$

where \vec{p} is a canonical momentum operator, $\vec{A}(\vec{r}, t)$ and $\Phi(\vec{r}, t)$ are vector and scalar potentials of the external field and $V(r)$ is an electrostatic atomic binding potential. The Hamiltonian (3.1) can be derived from the principles of a gauge invariance and in what follows we will use a gauge in which $\Phi(\vec{r}, t) = 0$ and $\nabla \cdot \vec{A}(\vec{r}, t) = 0$. Let us consider a situation when the electron is bound by the potential of a nucleus located at \vec{r}_0 . The entire atom will experience an action from the plane electromagnetic wave described by the vector potential $\vec{A}(\vec{r} + \vec{r}_0, t)$ which can be further expanded in a series

$$\begin{aligned} \vec{A}(\vec{r} + \vec{r}_0, t) &= \vec{A}(t) \exp(i\vec{k} \cdot \vec{r}_0)(1 + i\vec{k} \cdot \vec{r} + \dots) \\ &\approx \vec{A}(t) \exp(i\vec{k} \cdot \vec{r}_0) = \vec{A}(\vec{r}_0, t) \end{aligned} \quad (3.2)$$

Where in the last equation (3.2) the dipole approximation has been applied i.e. we assume that $\vec{k} \cdot \vec{r} \ll 1$ and the only non-vanishing contribution is of the zeroth order. This supposition allows us further simplification of the Hamiltonian (3.1) so that it can be rewritten as

$$\mathcal{H} = \mathcal{H}_0 + \mathcal{H}_{int}, \quad (3.3)$$

with

$$\mathcal{H}_0 = \frac{p^2}{2m} + V(r) \quad (3.4)$$

$$\mathcal{H}_{int} = -e\vec{r} \cdot \vec{E}(\vec{r}_0, t) \quad (3.5)$$

here we change the field description from the vector potential $\vec{A}(\vec{r}, t)$ to an electric field vector $\vec{E}(\vec{r}, t)$ using $\vec{E} = -\frac{\partial \vec{A}}{\partial t}$. Hamiltonian (3.4) describes an unperturbed atom

considered as a quantum system whereas Hamiltonian (3.5) governs an interaction between the atom and the classical electromagnetic field.

The next step is to replace the classical field by its quantum counterpart assuming, however, that the coupling between the atom and quantum field remains unchanged and therefore can be expressed in terms of the Hamiltonian (3.5). In this case the complete Hamiltonian of the interacting quantum atom and field reads

$$\mathcal{H} = \mathcal{H}_a + \mathcal{H}_f + \mathcal{H}_{int}, \quad (3.6)$$

here \mathcal{H}_a and \mathcal{H}_f are Hamiltonians of the free atom and the free electromagnetic field correspondingly and \mathcal{H}_{int} is the interaction Hamiltonian given by (3.5). Since we are dealing now with the quantized field, it is convenient to present its free Hamiltonian \mathcal{H}_f in terms of creation(annihilation) operators of a photon $a_{\mathbf{k}}^\dagger(a_{\mathbf{k}})$ in the \mathbf{k} -th mode of the field as

$$\mathcal{H}_f = \sum_{\mathbf{k}} \hbar\omega_{\mathbf{k}}(a_{\mathbf{k}}^\dagger a_{\mathbf{k}} + \frac{1}{2}). \quad (3.7)$$

Operators $a_{\mathbf{k}}^\dagger$ and $a_{\mathbf{k}}$ obey the following permutation relations

$$[a_{\mathbf{k}}, a_{\mathbf{k}'}] = 0; [a_{\mathbf{k}}^\dagger, a_{\mathbf{k}'}^\dagger] = 0; [a_{\mathbf{k}}, a_{\mathbf{k}'}^\dagger] = \delta_{\mathbf{k}\mathbf{k}'} \quad (3.8)$$

and act on the infinitely dimensional Hilbert space consisted of the Fock states of a harmonic oscillator $|n_1, \dots, n_k\rangle, n_i = \overline{0, \infty}, i = \overline{1, k}$ so that

$$a_i |n_1, \dots, n_i, \dots, n_k\rangle = \sqrt{n_i} |n_1, \dots, n_i - 1, \dots, n_k\rangle, \quad (3.9)$$

$$a_i^\dagger |n_1, \dots, n_i, \dots, n_k\rangle = \sqrt{n_i + 1} |n_1, \dots, n_i + 1, \dots, n_k\rangle. \quad (3.10)$$

The electric field operator appearing in the interaction Hamiltonian (3.5) is evaluated in the dipole approximation at the position of the point atom and in the terms of $a_{\mathbf{k}}^\dagger$ and $a_{\mathbf{k}}$ reads

$$\vec{E} = \sum_{\mathbf{k}} \vec{\epsilon}_{\mathbf{k}} \mathcal{E}_{\mathbf{k}} (a_{\mathbf{k}}^\dagger + a_{\mathbf{k}}), \quad (3.11)$$

where $\mathcal{E}_{\mathbf{k}} = \sqrt{\hbar\omega_{\mathbf{k}}/2\epsilon_0 V}$, $\vec{\epsilon}_{\mathbf{k}}$ - polarization vector and V is a quantization volume. We suppose now that the atom has discrete energy level structure i.e. $\mathcal{H}_a|i\rangle = E_i|i\rangle$ where $|i\rangle$ is a complete set of atomic energy eigenstates. In other words the relation $\sum_i |i\rangle\langle i| = \mathbb{1}$ is fulfilled. Hence the free atomic Hamiltonian in terms of its eigenstates reads

$$\mathcal{H}_a = \sum_{i,j} |i\rangle\langle i| \mathcal{H}_a |j\rangle\langle j| = \sum_i E_i |i\rangle\langle i|, \quad (3.12)$$

and a dipole operator $e\vec{r}$ can be rewritten in the same manner i.e.

$$e\vec{r} = e \sum_{i,j} |i\rangle\langle i| \vec{r} |j\rangle\langle j| = \sum_{i,j} \Omega_{ij} \sigma_{ij}, \quad (3.13)$$

where $\Omega_{ij} = \langle i | \vec{r} | j \rangle$ are the matrix elements of the electric dipole operator and we have introduced the atomic transition operators $\sigma_{ij} = |i\rangle\langle j|$. With the help of equations (3.11) and (3.13) we obtain that the interaction between the atom with a discrete level structure and quantized field, deduced from the equation (3.5), is given by the interaction Hamiltonian

$$\mathcal{H}_{int} = \hbar \sum_{i,j} \sum_{\mathbf{k}} g_{\mathbf{k}}^{ij} \sigma_{ij} (a_{\mathbf{k}}^{\dagger} + a_{\mathbf{k}}), \quad (3.14)$$

with coupling coefficients $g_{\mathbf{k}}^{ij} = -\Omega_{ij} \vec{\epsilon}_{\mathbf{k}} \mathcal{E}_{\mathbf{k}} / \hbar$. Combining equations (3.7), (3.12) and (3.14) together we arrive finally at the explicit formulation of the Hamiltonian (3.6)

$$\mathcal{H} = \sum_i E_i \sigma_{ii} + \sum_{\mathbf{k}} \hbar \omega_{\mathbf{k}} a_{\mathbf{k}}^{\dagger} a_{\mathbf{k}} + \hbar \sum_{i,j} \sum_{\mathbf{k}} g_{\mathbf{k}}^{ij} \sigma_{ij} (a_{\mathbf{k}}^{\dagger} + a_{\mathbf{k}}), \quad (3.15)$$

Although we have already made the dipole approximation (3.2) our consideration till now has been pretty general and has allowed us to derive the Hamiltonian (3.15) which describes the coupling of the many-level atom with the quantized electromagnetic field. This, however, cannot serve as a model of a matter-light interaction due to the following reason. Introducing a model one wants to describe some complex physical phenomenon in terms of a relatively simple concept which could give a quantitative estimation to a real physical process. Unfortunately, the Hamiltonian (3.15) in its present form is non diagonalizable and, therefore, is a bad candidate to model the matter-light interaction. In order to simplify our consideration we assume that the level structure of the atom coupled to the quantized field consists only of two relevant levels. Let us call them $|g\rangle$ for the lower energy state and $|e\rangle$ for the higher one. Consequently, the first and the second terms in the Hamiltonian (3.15) can be modified using the following notations

$$\begin{aligned} \mathcal{H}_a &= E_e \sigma_{ee} + E_g \sigma_{gg} = \frac{1}{2} \hbar \omega \sigma_z, \\ \sigma_z &= \sigma_{ee} - \sigma_{gg} = |e\rangle\langle e| - |g\rangle\langle g|, \\ \sigma_+ &= \sigma_{eg} = |e\rangle\langle g|, \\ \sigma_- &= \sigma_{ge} = |g\rangle\langle e|, \end{aligned} \quad (3.16)$$

where we have defined the ground and excited states energies as $E_g = -(1/2)\hbar\omega$ and $E_e = (1/2)\hbar\omega$, with ω - $|g\rangle \rightarrow |e\rangle$ transition frequency. So that the Hamiltonian (3.15) for the case of a two-level atom reads

$$\mathcal{H} = \frac{1}{2} \hbar \omega \sigma_z + \sum_{\mathbf{k}} \hbar \omega_{\mathbf{k}} a_{\mathbf{k}}^{\dagger} a_{\mathbf{k}} + \hbar \sum_{\mathbf{k}} g_{\mathbf{k}} (\sigma_+ + \sigma_-) (a_{\mathbf{k}}^{\dagger} + a_{\mathbf{k}}), \quad (3.17)$$

here we have put $g_{\mathbf{k}}^{eg} = g_{\mathbf{k}}^{ge} = g_{\mathbf{k}}$ for the sake of simplicity. We should notice here that the operators σ_z , σ_+ and σ_- obey the spin-1/2 algebra of the Pauli matrices i.e.,

$$[\sigma_+, \sigma_-] = \sigma_z, [\sigma_{\pm}, \sigma_z] = \mp 2\sigma_{\pm}, \quad (3.18)$$

and therefore the two-level atom model is equivalent to the model of a spin-1/2 particle. The Hamiltonian (3.17) could be further reduced if we select a particular mode, with the given polarization, from a set of the field modes. In other words, we are interested in the interaction between the selected field mode and the two-level atom. Physically, such a selection, can be performed by using a resonator which cuts the modes which are not relevant to our consideration in order to reduce drastically a coupling of the atom to the other left modes of resonator by selecting a proper polarization of the mode of interest so as to at the end the only relevant contribution to the third term in (3.17) is given by the $g_{\mathbf{k}_0} = g$. Finally, we obtain that the dynamics of the interaction of the two-level atom with the single mode of the quantized field is governed by the following Hamilton operator

$$\mathcal{H} = \frac{1}{2}\hbar\omega\sigma_z + \hbar\omega_f a^\dagger a + \hbar g(\sigma_+ + \sigma_-)(a^\dagger + a). \quad (3.19)$$

The third term in the Hamiltonian (3.19) responds for the atom-field interaction and consists of four terms $\sigma_+ a^\dagger$, $\sigma_- a^\dagger$, $\sigma_+ a$ and $\sigma_- a$. Atomic operators σ_- and σ_+ has a transparent physical meaning, namely, σ_- operator takes an atom in the upper state into the lower state whereas σ_+ does the opposite. Consequently $\sigma_+ a^\dagger$ atom-field operator takes an atom into the upper state and creates a photon in a field mode, on the contrary the operator $\sigma_- a$ takes an atom into the lower state and destroys a photon. The both processes lead to a generation(destruction) of two quanta of energy and therefore are nonconservative. The other pair of operators $\sigma_- a^\dagger$ and $\sigma_+ a$ conserves a number of quanta in the closed atom-field system and induce an oscillatory exchange of an energy quanta between the atom and the field. Dropping the energy nonconservative terms in the Hamiltonian (3.19) corresponds to the rotating-wave approximation(RWA). The other way to justify an applicability of the RWA is to look at the oscillation frequencies of the conservative and nonconservative terms. Indeed, for conservative terms they are proportional to $|\omega_f - \omega|$ whereas for nonconservative ones they are $|\omega_f + \omega|$. If the detuning between an atomic transition frequency and a frequency of the field is small than we immediately conclude that the nonconservative terms oscillate much faster(especially in a high-frequency domain) when compared to the conservative ones and hence their contribution to the dynamics is negligible. Nevertheless, that is not always the case and there are certain situations when the RWA fails. However, in what follows, we suppose that the RWA takes place. Applying the RWA to the Hamiltonian (3.19) we obtain

$$\mathcal{H}_{J.-C.} = \frac{1}{2}\hbar\omega\sigma_z + \hbar\omega_f a^\dagger a + \hbar g(\sigma_+ a + \sigma_- a^\dagger). \quad (3.20)$$

The Hamiltonian (3.20) is called Jaynes-Cummings Hamiltonian [24] and is the central point of this section. It is an essential point of the Jaynes-Cummings model which one can briefly summarize as follows:

- It is a fully quantum model which describes an interaction between a two-level atom and a single mode of a quantized electromagnetic field by means of the Hamiltonian (3.20).

- It is based on two approximations, namely, the dipole approximation and the rotating-wave approximation.

Having at our disposal the Jaynes-Cummings Hamiltonian (3.20) we can start to address the quantitative questions of an atom-field evolution. For the sake of simplicity we will consider a case in which an atom couples resonantly to a single mode of a cavity i.e. $\omega_f = \omega$. We pass in the Hamiltonian (3.20) to the interaction picture what leads to the following Hamilton operator

$$\mathcal{W} = e^{(i/\hbar)\mathcal{H}_0 t} \hbar g (\sigma_+ a + \sigma_- a^\dagger) e^{-(i/\hbar)\mathcal{H}_0 t}, \quad (3.21)$$

where $\mathcal{H}_0 = \frac{1}{2}\hbar\omega\sigma_z + \hbar\omega_f a^\dagger a$ is the free Hamiltonian of an atom and a field. After some algebra we deduce that the Jaynes-Cummings Hamiltonian in the interaction picture reads

$$\mathcal{W} = \hbar g (\sigma_+ a + \sigma_- a^\dagger). \quad (3.22)$$

Calculating the unitary time-evolution operator $U(t)$ for the Hamiltonian (3.22) we arrive at

$$\begin{aligned} U(t) &= e^{-(i/\hbar)\mathcal{W}t} \\ &= \cos(gt\sqrt{a^\dagger a + 1})|e\rangle\langle e| + \cos(gt\sqrt{a^\dagger a})|g\rangle\langle g| \\ &\quad - i\frac{\sin(gt\sqrt{a^\dagger a + 1})}{\sqrt{a^\dagger a + 1}}a|e\rangle\langle g| - i\frac{\sin(gt\sqrt{a^\dagger a})}{\sqrt{a^\dagger a}}a^\dagger|g\rangle\langle e|. \end{aligned} \quad (3.23)$$

Assume that initially we have an atom prepared in the upper state $|e\rangle\langle e|$ and a field is in the $\rho_f(0) = \sum_{n,m=0}^{\infty} \rho_{n,m}(0)|n\rangle\langle m|$ than the probability to detect the atom, undergoing an interaction with the field via the interaction Hamiltonian (3.22), in the lower state $|g\rangle\langle g|$ after time t is given by

$$\begin{aligned} P_g(t) &= \text{Tr}\{U^\dagger(t)|e\rangle\langle e| \otimes \rho_f(0)U(t)|g\rangle\langle g|\} \\ &= \sum_{n=0}^{\infty} \rho_{nn}(0) \sin^2(gt\sqrt{n+1}). \end{aligned} \quad (3.24)$$

In the same manner one can derive an expression for the probability to detect the initially excited atom in the excited state again

$$\begin{aligned} P_e(t) &= \text{Tr}\{U^\dagger(t)|e\rangle\langle e| \otimes \rho_f(0)U(t)|e\rangle\langle e|\} \\ &= \sum_{n=0}^{\infty} \rho_{nn}(0) \cos^2(gt\sqrt{n+1}). \end{aligned} \quad (3.25)$$

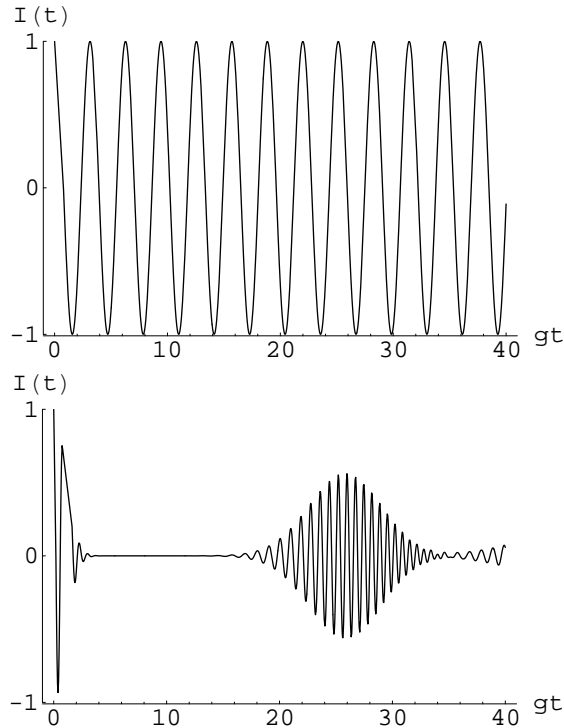


Figure 3.1: Rabi oscillation of an atomic inversion. Vacuum Rabi oscillations (top) and Rabi oscillations for an initial coherent state of a field (bottom) with $|\alpha| = 4$.

Defining the atomic population inversion as $I(t) = P_e(t) - P_g(t)$ we obtain that its time evolution reads

$$I(t) = \sum_{n=0}^{\infty} \rho_{nn}(0) \cos(2gt\sqrt{n+1}). \quad (3.26)$$

From Eq.(3.26) we immediately conclude that the time evolution of the atomic inversion strongly depends on the initial state of the field. For example, if the field was initially in the vacuum i.e. $\rho_f(0) = |0\rangle\langle 0|$ than the only contribution to the sum in the equation (3.26) is for $n = 0$ with $\rho_{00} = 1$ so that $I(t) = \cos(2gt)$. In other words, for such initial conditions, the atomic population inversion exhibits so-called vacuum Rabi oscillations fig.(3.1), where $\Omega_0 = gt$ is frequently regarded as the vacuum Rabi frequency. These oscillations are the direct consequence of the Jaynes-Cummings interaction (3.22) which conserves the number of excitation quanta in the entire atom-field system and allows an oscillatory exchange of them. If the entire system is closed then these oscillations can last infinitely long. Another interesting behaviour of the atomic inversion can be seen when the field is initially prepared in a coherent state $|\alpha\rangle$. In this case $\rho_{nn}(0) = (|\alpha|^{2n}/n!)e^{-|\alpha|^2}$ and for large values of α atomic inversion suffers the collapses and revivals fig.(3.1). This phenomenon can also be understood from Eq.(3.26). Each term in the summation oscillates with its own Rabi frequency depending on a value of n . Thus, an initial packet, in the course of time, becomes uncorrelated leading to a collapse of inversion. Further time evolution restores the correlation and leads to

a revival of inversion. This process continues and an infinite sequence of collapses and revivals follows.

3.2 Jaynes-Cummings model in the presence of a strong classical field

Vacuum Rabi oscillations and collapses and revivals of atomic inversion are direct consequences of the Jaynes-Cummings atom-field evolution (3.23) enlightening the pure quantum nature of atom-field interaction. In this section we analyze an influence of external classical field on the Jaynes-Cummings dynamics studied in the previous section.

The model considered in this section consists of a two-level atom interacting with a single mode of electromagnetic field via the resonant Jaynes-Cummings interaction (3.20) in the presence of a strong classical driving field [27, 28]. We assume that the classical driving field couples only to the atom and a cavity-driving-field interaction is negligible. Practically, this can be achieved by applying a driving field which is transversal with respect to the cavity field. Coupling of a two-level atom to a classical field can be described in terms of the Hamiltonian (3.5) and leads to

$$\mathcal{H}' = \hbar\Omega(e^{i\omega_L t}\sigma_+ + e^{-i\omega_L t}\sigma_-), \quad (3.27)$$

where ω_L is a frequency of the driving field, Ω is a coupling constant of the atom-driving-field interaction and σ_+ , σ_- are the atomic transition operators defined in Eq.(3.16). Hence, combining the Hamilton operators (3.20) and (3.27) together we arrive at a Hamilton operator for our model, that is

$$\mathcal{H} = \frac{1}{2}\hbar\omega\sigma_z + \hbar\omega a^\dagger a + \hbar g(\sigma_+ a + \sigma_- a^\dagger) + \hbar\Omega(e^{i\omega_L t}\sigma_+ + e^{-i\omega_L t}\sigma_-), \quad (3.28)$$

likewise in the preceding section, here a and a^\dagger are annihilation and creation operators of the quantized cavity field. For the sake of simplicity we set $\omega_L = \omega$ hereafter and proceed to transform the Hamiltonian (3.28) into a frame rotating with the external field frequency ω_L so that the result of the transformation reads

$$\begin{aligned} \mathcal{H}_1 &= e^{i\omega_L t(\sigma_z + a^\dagger a)} \{ \hbar g(\sigma_+ a + \sigma_- a^\dagger) + \hbar\Omega(e^{i\omega_L t}\sigma_+ + e^{-i\omega_L t}\sigma_-) \} e^{-i\omega_L t(\sigma_z + a^\dagger a)} \\ &= \hbar g(\sigma_+ a + \sigma_- a^\dagger) + \hbar\Omega(\sigma_+ + \sigma_-). \end{aligned} \quad (3.29)$$

Finally, passing in the Hamiltonian \mathcal{H}_1 into the interaction picture with respect to $\hbar\Omega(\sigma_+ + \sigma_-)$ we arrive at the following expression

$$\begin{aligned} \mathcal{H}_2 &= e^{i\Omega t(\sigma_+ + \sigma_-)} \hbar g(\sigma_+ a + \sigma_- a^\dagger) e^{-i\Omega t(\sigma_+ + \sigma_-)} \\ &= \frac{\hbar g}{2} (|+\rangle\langle +| - |-\rangle\langle -| + e^{2i\Omega t}|+\rangle\langle -| - e^{2i\Omega t}|-\rangle\langle +|) a + h.c., \end{aligned} \quad (3.30)$$

3.2 Jaynes-Cummings model in the presence of a strong classical field 29

here we have introduced the so-call dressed states $|\pm\rangle = (|g\rangle \pm |e\rangle)/\sqrt{2}$ - eigenstates of a $\sigma_x = \sigma_+ + \sigma_-$ operator with eigenvalues ± 1 respectively. We notice immediately that the model Hamiltonian (3.28), in contrast to the pure Jaynes-Cummings model Hamiltonian (3.22), has an explicit time dependence in the interaction picture. However, in the limiting situation when the atom-driving-field interaction goes to zero i.e. when $\Omega \rightarrow 0$ we recover in the Hamiltonian (3.30) the time independent Jaynes-Cummings Hamiltonian (3.22). In order to avoid any explicit time dependence in the Hamiltonian (3.30) for non-zero values of Ω we can suppose that a coupling strength of the atom-driving field interaction - Ω is much larger than the one of the atom-cavity - g . In this case, terms which contain the time explicitly i.e. $e^{2i\Omega t}|-\rangle\langle+|$, $e^{-2i\Omega t}|+\rangle\langle-|$ and hermitian conjugated oscillate with much higher frequency when compared with the rest and therefore the RWA can be applied and time dependent terms in (3.30) omitted. So that the Hamiltonian (3.30) after the RWA reads

$$\begin{aligned}\mathcal{H}'_2 &= \frac{\hbar g}{2}(|+\rangle\langle+| - |-\rangle\langle-|)(a + a^\dagger) \\ &= \frac{\hbar g}{2}(\sigma_- + \sigma_+)(a + a^\dagger) = \frac{\hbar g}{2}\sigma_x(a + a^\dagger).\end{aligned}\quad (3.31)$$

Hamiltonian (3.31) is an *interaction picture expression* for the starting model Hamiltonian (3.28) and combines simultaneously both Jaynes-Cummings term $\sigma_- a^\dagger + \sigma_+ a$ and anti-Jaynes-Cummings term $\sigma_- a + \sigma_+ a^\dagger$. Therefore it does not conserve a number of excitations in an atom-cavity-field system. This can be explained by a presence of an external field which is an additional source of energy when compared to the standard Jaynes-Cummings model. Hence the external driving preserves the energy nonconservative terms which in the standard Jaynes-Cummings model are neglected due to the RWA and leads to the Hamiltonian (3.31) instead of one given by equation (3.22).

Corresponding unitary atom-cavity-external-driving dynamics in the limit of strong driving field ($\Omega \gg g$) is given by

$$\begin{aligned}U(t) &= e^{-(i/\hbar)\mathcal{H}'_2 t} \\ &= e^{-(igt/2)(a+a^\dagger)}|+\rangle\langle+| + e^{(igt/2)(a+a^\dagger)}|-\rangle\langle-| \\ &= D(\xi)|+\rangle\langle+| + D(-\xi)|-\rangle\langle-|,\end{aligned}\quad (3.32)$$

where $D(\xi) = e^{\xi a^\dagger - \xi^* a}$ is a displacement operator acting on a cavity field, $\xi = -igt/2$ is a displacement parameter and we have used a completeness property of the eigenstates of σ_x operator i.e. $|+\rangle\langle+| + |-\rangle\langle-| = \mathbb{1}$. We remember that $D(\alpha)$ is unitary operator and its action on a vacuum state of a field leads to a displacement of the field into the coherent state $|\alpha\rangle$. In other words, $D(\pm\alpha)|0\rangle = |\pm\alpha\rangle$.

Suppose that an atom was initially prepared in the lower state $|g\rangle$ and a cavity field in vacuum $|0\rangle$, so that the initial atom-field state is $|\psi_{in}\rangle = |g\rangle \otimes |0\rangle$. When the initial state $|\psi_{in}\rangle$ is subjected to the unitary evolution (3.32) it transforms with the course of

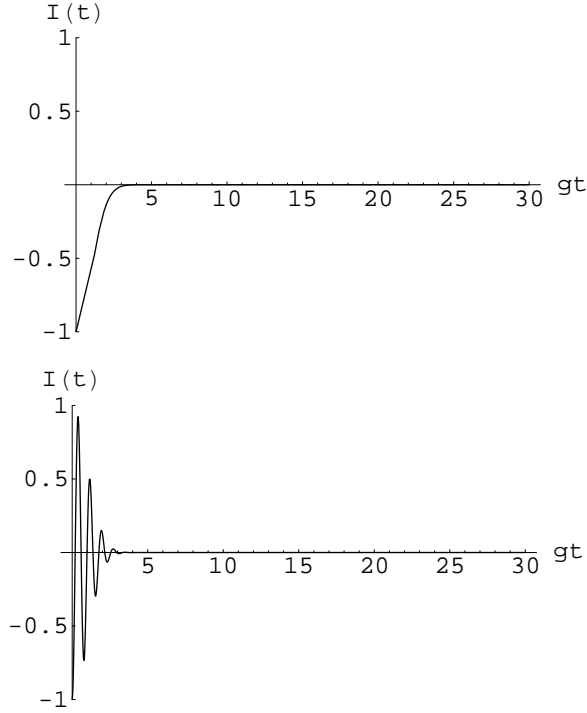


Figure 3.2: Atomic inversion as a function of time in the case of a two-level atom interacting with a cavity mode and strong external field for the vacuum initial state of the cavity (top) and coherent initial state $|\alpha| = 4$ (bottom).

time into the following atom-field state

$$|\psi(t)\rangle = U(t)|\psi_{in}\rangle = \frac{1}{\sqrt{2}}(|\xi\rangle|+\rangle + |-\xi\rangle|-\rangle), \quad (3.33)$$

that is, into the atom-field entangled state which is frequently regarded as the Schrödinger cat state. Thus, an external driving leads to the interaction which generates mesoscopic-microscopic superposition states of the form (3.33) in a fast resonant manner as compared with the conventional methods based on an atom-field dispersive interaction [29]. Such a behaviour differs noticeably from those we have noticed while we have been considering the Jaynes-Cummings model. Indeed, an external driving cancels the familiar concept of the oscillatory energy exchange between an atom and cavity field inherent in the Jaynes-Cummings model and provides us with logic of atomic state dependent displacements of cavity field. In order to illustrate this, we compute a time dependence of atomic population inversion for a case of the initial atom-field state $\rho_{in} = |g\rangle\langle g| \otimes |0\rangle\langle 0|$. According to Eq.(3.26) atomic inversion reads

$$\begin{aligned} I(t) &= \text{Tr}\{U^\dagger(t)|g\rangle\langle g| \otimes |0\rangle\langle 0|U(t)(|e\rangle\langle e| - |g\rangle\langle g|)\} \\ &= -\text{Re}\{\text{Tr}\{|0\rangle\langle 0|D(2\xi)\}\} = -e^{-|2\xi|^2/2} = -e^{-(gt)^2/2}. \end{aligned} \quad (3.34)$$

It follows immediately from Eq.(3.34) that in contrast to the vacuum Rabi oscillations

in the case of the Jaynes-Cummings model presence of external field leads to an exponential decay of initial atomic inversion to the zero value fig.(3.2) i.e. starting from any initial distribution of the upper and lower atomic states populations we always arrive at a final distribution with the population of the both atomic states equal to $\frac{1}{2}$.

In the same manner, if a cavity field was prepared initially in the coherent state $|\alpha\rangle$ and an atom in the lower state $|g\rangle$ we obtain that the time evolution of the atomic inversion reads

$$\begin{aligned} I(t) &= \text{Tr}\{U^\dagger(t)|g\rangle\langle g| \otimes |\alpha\rangle\langle\alpha|U(t)(|e\rangle\langle e| - |g\rangle\langle g|)\} \\ &= -\text{Re}\{\text{Tr}\{|\alpha\rangle\langle\alpha|D(2\xi)\}\} \\ &= -\cos(2\text{Im}\{2\xi\alpha^*\})e^{-|2\xi|^2/2} = -\cos(2gt\text{Re}\{\alpha\})e^{-(gt)^2/2}. \end{aligned} \quad (3.35)$$

Hence we notice in Eq.(3.35) an explicit exponential factor which leads to a decay of the atomic inversion to zero despite an oscillatory behaviour due to the initial coherent state fig.(3.2). Such a dynamics of atomic inversion is opposite to the collapses and revivals of the Jaynes-Cummings model and emphasizes a striving of external driving to populate equally both upper and lower states.

3.3 Micromaser

Enormous progress in fabrication of high-Q superconductive microwave resonators in the last decades has allowed to study experimentally an interaction of a single cavity mode with a two-level atom considered theoretically in the section 3.1. Experimental realization of a single-atom maser or a micromaser [10, 11, 30] - a device in which a single mode of a cavity field interacts with a stream of two-level atoms in such a way that only one atom is inside the cavity at any time - has improved our understanding of light-matter interaction. The micromaser experimental setup can be schematically presented consisting of three main parts:

1. *Atomic beam preparation stage.* Here a collimated beam of neutral alkaline atoms coming from an oven are subjected to a velocity selection, in order to have all atoms with the same atom-cavity interaction time, and are excited to the upper level of the atomic masing transition. Practically, this masing transition is selected to be between two highly-excited Rydberg states of an atom. The reasons to choose the Rydberg states are the following:
 - Rydberg states are atomic states with big principal quantum numbers($n > 50$) and transitions between them are in the convenient microwave range where the ultrahigh-Q resonators are available.
 - Atoms in the Rydberg states are atoms with one highly excited electron and therefore they possess an enormous dipole moment which leads to the very strong interaction with a cavity field, so that the masing transition is saturated with only one photon.

- Rydberg states are extremely resistant to the spontaneous emission. As a consequence, spontaneous emission has no relevant influence for micromaser since an operation time is smaller than the Rydberg levels lifetime.
2. *Atom-field interaction region.* Here an atom, passed through the preparation stage, enters a high-Q microwave cavity¹ and undergoes the resonant Jaynes-Cummings interaction with a single mode of the cavity for time τ . The interaction time τ is a well controlled parameter and can be varied in a wide range of values by changing the atomic velocity. Since the atom was initially prepared in the upper level of a masing transition, it can deposit a quantum of excitation in the cavity mode and leave the cavity in the lower state as the conservation law requires. The next atom enters the cavity again in the excited state and can leave one more excitation quantum in it. Thus the cavity field can be built up as a tradeoff between atomic pumping process and dissipation of the cavity field due to the finite quality of the resonator.
 3. *Detection of atomic states.* Here a level statistics of atom, left the cavity is measured by means of the state-selective detection. This, of course, is a projective measurement, since we determine in which state the atom has left the cavity and therefore projects the cavity field state as well. Such a procedure destroys a quantum interference and leads to the final mixed state of the cavity field.

In this section we discuss the theory of the micromaser, statistical properties of a micromaser field and the ways of generation of non-classical field states using the micromaser.

3.3.1 Model of the Micromaser

In order to build a theoretical model which closest fits the real micromaser experiment, we assume the following:

- *One-atom events.* The standard experimental situation, if no special manipulation with the atomic beam is made, is when all atoms are uncorrelated i.e. they arrive at random times. Therefore, the probability to have one atom interacting with a cavity at any time is $\exp(-2r\tau)$, where r is the rate at which atoms arrive and τ is the atom-cavity interaction time. Thus, for typical experimental parameters $r = 100$ and $\tau = 50\mu s$ this probability is around 99%. Hence, in what follows we can suppose that at any time there is only one atom undergoes an interaction with a cavity.
- *Leakage of the cavity field.* Since the photon lifetime in a cavity is of the order of a fraction of a second and a cavity passage time of an atom is typically less than

¹Quality factor is about 10^{10} (photon lifetime is of a fraction of a second) in the current experiments of group in Garching

$100\mu s$ we can neglect, for all practical purposes, a dissipation of a cavity field during the atom-field interaction. Indeed, we assume that the field decays only in the time interval between two successive atom-field interactions when there is no atom inside a cavity.

- *Atom-field interaction.* The coupling g between an atom and a cavity mode switches on when the atom enters the cavity and follows the sinusoidal mode profile inside the cavity. Hence the coupling $g = g(\tau)$ is a function of interaction time. However, for simplicity sake, we suppose that the atom-field coupling is constant at the average value of $\bar{g} = \frac{1}{\tau} \int_0^{\tau} dt g(t)$ during the atomic transit through a cavity.

Taking into account the assumptions introduced above we are ready to formulate the model of micromaser [31, 32]:

Micromaser is a system aimed at building up a cavity field via its resonant interaction with a beam of two-levels atoms entering the cavity in the upper state. The resulting cavity field is a tradeoff between the gaining process due to the resonant Jaynes-Cummings interaction for the time τ with the coupling rate \bar{g} between an each atom from a pumping beam and a cavity and the loss process due to the coupling of the cavity mode to a thermal bath when no atom is in the cavity.

3.3.2 Dynamics of the Micromaser

Having at our disposal a qualitative description of the micromaser, given by the model introduced in preceding subsection, we would like to have now a quantitative one. For this we take into consideration that the dynamics of cavity field can be considered consisting of two terms, namely, one corresponding to the gains and another corresponding to the losses, so that the time evolution of the density operator of cavity field ρ reads

$$\frac{\partial \rho}{\partial t} = \left(\frac{\partial \rho}{\partial t}\right)_{gain} + \left(\frac{\partial \rho}{\partial t}\right)_{loss}. \quad (3.36)$$

We compute the contribution from the gains term, to start with. We employ the standard master equation approach i.e. we consider the changes of the cavity field on a coarse grain time scale. In other words this means that we ignore any changes in the field on the short time scale - the time scale of the order of the atom-field interaction time and we are interested only in changes on the time scale of several interaction times. The changes in the cavity state per atom is given by

$$\delta \rho = \rho(t_0 + \tau) - \rho(t_0), \quad (3.37)$$

Since the only source of gains in our model is the unitary resonant Jaynes-Cummings interaction we can express $\rho(t_0 + \tau)$ as

$$\rho(t_0 + \tau) = \text{Tr}_{at}\{U^\dagger(\tau)\rho_{at+f}(t_0)U(\tau)\}$$

$$\begin{aligned}
&= \cos(g\tau\sqrt{a^\dagger a + 1})\rho(t_0)\cos(g\tau\sqrt{a^\dagger a + 1}) + \\
&\quad a^\dagger \frac{\sin(g\tau\sqrt{a^\dagger a + 1})}{\sqrt{a^\dagger a + 1}}\rho(t_0)\frac{\sin(g\tau\sqrt{a^\dagger a + 1})}{\sqrt{a^\dagger a + 1}}a, \tag{3.38}
\end{aligned}$$

where the Jaynes-Cummings unitary evolution operator $U(\tau)$ is given by Eq.(3.23) and we assume that all atoms enter a cavity in the upper state so that an initial atom-field state $\rho_{at+f}(t_0) = \rho(t_0) \otimes |e\rangle\langle e|$. We have traced the atomic degrees of freedom, in order to obtain in the Eq.(3.38) an expression for the time evolution of the cavity field. Hence, the overall change of the cavity field due to the interaction with the atomic beam reads

$$\Delta\rho = r\Delta t\delta\rho = r\Delta t(\rho(t_0 + \tau) - \rho(t_0)). \tag{3.39}$$

Consequently, from the Eq.(3.39) we conclude that the gain term in the master equation Eq.(3.36) in the coarse-grain approximation can be explicitly written as follows

$$\left(\frac{\partial\rho}{\partial t}\right)_{gain} = \lim_{\Delta t \rightarrow 0} \frac{\Delta\rho}{\Delta t} = r(\mathcal{A} + \mathcal{B} - 1)\rho, \tag{3.40}$$

where τ is the atom-field interaction time, r is a number of atoms per second - beam rate, and

$$\mathcal{A}\rho = \cos(g\tau\sqrt{a^\dagger a + 1})\rho\cos(g\tau\sqrt{a^\dagger a + 1}) \tag{3.41}$$

$$\mathcal{B}\rho = a^\dagger \frac{\sin(g\tau\sqrt{a^\dagger a + 1})}{\sqrt{a^\dagger a + 1}}\rho\frac{\sin(g\tau\sqrt{a^\dagger a + 1})}{\sqrt{a^\dagger a + 1}}a. \tag{3.42}$$

Our model of micromaser dynamics assumes the losses of cavity field when no atom couples to it. In order to model a decay of cavity field we suppose that it happens due to an interaction between the single cavity mode of interest and a thermal bath consisting of infinitely many modes of the environment. This model has a standard description by means of the following master equation [33]

$$\begin{aligned}
\left(\frac{\partial\rho}{\partial t}\right)_{loss} &= \mathcal{L}\rho \\
&= -\frac{1}{2}\gamma(\bar{n}_{th} + 1)(a^\dagger a\rho - 2a\rho a^\dagger + \rho a^\dagger a) - \\
&\quad \frac{1}{2}\gamma\bar{n}_{th}(a^\dagger a\rho - 2a\rho a^\dagger + \rho a^\dagger a), \tag{3.43}
\end{aligned}$$

where γ is a cavity decay constant, $\bar{n}_{th} = (e^{\frac{\hbar\omega}{kT}} - 1)^{-1}$ is an average number of thermal photons in the cavity at the temperature T for the frequency ω .

By substituting Eq.(3.40) and Eq.(3.43) into Eq.(3.36) we arrive at the micromaser master equation

$$\frac{\partial\rho}{\partial t} = r(\mathcal{A} + \mathcal{B} - 1 + \mathcal{L})\rho. \tag{3.44}$$

Master equation Eq.(3.44) describes an open quantum driven system and can not be solved analytically for any moment of time. However, in the steady-state regime of the micromaser dynamics when the gains are equal to the losses i.e. when $\frac{\partial \rho}{\partial t} = 0$ it possesses an analytical steady-state solution. In order to show this, let us rewrite the micromaser steady-state master equation in the Fock basis

$$\begin{aligned} 0 &= \langle n | r(\mathcal{A} + \mathcal{B} - 1 + \mathcal{L}) \rho | n \rangle \\ &= r(\sin^2(g\tau\sqrt{n})\rho_{n-1n-1} - \sin^2(g\tau\sqrt{n+1})\rho_{nn}) - \\ &\quad \gamma(2\bar{n}_{th} + 1)(n\rho_{nn} - (n+1)\rho_{n+1n+1}), \end{aligned} \quad (3.45)$$

for $n = \overline{0, \infty}$. After some algebra in the Eq.(3.45) we arrive at the following recursion relations

$$\frac{r}{\gamma(2\bar{n}_{th} + 1)} \sin^2(g\tau\sqrt{n})\rho_{n-1n-1} - n\rho_{nn} = \frac{r}{\gamma(2\bar{n}_{th} + 1)} \sin^2(g\tau\sqrt{n+1})\rho_{nn} - (n+1)\rho_{n+1n+1}. \quad (3.46)$$

From the latest we immediately obtain that the steady state solution ρ_{nn}^{ss} reads

$$\rho_{nn}^{ss} = \rho_{00}^{ss} \prod_{k=1}^n \left[\frac{\bar{n}_{th}}{\bar{n}_{th} + 1} + \frac{r/\gamma}{\bar{n}_{th} + 1} \frac{\sin^2(g\tau\sqrt{k})}{k} \right], \quad (3.47)$$

where ρ_{00}^{ss} is the normalization constant and can be deduced from the normalization condition $\text{Tr}[\rho] = \sum_{n=0}^{\infty} \rho_{nn} = 1$. The steady-state solution Eq.(3.47) of the micromaser master equation Eq.(3.44) is the central result of the micromaser theory and allows one to calculate all statistical properties of the micromaser field. For example, the mean photon number of the steady-state micromaser field is given by

$$\langle n \rangle = \langle a^\dagger a \rangle = \text{Tr}[\rho^{ss} a^\dagger a] = \sum_{k=0}^{\infty} k \rho_{kk}^{ss}. \quad (3.48)$$

As it is depicted on fig.(3.3) the values of $\langle n \rangle$ vary strongly in the interval from several till hundreds of photons depending on the micromaser operating parameters $N_{ex} = \frac{r}{\gamma}$ and so-called ‘‘pump parameter’’ $\theta = g\tau\sqrt{r/\gamma}$ opening an avenue for a generation of the field states on demand. The next statistical parameter, which shows how close(far) is the given field state to a correspondent ‘‘classical’’ state, is the Fano-Mandel Q parameter defined as

$$Q = \frac{\langle (a^\dagger a)^2 \rangle - \langle a^\dagger a \rangle^2}{\langle a^\dagger a \rangle} = \frac{\langle n^2 \rangle - \langle n \rangle^2}{\langle n \rangle}. \quad (3.49)$$

In other words, the Fano-Mandel Q parameter shows how much differs the given field state from a state obeying the Poissonian field statistics i.e. the state for which $\langle n \rangle^2 - \langle n^2 \rangle = \langle n \rangle$ and $Q = 1$ respectively. For instance, the coherent state

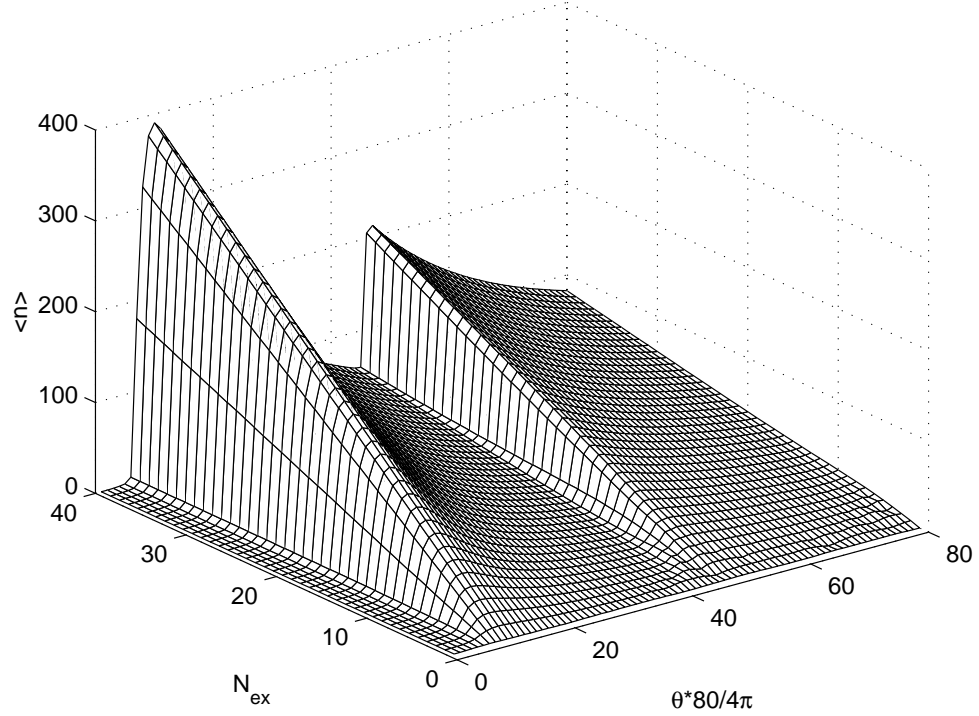


Figure 3.3: Steady-state mean photon number of the micromaser field as a function of θ and N_{ex} for the mean thermal photon number $\bar{n}_{th} = 0.01$.

$|\alpha\rangle$ satisfies the Poissonian statistics and is the “classical” quantum state. States for which $Q < 1$ ($Q > 1$) are frequently regarded as the states with sub-Poissonian (super-Poissonian) statistics and called “nonclassical” (“classical”) states of radiation field. Typical example of the “nonclassical” states are Fock states, whereas a thermal field state is called “classical”. It follows from the fig.(3.4) that the micromaser field, depending on the operating parameters, can exhibit both sub-Poissonian and super-Poissonian behaviour and therefore the micromaser is an ideal generating device of the nonclassical field states.

3.4 Strongly-driven micromaser

In this section we discuss a theory of a micromaser where the pumping atoms are strongly driven by a resonant classical field during their transit through the cavity mode. We formulate a master equation for the cavity field density operator of this strongly-driven micromaser (SDM [34]), where the gain originates in the coherent interaction of the field with two-level atoms which are strongly driven by an external driving while they are inside the cavity [27]. The losses in the master equation stem from the interaction of the cavity field with a thermal bath. The additional strong driving acting on the atoms changes drastically the SDM dynamics as compared with the conventional micromaser.

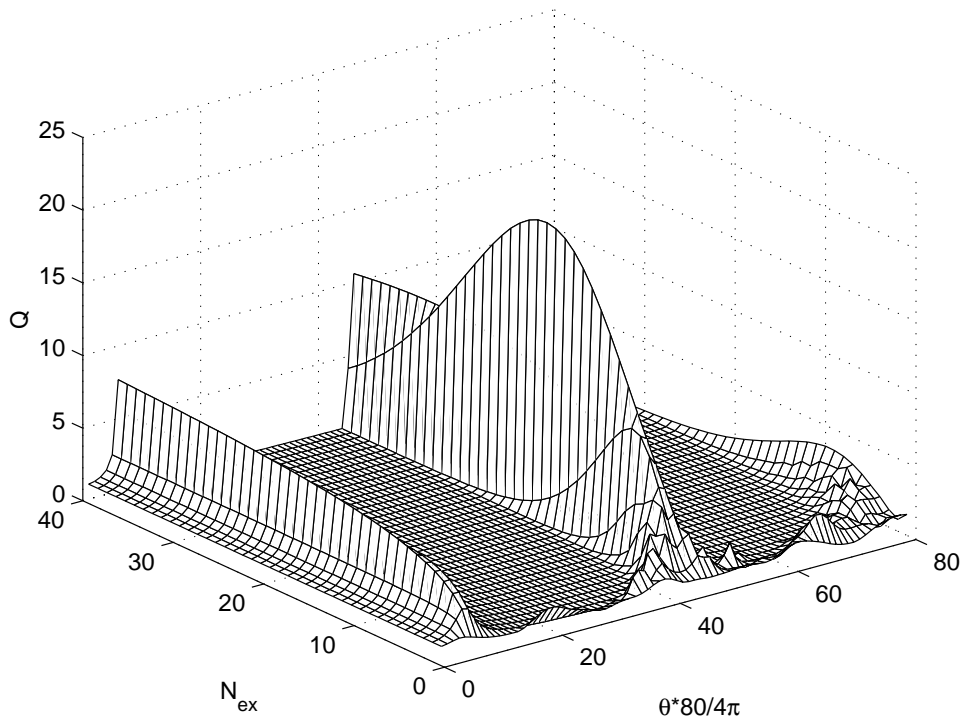


Figure 3.4: Fano-Mandel Q parameter of the stationary micromaser field as a function of θ and N_{ex} for the mean thermal photon number $\bar{n}_{th} = 0.01$.

We show that the SDM master equation can be solved analytically by means of phase-space methods, providing an unusual integrable model of an open quantum system under realistic conditions. In this way we are able to trace the temporal evolution of the SDM field from an arbitrary initial state to the final steady-state, which happens to be superpoissonian. We derive closed expressions for the main quantities which characterize the statistics of the cavity photons and the detected atoms. We find that, despite the classicality of the SDM field steady-state, the atomic correlations exhibit stronger nonclassical features when compared with the conventional micromaser. The description of system dynamics is illustrated also by numerical results which support and complement the analytical ones.

3.4.1 Hamiltonian and coherent dynamics

As it was already shown in section 3.2 the effective coupling between an atom and a single cavity mode is drastically modified in the presence of a strong external driving field. Under the resonant conditions among the atomic transition, the cavity mode and the external field, it is possible to engineer a resonant Jaynes-Cummings and anti-Jaynes-Cummings interaction simultaneously. The latter is usually negligible in CQED, whereas they can be of importance in other systems, like ion traps [35]. In this case, the usual atom-field Rabi oscillations do not rule anymore, leaving their place to conditional

field displacements depending on the atomic internal states: “Schrödinger cat states.” In fact, this opens an avenue to the entanglement generation and measurement, which is a very active field in CQED with diverse implications in fundamental and applied quantum physics [17, 15].

Before studying a general SDM dynamics, it is useful to consider a coherent dynamics of an atom-cavity-driving interaction in more details, since the later governs amplification processes of the cavity field. In this connection, an influence of a measurement of the atomic levels on the resulting cavity field is of great importance. We show that the situation when atoms are measured after their interaction with a cavity field markedly differs from the one when they are unobserved and leads to a building up of a superposition states of the cavity field. However, such superposition states are only possible when the dissipation processes are not considered. Indeed, in the next subsections we see that the cavity field superposition states are ruled out in the SDM as a consequence of decoherence.

To start with, we consider a coherent dynamics of the fully resonant interaction between one mode of a high-Q cavity and a two-level atom strongly driven by a classical external field. It is described by the Hamiltonian (3.31) and reads

$$\mathcal{H} = \frac{\hbar g}{2}(\sigma^\dagger + \sigma)(a^\dagger + a), \quad (3.50)$$

where g is the atom-cavity mode coupling constant, a (a^\dagger) the field annihilation (creation) operator, and $\sigma = |g\rangle\langle e|$ ($\sigma^\dagger = |e\rangle\langle g|$) the atomic lowering (raising) operator.

It is worth to note that the Hamiltonian (3.50) is already written in the interaction picture, and was derived in section 3.2 under the strong driving condition $\Omega \gg g$, where Ω is the Rabi frequency associated with the external field. There, it was assumed that the external field interacts only with the atom and not with the cavity. This theoretical consideration can be achieved experimentally in different ways depending on the chosen setup. In the case of open cavities [15], the external field can be driven transversally to the axis of the pumping atoms by means of microwave guides, without feeding the cavity at any moment. In the case of closed cavities [36, 37], it is enough that the external field has a polarization orthogonal to the cavity mode of interest.

The unitary evolution operator $U = \exp(-i/\hbar)\mathcal{H}\tau$ associated with the Hamiltonian (3.50), where τ is the interaction time between the atom and the cavity, has been introduced in the Eq.(3.32) and reads

$$U(\xi) = D(\xi)|+\rangle\langle +| + D(-\xi)|-\rangle\langle -|. \quad (3.51)$$

Here, the parameter $\xi = -ig\tau/2$ is proportional to the interaction time τ and $D(\alpha) = \exp(\alpha a^\dagger - \alpha^* a)$ is a unitary displacement operator, where α is a complex number determining the displacement produced in the associated phase space.

Starting from an initial state with the cavity field in a state $\rho_{F,0}$ and one atom injected in the excited state,

$$\rho_0 = \rho_{F,0} \otimes |e\rangle\langle e|, \quad (3.52)$$

the density operator evolves to the state

$$\rho_1 = U(\xi)\rho_0U(-\xi). \quad (3.53)$$

We consider two cases, one in which the atoms are not observed when they leave the cavity and the other in which they are detected in the upper or lower level.

Atoms are not observed. If we are interested in the cavity field after the atomic transit without measuring the state of the outgoing atom, the cavity field density operator is

$$\rho_{F,1} = \text{Tr}_A \rho_1 = \frac{1}{2} [D(\xi)\rho_{F,0}D(-\xi) + D(-\xi)\rho_{F,0}D(\xi)], \quad (3.54)$$

where Tr_A is the partial trace over the atomic degrees of freedom, and we used Eqs. (3.51-3.53). If the cavity is initially in the vacuum state, $\rho_{F,0} = |0\rangle\langle 0|$, its state turns into

$$\rho_{F,1} = \frac{1}{2} (|\xi\rangle\langle \xi| + |-\xi\rangle\langle -\xi|), \quad (3.55)$$

which is a statistical mixture of two coherent states with the same amplitude and opposite phases.

It is of interest for what follows to describe the time evolution of the cavity field in phase space. While for the vacuum state the Wigner function is the Gaussian $W_0(\alpha) = 2 \exp(-2|\alpha|^2)$, for the state of Eq. (3.55) we have

$$W_1(\alpha) = 2 \exp[-2(|\alpha|^2 + |\xi|^2)] \cosh(4|\xi|\text{Im}\alpha). \quad (3.56)$$

This last expression shows that the interaction with a driven atom can affect the rotational symmetry of the initial vacuum state. The section of $W_1(\alpha)$ along the real axis remains a Gaussian with the initial minimum uncertainty, while the section along the imaginary axis is broadened, showing a two-peaked structure that results from the superposition of two Gaussians centered at $\alpha = \pm\xi$. The two peaks are well resolved if $|\xi| > 1/2$, which requires that the system is operated in the strong-coupling regime i.e. ($g\tau \gg 1$).

If the cavity mode, initially in the vacuum state, interacts with $1, 2, \dots, m$ strongly driven atoms, all assumed to pass through the cavity (one by one) with the same interaction time τ and to leave it unobserved, the final field state is given by the density operator

$$\rho_{F,m} = \frac{1}{2^m} \sum_{n=0}^m \binom{m}{n} |(m-2n)\xi\rangle\langle (m-2n)\xi|, \quad (3.57)$$

which describes a statistical mixture of $m+1$ coherent states. This state is represented in phase space by the Wigner function

$$W_m(\alpha) = \frac{1}{2^{m-1}} \sum_{n=0}^m \binom{m}{n} \exp[-2|\alpha - (m-2n)\xi|^2]. \quad (3.58)$$

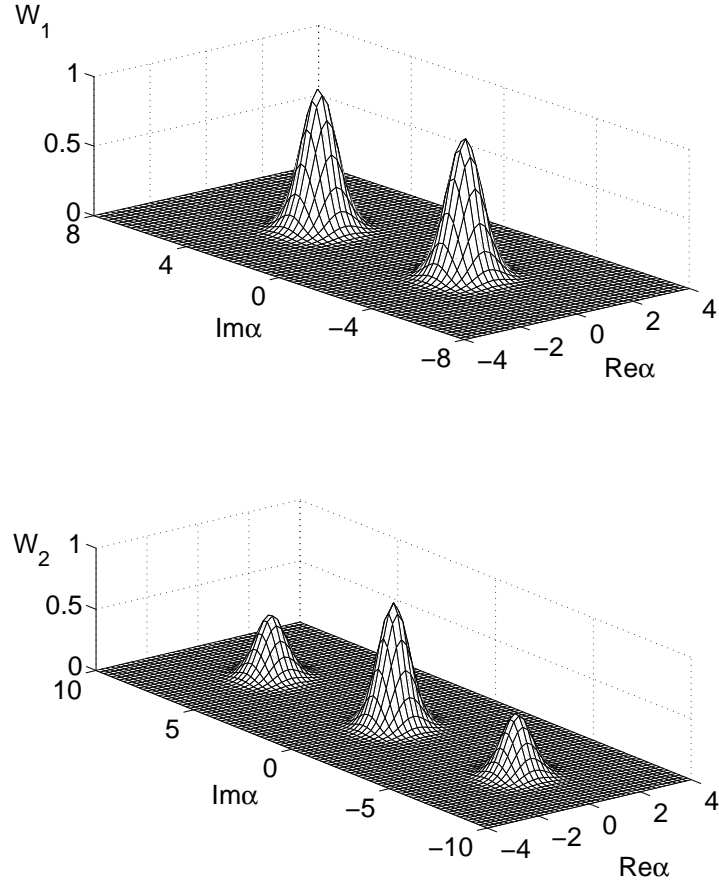


Figure 3.5: Wigner distributions $W_1(\alpha)$ and $W_2(\alpha)$ of the cavity field, see Eq. (3.58), in the case of one and two crossing atoms, respectively, provided that no attempt is made to determine the final internal state of the atoms. Here, as well as in all the following figures, $|\xi| = \pi$, the cavity field is initially in the vacuum state, and the atoms are in the excited state.

Hence, in the strong coupling regime and with negligible dissipation effects, multi-peaked cavity field distributions can be generated in phase-space, where the number of peaks increases with the number of driven atoms injected in the cavity. The subsequent generation of such cavity field states is illustrated in Fig.(3.5), where we show the Wigner functions $W_1(\alpha), W_2(\alpha)$ calculated from Eq. (3.58). After the transit of m atoms the function $W_m(\alpha)$ exhibits $m + 1$ peaks, all centered on the imaginary axis and with a center-to-center distance of $2|\xi| = g\tau$. If m is even, the peaks are centered at $\text{Re}\alpha = 0$ and $\text{Im}\alpha = 0, \pm 2|\xi|, \dots$, where the central peak in the origin is the highest one. If m is odd, the centers are at $\text{Re}\alpha = 0$ and $\text{Im}\alpha = \pm|\xi|, \pm 3|\xi|, \dots$, the highest peaks being at $\alpha = \pm\xi$.

Atoms are detected Now we consider the cavity field in the case in which the strongly driven atoms are detected when they leave the cavity, e.g. their state is determined by selective field ionization, where for simplicity we assume perfect detector efficiency. We are again interested in the cavity field properties after interaction. Proceeding again from the initial condition of Eq. (3.52), and using Eqs. (3.51-3.53), the cavity field density operators after detecting an atom in the excited state $\rho_{F,1}^{(e)}$ or in the ground state $\rho_{F,1}^{(g)}$ are

$$\begin{aligned}\rho_{F,1}^{(e)} &= \frac{[D(\xi) + D(-\xi)] \rho_{F,0} [D(\xi) + D(-\xi)]}{2[\operatorname{Re}\chi(2\xi) + 1]}, \\ \rho_{F,1}^{(g)} &= \frac{[D(\xi) - D(-\xi)] \rho_{F,0} [D(\xi) - D(-\xi)]}{2[\operatorname{Re}\chi(2\xi) - 1]},\end{aligned}\quad (3.59)$$

where $\chi(\beta) = \operatorname{Tr}_F \{\rho_{F,0} D(\beta)\}$ is the characteristic function for symmetrical ordering of the field operators and Tr_F is the partial trace over the field variables. If the cavity is initially in the vacuum state, then

$$\begin{aligned}\rho_{F,1}^{(e)} &= \frac{|\xi\rangle\langle\xi| + |-\xi\rangle\langle-\xi| + |\xi\rangle\langle-\xi| + |-\xi\rangle\langle\xi|}{2[1 + \exp(-2|\xi|^2)]}, \\ \rho_{F,1}^{(g)} &= \frac{|\xi\rangle\langle\xi| + |-\xi\rangle\langle-\xi| - |\xi\rangle\langle-\xi| - |-\xi\rangle\langle\xi|}{2[1 - \exp(-2|\xi|^2)]},\end{aligned}\quad (3.60)$$

which are pure states of the cavity field instead of the statistical mixtures of Eq. (3.55). Actually, the cavity field state vectors are $|\psi_{F,1}\rangle^{(e),(g)} \propto (|\xi\rangle \pm |-\xi\rangle)$, that is the superposition of two coherent states of the kind generated and monitored in the dispersive regime of cavity QED in [29]. More elaborated superposition states were investigated in Ref. [27], where also many-atom states were considered. The mean photon number of the field states of Eq. (3.60) are

$$\langle N_1 \rangle^{(e),(g)} = |\xi|^2 \frac{1 \mp \exp(-2|\xi|^2)}{1 \pm \exp(-2|\xi|^2)},\quad (3.61)$$

whereas $\langle N_1 \rangle = |\xi|^2$ in the case of an unmeasured atom Eq.(3.55).

The corresponding Wigner functions representing the states of Eq. (3.60) are

$$W_1^{(e),(g)}(\alpha) = 2e^{-2|\alpha|^2} [e^{-2|\xi|^2} \cosh(4|\xi|\operatorname{Im}\alpha) \pm \cos(4|\xi|\operatorname{Re}\alpha)] / (1 \pm e^{-2|\xi|^2}).\quad (3.62)$$

Beyond the two-peaked structure, present in Eq. (3.56) for an unmeasured atom (see also Fig. 3.5), the presence of the sinusoidal interference term implies that the Wigner functions in Eq. (3.62) can exhibit strong oscillations with period $\pi/2|\xi|$. They can even take negative values (see Fig. 3.6), which is a signature of the quantum nature of the cavity field states of Eq. (3.60). In particular, in the origin of phase space, $W_1^{(e),(g)}(0) = \pm 2$.

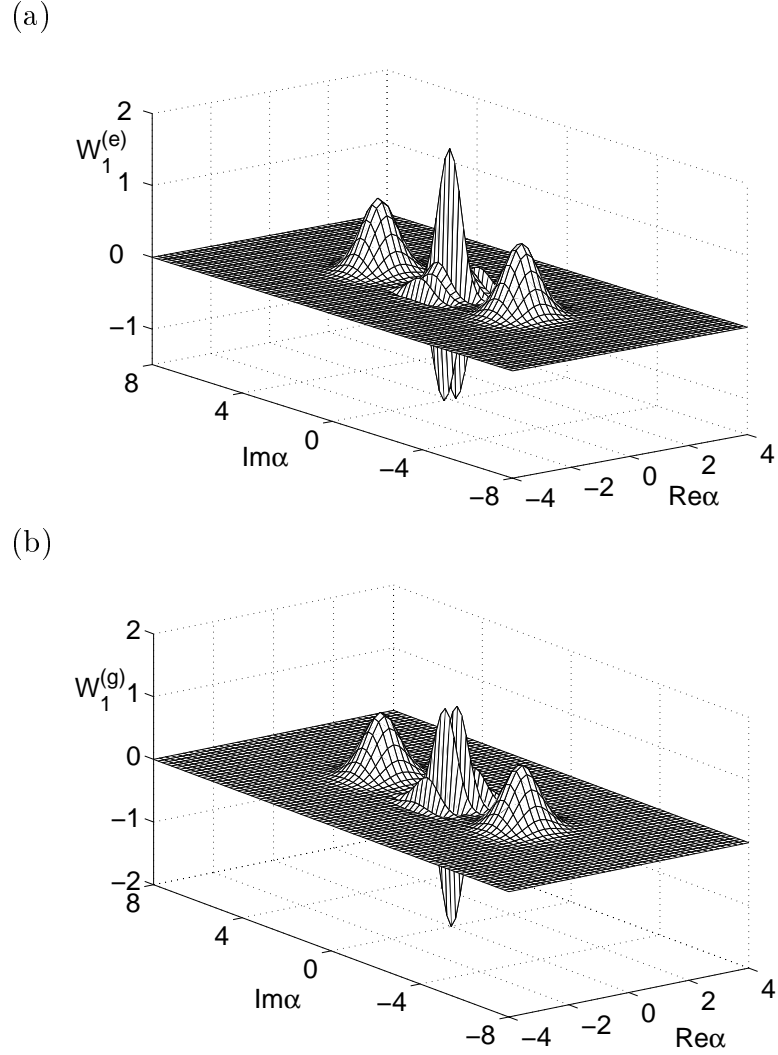


Figure 3.6: Wigner distribution of the cavity field for the case of one crossing atom detected (a) in the excited state, $W_1^{(e)}(\alpha)$; (b) in the ground state, $W_1^{(g)}(\alpha)$; see Eq. (3.62).

If the second atom crosses the cavity and is also detected in the upper or lower state soon after, the cavity field is projected onto one of the following states,

$$\begin{aligned} \rho_{F,2}^{(ee)} &= [|2\xi\rangle\langle 2\xi| + 4|0\rangle\langle 0| + |-2\xi\rangle\langle -2\xi| + |2\xi\rangle\langle -2\xi| \\ &\quad + |-2\xi\rangle\langle 2\xi| + 2(|2\xi\rangle\langle 0| + |0\rangle\langle 2\xi| + |0\rangle\langle -2\xi| \\ &\quad + |-2\xi\rangle\langle 0|)] / [2(3 + 4e^{-2|\xi|^2} + e^{-8|\xi|^2})], \end{aligned}$$

$$\begin{aligned} \rho_{F,2}^{(eg)} &= \rho_{F,2}^{(ge)} = [|2\xi\rangle\langle 2\xi| + |-2\xi\rangle\langle -2\xi| \\ &\quad - |2\xi\rangle\langle -2\xi| - |-2\xi\rangle\langle 2\xi|] / [2(1 - e^{-8|\xi|^2})], \end{aligned}$$

$$\begin{aligned}
\rho_{F,2}^{(gg)} &= [|2\xi\rangle\langle 2\xi| + 4|0\rangle\langle 0| + | -2\xi\rangle\langle -2\xi| + |2\xi\rangle\langle -2\xi| \\
&\quad + | -2\xi\rangle\langle 2\xi| - 2(|2\xi\rangle\langle 0| + |0\rangle\langle 2\xi| + |0\rangle\langle -2\xi| \\
&\quad + | -2\xi\rangle\langle 0|)] / [2(3 - 4e^{-2|\xi|^2} + e^{-8|\xi|^2})], \tag{3.63}
\end{aligned}$$

where, for instance, (eg) means that the first atom is detected in the upper state and the second one in the lower state. The expressions of Eq. (3.63) should be compared with the statistical mixture of Eq. (3.57) in the case of two unobserved atoms ($m = 2$). The density operators in Eq. (3.63) describe mesoscopic Schrödinger-cat-like states of the cavity field, the corresponding state vectors being

$$\begin{aligned}
|\psi_{F,2}\rangle^{(ee)} &\propto (|2\xi\rangle + 2|0\rangle + | -2\xi\rangle), \\
|\psi_{F,2}\rangle^{(gg)} &\propto (|2\xi\rangle - 2|0\rangle + | -2\xi\rangle), \\
|\psi_{F,2}\rangle^{(eg)} = |\psi_{F,2}\rangle^{(ge)} &\propto (|2\xi\rangle - | -2\xi\rangle). \tag{3.64}
\end{aligned}$$

The Wigner functions which represent the above states in phase space, whose behavior is depicted in Fig. 3.7, can be written as

$$\begin{aligned}
W_2^{(ee)}(\alpha) &= 2e^{-2|\alpha|^2} [2 + e^{-8|\xi|^2} \cosh(8|\xi|\text{Im}\alpha) \\
&\quad + 4e^{-2|\xi|^2} \cosh(4|\xi|\text{Im}\alpha) \cos(4|\xi|\text{Re}\alpha) \\
&\quad + \cos(8|\xi|\text{Re}\alpha)] / (3 + 4e^{-2|\xi|^2} + e^{-8|\xi|^2}), \\
W_2^{(eg)}(\alpha) &= W_2^{(ge)}(\alpha) = 2e^{-2|\alpha|^2} [-\cos(8|\xi|\text{Re}\alpha) \\
&\quad + e^{-8|\xi|^2} \cosh(8|\xi|\text{Im}\alpha)] / (1 - e^{-8|\xi|^2}), \\
W_2^{(gg)}(\alpha) &= 2e^{-2|\alpha|^2} [2 + e^{-8|\xi|^2} \cosh(8|\xi|\text{Im}\alpha) \\
&\quad - 4e^{-2|\xi|^2} \cosh(4|\xi|\text{Im}\alpha) \cos(4|\xi|\text{Re}\alpha) \\
&\quad + \cos(8|\xi|\text{Re}\alpha)] / (3 - 4e^{-2|\xi|^2} + e^{-8|\xi|^2}). \tag{3.65}
\end{aligned}$$

We consider now the atomic statistics at the exit of the cavity independent of the cavity field state. If an atom is injected in the cavity, so that the initial state is $\rho_F \otimes |e\rangle\langle e|$, the atomic state after the interaction will be

$$\begin{aligned}
\rho_A &= \text{Tr}_F\{U(\xi)\rho_F \otimes |e\rangle\langle e|U(-\xi)\} \\
&= \frac{1}{2} \left[1_A + \text{Re}\chi(2\xi)(|e\rangle\langle e| - |g\rangle\langle g|) + i\text{Im}\chi(2\xi)(|g\rangle\langle e| - |e\rangle\langle g|) \right]. \tag{3.66}
\end{aligned}$$

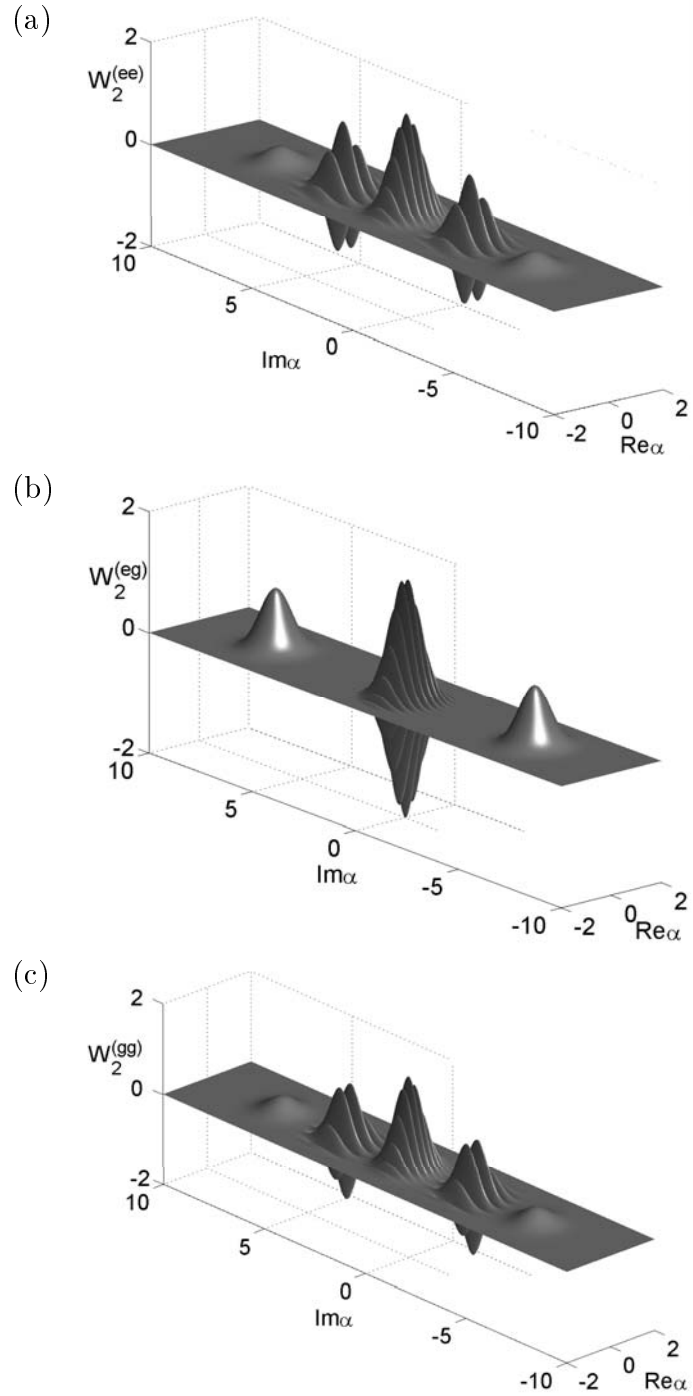


Figure 3.7: Wigner distribution of the cavity field for the case of two crossing atoms detected (a) both in the excited state, $W_2^{(ee)}(\alpha)$; (b) one in the excited state and the other in the ground state, $W_2^{(eg)}(\alpha)$; (c) both in the ground state, $W_2^{(gg)}(\alpha)$; see Eq. (3.65).

Here, Tr_F is the partial trace over the cavity mode degrees of freedom. In the derivation of Eq. (3.66) we used also Eqs. (3.51) and (3.52) as well as the property $\chi(\beta) = \chi(-\beta)^*$. Finally, we can calculate the probability $p_{e,g}$ for atomic detection in the upper or lower state as

$$p_{e,g} = \langle e, g | \rho_A | e, g \rangle = \frac{1}{2} [1 \pm \text{Re } \chi(2\xi)]. \quad (3.67)$$

3.4.2 SDM master equation and analytical solutions

The model of SDM is based on the model of the conventional micromaser introduced in the section 3.3 and absorbs its main features and approximations. Therefore, it can be briefly summarized as follows:

- We consider a beam of two-level Rydberg atoms, satisfying the poissonian arrival time statistics, with pumping rate r , interacting with a single mode of a microwave high-Q cavity.
- We study a regime where at most one atom is present inside the cavity at a time, that is, $\tau \ll r^{-1}$, τ being atom-cavity interaction time, and where the decay of atomic Rydberg levels is negligible.
- While the atoms are inside the cavity, during an interaction time τ , they are strongly driven by an additional strong classical field, the whole system being in resonance.
- Between two successive atoms, the cavity field decays due to its interaction with a thermal bath.

Hence, even though the present SDM model looks quite similar to the conventional micromaser, there is a crucial difference in the pumping dynamics. In the case of SDM an atom-cavity interaction is described in terms of the interaction Hamiltonian (3.50) instead of the Jaynes-Cummings Hamiltonian (3.22) for the micromaser. It has been already discussed in the preceding subsection, that the Rabi oscillations do not rule any more the unitary atom-field interaction. Their role is taken over by field displacements conditioned on the atomic internal states.

The dynamics of the SDM field is governed by an interplay between the amplification process, due to the interaction with the driven atoms, and the dissipation process, occurring when no atom crosses the cavity. The gain rate of the cavity mode of SDM can be obtained using a coarse-grained description in a similar manner as it has been already done in the case of conventional micromaser (see Eq.(3.37-3.40)). However, now one should make use of the unitary evolution operator Eq.(3.51) instead of the one corresponding to the Jaynes-Cummings model, so that the gains of the SDM field read

$$\left. \frac{\partial \rho_F}{\partial t} \right|_{\text{gain}} = \frac{r}{2} [D(\xi) \rho_F D(-\xi) + D(-\xi) \rho_F D(\xi) - 2\rho_F]. \quad (3.68)$$

The loss rate, due to the interaction of the cavity field with a thermal bath [33], is given by a standard expression

$$\begin{aligned} \left. \frac{\partial \rho_F}{\partial t} \right|_{\text{loss}} &= -\frac{\gamma(\bar{n}_{th} + 1)}{2} [a^\dagger a \rho_F - 2a \rho_F a^\dagger + \rho_F a^\dagger a] \\ &\quad - \frac{\gamma \bar{n}_{th}}{2} [a a^\dagger \rho_F - 2a^\dagger \rho_F a + \rho_F a a^\dagger] \equiv \mathcal{L} \rho_F, \end{aligned} \quad (3.69)$$

where γ is the cavity photon decay rate and \bar{n}_{th} is the mean thermal photon number. Bringing Eqs. (3.68) and (3.69) together we arrive at the master equation of SDM

$$\frac{\partial \rho_F}{\partial t} = \frac{r}{2} [D(\xi) \rho_F D(-\xi) + D(-\xi) \rho_F D(\xi) - 2\rho_F] + \mathcal{L} \rho_F. \quad (3.70)$$

At variance with the conventional micromaser, whose master equation Eq.(3.44) has an analytical solution only in a steady-state [31, 32], the SDM master equation (3.70) is completely integrable for any time. In order to demonstrate that, we perform a transformation from the equation of motion (3.70) for the density operator into the corresponding partial differential equation for its symmetrically ordered characteristic function $\chi(\beta)$. We employ a one-to-one correspondence between $\chi(\beta)$ and a related field density operator, which is given by

$$\rho_F = \pi^{-1} \int \chi(\beta) D^{-1}(\beta) d^2 \beta. \quad (3.71)$$

We note here that the Wigner function, $W(\alpha)$, is the 2D Fourier transform of the characteristic function $\chi(\beta)$.

Thus, using known operator techniques [38], we map both parts of the operator equation (3.70) into the following complex functions:

$$\begin{aligned} \frac{\partial \rho_F}{\partial t} &\rightarrow \frac{\partial}{\partial t} \chi(\beta, \beta^*, t), \\ D(\xi) \rho_F D(-\xi) &\rightarrow e^{\xi^* \beta - \xi \beta^*} \chi(\beta, \beta^*, t), \\ \mathcal{L} \rho_F &\rightarrow -\frac{\gamma}{2} \left[(2\bar{n}_{th} + 1) |\beta|^2 + \beta \frac{\partial}{\partial \beta} + \beta^* \frac{\partial}{\partial \beta^*} \right] \chi(\beta, \beta^*, t), \end{aligned} \quad (3.72)$$

so that correspondent partial differential equation for $\chi(\beta, \beta^*, t)$ reads

$$\begin{aligned} \frac{\partial}{\partial t} \chi(\beta, \beta^*, t) &= \left[\frac{r}{2} (e^{\xi^* \beta - \xi \beta^*} + e^{-\xi^* \beta + \xi \beta^*} - 2) - \frac{\gamma}{2} (2\bar{n}_{th} + 1) |\beta|^2 \right] \chi(\beta, \beta^*, t) \\ &\quad - \frac{\gamma}{2} \left(\beta \frac{\partial}{\partial \beta} + \beta^* \frac{\partial}{\partial \beta^*} \right) \chi(\beta, \beta^*, t). \end{aligned} \quad (3.73)$$

We transform Eq. (3.73) to cartesian coordinates by setting $\xi^* \beta \equiv |\xi|(x + iy)$, which gives

$$\left(\frac{\partial}{\partial t} + \frac{\gamma}{2} \left[x \frac{\partial}{\partial x} + y \frac{\partial}{\partial y} + x G'(x) + y F'(y) \right] \right) \chi(x, y, t) = 0, \quad (3.74)$$

where

$$\begin{aligned} G(x) &= \frac{2\bar{n}_{th} + 1}{2} x^2, \\ F(y) &= \int_0^y \frac{4N_{ex} \sin^2(|\xi|z) + (2\bar{n}_{th} + 1)z^2}{z} dz, \end{aligned} \quad (3.75)$$

and $N_{ex} = r/\gamma$. The solution of Eq. (3.74) reads

$$\chi(x, y, t) = \frac{\chi^{(ss)}(x, y) \chi_0(xe^{-\frac{\gamma t}{2}}, ye^{-\frac{\gamma t}{2}})}{\chi^{(ss)}(xe^{-\frac{\gamma t}{2}}, ye^{-\frac{\gamma t}{2}})}. \quad (3.76)$$

Here,

$$\chi^{(ss)}(x, y) = e^{-G(x) - F(y)} \quad (3.77)$$

is the steady-state solution of Eq. (3.74) that is reached for $t \rightarrow \infty$, and $\chi_0 = \text{Tr}_F[\rho_F(0)D]$ is the characteristic function corresponding to the initial field state $\rho_F(0)$. By substituting the expressions of Eq. (3.75) into Eq. (3.77), we arrive at the steady-state characteristic function

$$\chi^{(ss)}(x, y) = \exp\left(-(\bar{n}_{th} + \frac{1}{2})(x^2 + y^2) + 4N_{ex}[-\gamma_e - \ln(2|\xi|y) + \text{Ci}(2|\xi|y)]\right), \quad (3.78)$$

where γ_e is Euler's constant and $\text{Ci}(2|\xi|y)$ is the Cosine Integral defined as

$$\text{Ci}(2|\xi|y) = \gamma_e + \ln(2|\xi|y) + \int_0^{2|\xi|y} \frac{\cos(z) - 1}{z} dz. \quad (3.79)$$

Note that starting from a real initial function, the time-dependent solution in Eq. (3.76) will always produce a real characteristic function. This follows from the invariance of the time evolution equation in Eq. (3.73) under the transformation $\beta \rightarrow -\beta$, and from the property $\chi(\beta) = \chi(-\beta)^*$. Accordingly, the solution of Eq. (3.76) depends only on the modulus of the (imaginary) parameter ξ , which is in agreement with the invariance of the master equation (3.70) under the transformation $\xi \rightarrow -\xi$.

3.4.3 SDM field statistics

It is clear that from the general solution of the characteristic function, Eq. (3.76), we can calculate the field density operator $\rho_F(t)$, following Eq. (3.71), and have access to the field statistics. However, this information can be directly extracted from the characteristic function itself, since the expectation value of any symmetrically ordered product of the operators a and a^\dagger is given by

$$\langle (a^\dagger)^m a^n \rangle_{\text{sym}} = \left. \frac{\partial^{m+n} \chi(\beta, \beta^*)}{\partial \beta^m \partial (-\beta^*)^n} \right|_{\beta=\beta^*=0}. \quad (3.80)$$

For example, we have

$$\begin{aligned}\langle a(t) \rangle &= \langle a(0) \rangle e^{-\frac{\gamma}{2}t}, \\ \langle a^\dagger(t)a(t) \rangle &= \langle a^\dagger(0)a(0) \rangle e^{-\gamma t} + (N_{ex}|\xi|^2 + \bar{n}_{th})(1 - e^{-\gamma t}), \\ \langle a^2(t) \rangle &= \langle a^2(0) \rangle e^{-\gamma t} + N_{ex}\xi^2(1 - e^{-\gamma t}).\end{aligned}\quad (3.81)$$

From the expressions in Eq. (3.81) and their complex conjugates, we derive the steady-state expectation values of the field amplitude, photon number, and quadrature variances $(\Delta x_{1,2})^2$, with $x_1 = (1/2)(a^\dagger + a)$ and $x_2 = (i/2)(a^\dagger - a)$,

$$\begin{aligned}\langle a \rangle^{(ss)} &= 0, \\ \langle a^\dagger a \rangle^{(ss)} &= N_{ex}|\xi|^2 + \bar{n}, \\ (\Delta x_1^{(ss)})^2 &= \frac{1}{4}(1 + 2\bar{n}), \\ (\Delta x_2^{(ss)})^2 &= \frac{1}{4}(1 + 2\bar{n} + 4N_{ex}|\xi|^2).\end{aligned}\quad (3.82)$$

We see that in the steady state the expectation value of the SDM field is zero, whereas the mean photon number is a quadratic function of the modulus of the single atom displacement parameter ξ . Also, for vanishing cavity temperature ($\bar{n}_{th} \rightarrow 0$), the variance of the quadrature operator x_1 remains at the minimum value $1/4$, whereas the variance of the orthogonal quadrature x_2 , the one that is being driven by the system, is broadened by a factor equal to $\langle a^\dagger a \rangle^{(ss)}$.

Another important quantity describing the photon statistics is the Fano-Mandel parameter $Q = [(\Delta N)^2 - \langle N \rangle] / \langle N \rangle$, where $N \equiv \langle a^\dagger a \rangle$. For the SDM at steady-state we obtain

$$Q = N_{ex}|\xi|^2 + \bar{n}_{th} + \frac{N_{ex}|\xi|^4(N_{ex} + \frac{1}{2})}{N_{ex}|\xi|^2 + \bar{n}_{th}},\quad (3.83)$$

which describes a persistent super-Poissonian behavior ($Q > 0$). This result is at variance with the conventional micromaser steady-state [31] (see Fig.(3.4)), which alternates between super-Poissonian and sub-Poissonian statistics.

3.4.4 Atomic correlations

Just as it is the case for the micromaser, in the SDM we are not able to measure the cavity field directly. Therefore, we use the atoms not only for pumping the cavity mode but also as a source of information about the SDM field. The theory of the detector clicks statistics as well as the connection between the statistics of the detected atoms and the cavity field was developed for the conventional micromaser in [39]. According to this approach, the detection of the exiting atom, initially prepared in the upper state, in the ground state is described by an operator \mathcal{A} whose action on the field density operator ρ_F is given by

$$\mathcal{A}\rho_F = \frac{1}{4}[D(-\xi)\rho_FD(\xi) + D(\xi)\rho_FD(-\xi) - D(-\xi)\rho_FD(-\xi) - D(\xi)\rho_FD(\xi)].\quad (3.84)$$

Likewise, the click operator \mathcal{B} for detection in the excited state acts as follows

$$\mathcal{B}\rho_F = \frac{1}{4}[D(-\xi)\rho_FD(\xi) + D(\xi)\rho_FD(-\xi) + D(-\xi)\rho_FD(-\xi) + D(\xi)\rho_FD(\xi)]. \quad (3.85)$$

Note that the above expressions have the same structure as the field state operators of Eqs. (3.59). The probability to detect the atom in the ground (excited) state p_g (p_e) can be calculated as $\text{Tr}_F[\mathcal{A}\rho_F]$ ($\text{Tr}_F[\mathcal{B}\rho_F]$), giving the results of Eq. (3.67), which can be further simplified after the derivation of a real expression for the characteristic function χ , so that

$$p_{e,g} = \frac{1}{2}[1 \pm \chi(2\xi)]. \quad (3.86)$$

The latest is in agreement with the expression Eq.(3.67). The introduction of the above click operators enables us to describe the atomic correlation functions, or conditional probabilities for two consecutive detector clicks. For instance, the correlation function for a detection of the second atom in the excited state after a detection of the first atom in the ground state separated by a time interval t is given by

$$G_{ge}(t) = \frac{\text{Tr}_F[\mathcal{B}e^{\mathcal{L}_0 t}\mathcal{A}\rho^{(\text{ss})}]}{\text{Tr}_F[\mathcal{B}\rho^{(\text{ss})}]\text{Tr}_F[\mathcal{A}\rho^{(\text{ss})}]} = \frac{1 + \tilde{\chi}(2\xi, t)}{1 + \chi^{(\text{ss})}(2\xi)}, \quad (3.87)$$

where $\mathcal{L}_0 = \mathcal{L} + r(\mathcal{A} + \mathcal{B} - 1)$, $\chi^{(\text{ss})}$ is the steady-state characteristic function(3.78) which reads

$$\tilde{\chi}(2\xi, t) = \frac{2\chi^{(\text{ss})}(2\xi e^{-\frac{\gamma}{2}t}) - 1 - \chi^{(\text{ss})}(4\xi e^{-\frac{\gamma}{2}t})}{2 - 2\chi^{(\text{ss})}(2\xi e^{-\frac{\gamma}{2}t})} \times \exp\left(-(\bar{n}_{th} + \frac{1}{2})|2\xi|^2(1 - e^{-\frac{\gamma}{2}t})\right), \quad (3.88)$$

and 100% detection efficiency has been assumed. In other words, we suppose that no atom escapes detection.

The two-click correlation function in Eq. (3.87) is the ratio between the conditional probability to have a second e -click at time t after a first g -click occurred at time 0, and the probability for an e -click when the cavity field is in the steady-state. All other correlation functions for click pairs G_{ee} , G_{gg} and G_{eg} are given by the following expressions

$$\begin{aligned} G_{gg}(t) &= \frac{\text{Tr}_F[\mathcal{A}e^{\mathcal{L}_0 t}\mathcal{A}\rho^{(\text{ss})}]}{(\text{Tr}_F[\mathcal{A}\rho^{(\text{ss})}])^2} = \frac{1 - \tilde{\chi}(2\xi, t)}{1 - \chi^{(\text{ss})}(2\xi)}, \\ G_{eg}(t) &= \frac{\text{Tr}_F[\mathcal{A}e^{\mathcal{L}_0 t}\mathcal{B}\rho^{(\text{ss})}]}{\text{Tr}_F[\mathcal{A}\rho^{(\text{ss})}]\text{Tr}_F[\mathcal{B}\rho^{(\text{ss})}]} = \frac{1 - \bar{\chi}(2\xi, t)}{1 - \chi^{(\text{ss})}(2\xi)}, \\ G_{ee}(t) &= \frac{\text{Tr}_F[\mathcal{B}e^{\mathcal{L}_0 t}\mathcal{B}\rho^{(\text{ss})}]}{(\text{Tr}_F[\mathcal{B}\rho^{(\text{ss})}])^2} = \frac{1 + \bar{\chi}(2\xi, t)}{1 + \chi^{(\text{ss})}(2\xi)}, \end{aligned} \quad (3.89)$$

where

$$\bar{\chi}(2\xi, t) = \frac{2\chi^{(\text{ss})}(2\xi e^{-\frac{\gamma}{2}t}) + 1 + \chi^{(\text{ss})}(4\xi e^{-\frac{\gamma}{2}t})}{2 + 2\chi^{(\text{ss})}(2\xi e^{-\frac{\gamma}{2}t})} \times \exp\left(-(\bar{n}_{th} + \frac{1}{2})|2\xi|^2(1 - e^{-\frac{\gamma}{2}t})\right). \quad (3.90)$$

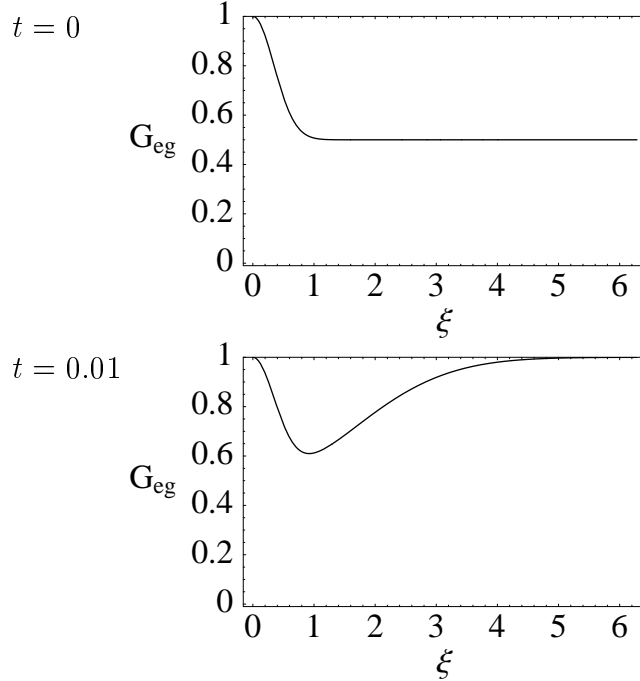


Figure 3.8: Atomic correlations G_{eg} with parameters $N_{ex} = 50$, $\bar{n}_{th} = 0.03$. The figures are plotted for time intervals $t = 0$ (top) and $t = 0.01$ (bottom) between detection clicks.

However, as in the case of the conventional micromaser, the two-click correlation functions of Eqs. (3.87) and (3.89) for the SDM reflect the statistics of all possible consecutive two-click events separated by a time t . In order to judge about the correlations between two truly successive atoms, one should take the limit $t \rightarrow 0$ in Eqs. (3.87) and (3.89). In this limit², two consecutive atoms interact with the cavity field and there is no time for decoherence to take place in between. Therefore, one expects stronger atomic correlations as a consequence of the discussion done in Sec. 3.4.1 .

In Fig. 3.8, we show the correlation function G_{eg} as a function of the displacement parameter ξ . We see that G_{eg} exhibits stronger correlations, when compared with the conventional micromaser, despite the complete classicality of the SDM steady-state. This is a counter intuitive result coming from the belief that stronger correlations should appear only when non-classical steady-states are involved. The stronger atomic correlations present in the SDM originate in the different nature of the unitary process. In the SDM, we rely on an interaction (see subsection 3.4.1) that naturally produces mesoscopic entangled atom-field states (“Schrödinger cat states”), while the conventional micromaser uses the Jaynes-Cummings interaction, producing Rabi oscillations

²We recall that the master equation of Eq. (3.70) was derived in the standard coarse-grained approximation, where the interaction time of each atom is considered as differential compared to the time scale of the global field dynamics. In this context, the limit $t \rightarrow 0$ in the two-atom correlations means that the first atom leaves the cavity in the moment in which the second one is entering. In consequence, no decoherence can happen between these two consecutive events.

inside well defined atom-field subspaces, and essentially exchanging a single photon per cycle.

3.4.5 Numerical simulations

In order to describe the SDM dynamics we have at our disposal the analytical expression of the symmetrically ordered characteristic function $\chi(\beta, \beta^*, t)$, Eq.(3.76). We can as well describe the time evolution of the Wigner function $W(\alpha, \alpha^*, t)$, that is the Fourier transform of $\chi(\beta, \beta^*, t)$, which gives a picture in the phase space associated to the cavity mode. We can further consider the time behavior of the density matrix $(\rho_F)_{m,n}(t) = \langle m | \rho_F(t) | n \rangle$, derived from the master equation in Eq. (3.70) when the field density operator is represented in the Fock basis. In this case, we can use quantum jumps techniques [40], already applied successfully in several problems in the domain of micromaser physics [41, 42] and CQED.

All these intertwined tools allow a consistent description of SDM dynamics which complements the analytical results and unveils additional features. As an example, in Fig. 3.9 we show the transient behavior of the Wigner distribution $W(\alpha)$ of the SDM field. Starting from the Gaussian function of the vacuum state (Fig. 3.9a), after a time interval $\gamma t = 0.1$ (Fig. 3.9b) we see the presence of two additional peaks, symmetrically placed along the imaginary axis. Here, we have chosen $|\xi| = \pi$, a large enough value to see a peaked structure. At later times in the transition, Fig. 3.9(c), we see the onset of other peak pairs symmetrically placed on the imaginary axis, while the distribution lowers and broadens along that axis. The underlying physical mechanism for the generation of this dynamics was described in subsection 3.4.1.

At later times decoherence destroys such structures, and when the steady-state is reached (Fig. 3.10) the distribution looks like the envelope of the multiply-peaked structure along the imaginary axis, while it preserves its initial minimum width along the real axis. Figure 3.11 shows the density matrix of the steady-state SDM field. The diagonal elements provide the photon statistics, and their wide distribution confirms the predicted super-poissonian behavior. Furthermore, we note the presence of off-diagonal density matrix elements or coherences, which rule the phase and spectral properties of the field.

Initially they are not excited in the cavity field, hence they are induced by the interaction with the strongly driven atoms. In order to investigate this effect, in Fig. 3.12, we show the steady-state Pegg-Barnett [43] phase distribution

$$P(\theta) = (2\pi)^{-1} \sum_{m,n=0}^{\infty} \rho_{n,m}^{(ss)} e^{i(m-n)\theta}. \quad (3.91)$$

The SDM phase distribution shows a particular feature, i.e., a narrow two-peaked structure centered on the values $\theta = \pm\pi/2$, which is already present in the transient regime. This feature is explained by the SDM gain dynamics, Eq. (3.68), which shows that the resonant interaction of the cavity field with strongly driven atoms implies an

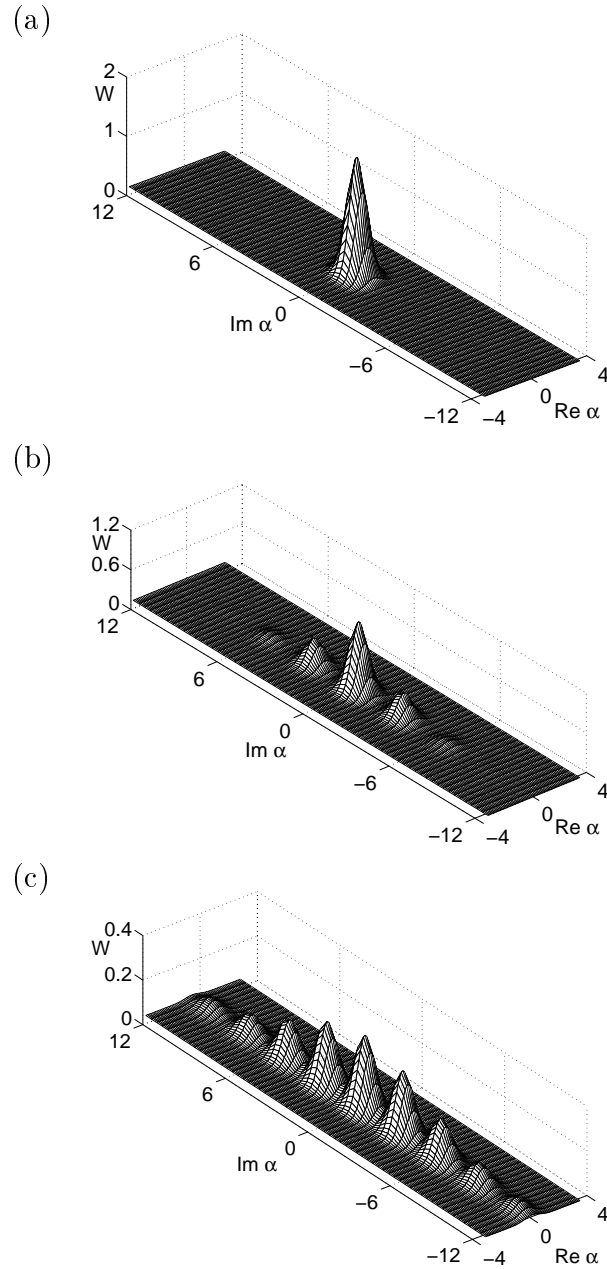


Figure 3.9: Generation of multi-peaked distributions in the transient SDM field dynamics: $W(\alpha, t)$ - Wigner distributions at $t = 0$ (top) and $\gamma t = 0.1, 0.5$ (proceeding downward), obtained from the master equation (3.70).

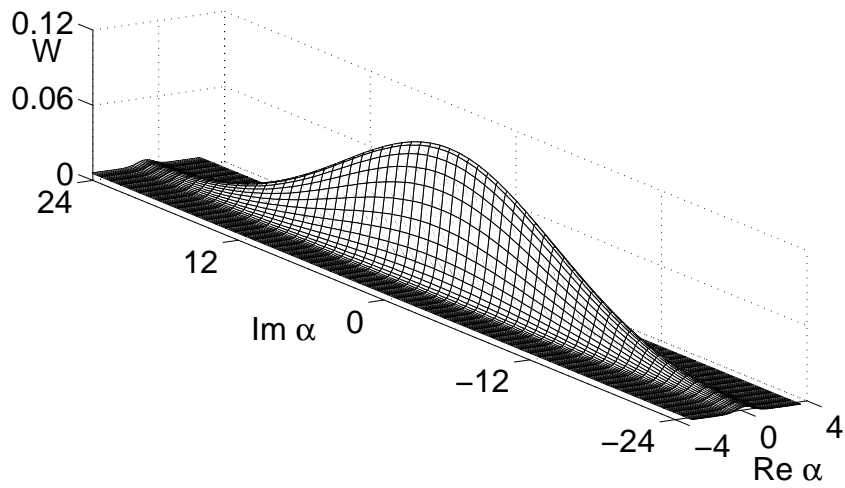


Figure 3.10: Steady-state cavity field after the transient evolution of Fig. 3.9: Wigner function $W(\alpha)$ for $\gamma t = 20$.

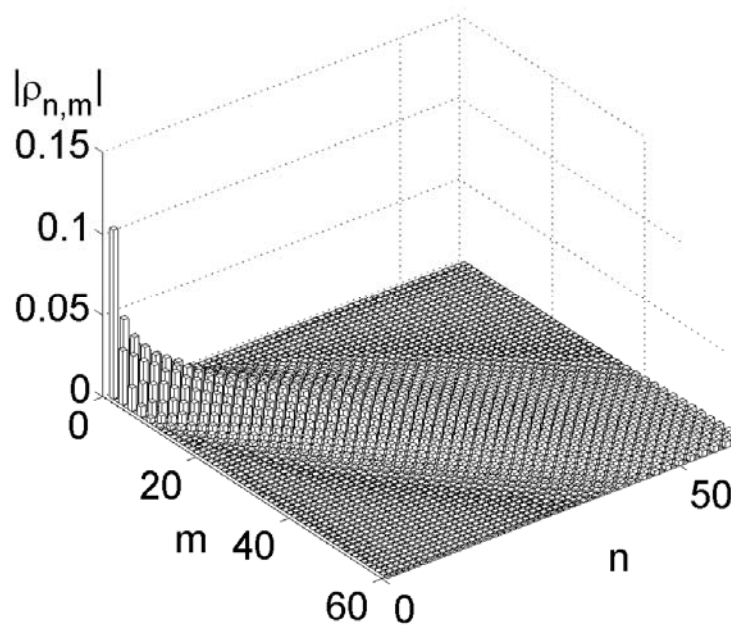


Figure 3.11: Density matrix of the steady-state cavity field.

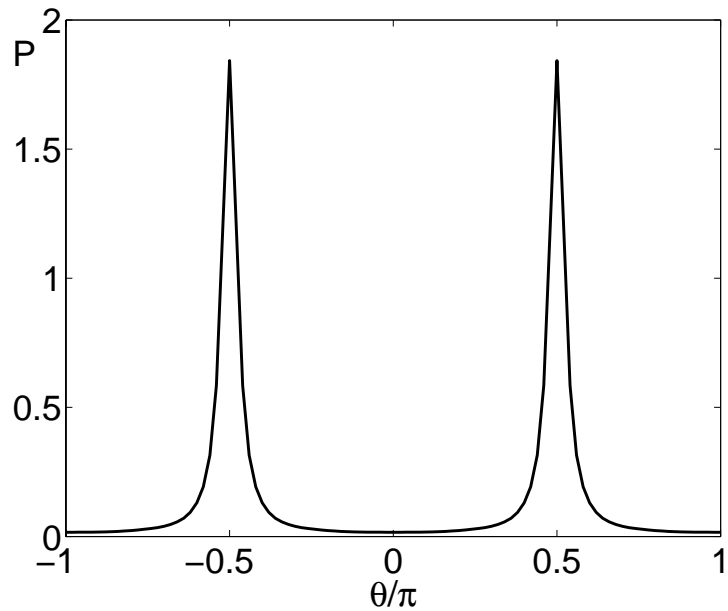


Figure 3.12: Pegg-Barnett phase distribution of the steady-state cavity field.

equal displacement of the field by the imaginary quantities $\pm\xi$. In turn, this effect is quite consistent with the narrow elongated form of the steady-state distribution along the imaginary axis in phase space, as well as with the vanishing of the steady-state field expectation value.

3.5 One-atom laser

We have already considered an important CQED model - model of the micromaser and its generalization to a case of driven micromaser. Both of them have a distinguishing feature, namely a cavity field is built up as a result of an interaction between a cavity mode with a large, in a limit with an infinite, sequence of atoms. The conventional macroscopic laser systems are built on a same principle. An output cavity field of a laser is generated as an interplay between losses of the field due to spontaneous incoherent emission of intracavity atoms and an amplified coherent stimulated emission of them. Whereas the micromaser can operate in a regime with only a few intracavity photons, lasers deal with a huge number of the field photons and as a consequence can be treated semi-classically [44] without taking into account an impact from a single quanta. However, a situation is modified drastically when a generating intracavity medium is reduced to a single atom. This leads to an interesting theoretical and experimental problem to study lasing properties of an atom pumped by a possibly coherent or incoherent radiation. Many theoretical works were devoted to studies of a one-atom laser [45, 46, 47, 48] and have shown that it can exhibit features which are

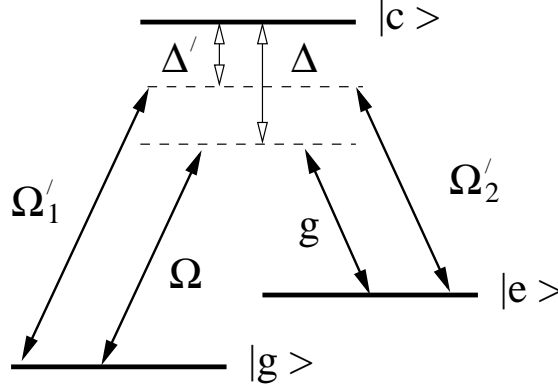


Figure 3.13: Atomic energy levels structure and the applied fields. Δ and Δ' denote the frequency detunings and g , Ω'_1 , Ω'_2 , Ω are corresponding coupling strengths.

not inherent in macroscopic lasers such as thresholdless generation and sub-poissonian field statistics. Recent advances in fabricating of high-Q optical cavities as well as a trapping and cooling [49, 22] of neutral atoms in an optical cavity have promoted an experimental realization of a one-atom laser [20]. In this section we present a theoretical integrable model of a one-atom laser and show how to use it for a monitoring of a cavity field decoherence.

3.5.1 Model

We consider an atom(ion) in a three level Λ -configuration trapped inside an optical cavity fig.(3.13) interacting off-resonantly with a single mode of a cavity field on a transition $|c\rangle \leftrightarrow |e\rangle$ and with a classical coherent pumping field of an amplitude Ω'_1 on a transition $|c\rangle \leftrightarrow |g\rangle$. We assume that the transition $|e\rangle \leftrightarrow |g\rangle$ is quadrupole and hence metastable states $|g\rangle$ and $|e\rangle$ cannot be coupled directly but through a level $|c\rangle$ by two effective far off-resonant interactions, one stemming from a laser field Ω'_1 and the cavity mode g and the other from two additional laser fields Ω'_2 and Ω . The later two fields are auxiliary and mediate a resonant interaction of $|e\rangle \leftrightarrow |g\rangle$ transition to the cavity mode and pumping field Ω'_1 . The level $|c\rangle$ is corrupted by spontaneous emission and therefore in order to avoid its population and as a result decay due to spontaneous emission, as well as to transfer adiabatically an atomic population between $|g\rangle$ and $|e\rangle$ we apply the external lasers and the cavity field detuned with respect to the corresponding transition frequencies. Moreover, the different frequency detunings, Δ and Δ' , of these Λ -processes prevent the system from undesired transitions.

We assume that both the cavity mode coupling strength g , and other coupling strengths $\{\Omega, \Omega'_1, \Omega'_2\}$ are real. Then, the Hamiltonian for the entire system can be written as

$$\begin{aligned} \mathcal{H} = & \hbar\omega_e|e\rangle\langle e| + \hbar\omega_c|c\rangle\langle c| + \hbar\omega_f a^\dagger a + \hbar g(a^\dagger|e\rangle\langle c| + a|c\rangle\langle e|) \\ & + \hbar\Omega(e^{-i(\omega_c-\Delta)t}|c\rangle\langle g| + h.c.) + \hbar\Omega'_2(e^{-i(\omega_c-\omega_e-\Delta')t}|c\rangle\langle e| + h.c.) \end{aligned}$$

$$+\hbar\Omega'_1(e^{-i(\omega_c-\Delta')t}|c\rangle\langle g| + h.c.). \quad (3.92)$$

Here, ω_c and ω_e are the Bohr frequencies associated with the transitions $|c\rangle \leftrightarrow |g\rangle$ and $|e\rangle \leftrightarrow |g\rangle$, respectively, while ω_f is the frequency of the cavity mode and a (a^\dagger) the associated annihilation (creation) operator. To eliminate level $|c\rangle$ adiabatically, so as to discard spontaneous emission from our model, we use a standard approach [50] and require

$$\left\{\frac{\Omega}{\Delta}, \frac{g}{\Delta}, \frac{\Omega'_1}{\Delta'}, \frac{\Omega'_2}{\Delta'}\right\} \ll 1. \quad (3.93)$$

Taking into account conditions (3.93) we rewrite the Hamiltonian (3.92) as

$$\begin{aligned} \tilde{\mathcal{H}} &= \hbar(\Delta + \Delta')|c\rangle\langle c| - \hbar\frac{g\Omega}{\Delta}(a^\dagger|e\rangle\langle g| + h.c.) + 2\hbar\frac{\Omega^2}{\Delta}(|c\rangle\langle c| - |g\rangle\langle g|) \\ &\quad - \hbar\frac{\Omega\Omega'_2}{\Delta}(e^{-i(\Delta'-\Delta)t}|e\rangle\langle g| + h.c.) + 2\hbar\frac{\Omega\Omega'_1}{\Delta}\cos((\Delta' - \Delta)t)(|c\rangle\langle c| - |g\rangle\langle g|) \\ &\quad - \hbar\frac{\Omega'_2\Omega'_1}{\Delta'}(|e\rangle\langle g| + h.c.) + \hbar\frac{g\Omega'_2}{\Delta'}(ae^{-i(\Delta'-\Delta)t} + h.c.)(|c\rangle\langle c| - |e\rangle\langle e|) \\ &\quad + \hbar\frac{\Omega'^2_2}{\Delta'}(|c\rangle\langle c| - |e\rangle\langle e|) + 2\hbar\frac{\Omega'^2_1}{\Delta'}(|c\rangle\langle c| - |g\rangle\langle g|) - \hbar\frac{g\Omega'_1}{\Delta'}(a^\dagger e^{i(\Delta'-\Delta)t}|e\rangle\langle g| + h.c.) \\ &\quad + \hbar\frac{g^2}{\Delta}(aa^\dagger|c\rangle\langle c| + a^\dagger a|e\rangle\langle e|) \end{aligned} \quad (3.94)$$

The Hamiltonian (3.94), in contrast to (3.92), does not couple the level $|c\rangle$ to the levels $|e\rangle$ and $|g\rangle$. Moreover, it performs an effective dynamics involving only the transition $|e\rangle \leftrightarrow |g\rangle$. However, it still contains the AC Stark shift terms as well as terms with an explicit time dependence. The presence of the latter can be neglected by implying the following rotating-wave-approximation (RWA) inequalities

$$\Delta - \Delta' \gg \left\{\frac{\Omega\Omega'_2}{\Delta'}, \frac{\Omega\Omega'_1}{\Delta'}, \frac{\Omega'_2 g}{\Delta'}, \frac{\Omega'_1 g}{\Delta'}\right\}, \quad (3.95)$$

turning Eq. (3.94) into the effective Hamiltonian

$$\mathcal{H}_{\text{eff}} = -\hbar g_{\text{eff}}(a^\dagger\sigma^\dagger + a\sigma) - \hbar\Omega_{\text{eff}}(\sigma^\dagger + \sigma), \quad (3.96)$$

where $g_{\text{eff}} = \Omega g/\Delta$ and $\Omega_{\text{eff}} = \Omega'_1\Omega'_2/\Delta'$, $\sigma^\dagger = |e\rangle\langle g|$ and $\sigma = |g\rangle\langle e|$ and the AC Stark shifts are assumed to be corrected by retuning the laser frequencies [51].

Thus, we have shown that the initial model described by the Hamiltonian (3.92) can be reduced by virtue of the conditions (3.93) and (3.95) to the effective Hamiltonian (3.96) exhibiting an effective coupling of metastable states $|g\rangle$ and $|e\rangle$ with the cavity mode according to the anti-Jaynes-Cummings model and with a classical external driving. Consequently, we have effectively discarded the spontaneous emission processes from the model.

We now consider a strong-driving regime, i.e. when $\Omega_{\text{eff}} \gg g_{\text{eff}}$. Then we may apply to the Hamiltonian (3.96) the same reasoning as in the section 3.2. In this way, and going to interaction picture with respect to the (effective) external driving term, the Hamiltonian of Eq. (3.96) can be written as

$$\mathcal{H}_{\text{eff}}^{\text{int}} = -\hbar \frac{g_{\text{eff}}}{2} (a^\dagger + a)(\sigma^\dagger + \sigma), \quad (3.97)$$

what is analogous to the Hamiltonian (3.31).

So far we have considered the only one possible source of dissipations in our model, namely, spontaneous emission of the upper level $|c\rangle$ which action was neglected using an adiabatic elimination procedure. However, to keep the discussion realistic enough one should take into account dissipation processes connected to the cavity field. Even though, that the modern optical cavities operate in a high quality factor regime, a leakage of the photons out of the cavity has a noticeable impact on an atom-field dynamics. Therefore, the most realistic description of the atom-field dynamics is given by the following master equation

$$\dot{\rho}_{at-f} = -\frac{i}{\hbar} [\mathcal{H}_{\text{eff}}^{\text{int}}, \rho_{at-f}] + \mathcal{L}\rho_{at-f}, \quad (3.98)$$

where the dissipative term is the standard Liouvillean for a damping harmonic oscillator and reads

$$\mathcal{L}\rho_{at-f} = -\frac{\kappa}{2} (a^\dagger a \rho_{at-f} - 2a \rho_{at-f} a^\dagger + \rho_{at-f} a^\dagger a). \quad (3.99)$$

We show in the next subsection how to integrate the master equation (3.98) and to employ its solution for a determination of a decoherence rate of the cavity field.

3.5.2 Monitoring the cavity field decoherence using a one-atom laser

We start by reminding that the unitary dynamics governed by the Hamiltonian (3.96) leads to entanglement of an atom and a cavity field. According to equation (3.33) a resulting atom-field state is a typical representative of the so-called ‘‘Schrödinger cat’’ states. The size of generated coherent states is proportional to an atom-field interaction time τ , so that if the interaction lasts long enough for coherent states $|\alpha\rangle$ and $|-\alpha\rangle$ to become orthogonal, the atom-field state gets a face of EPR state involving two parties, namely, the atom and the field.

However, in a more realistic consideration the dissipation effects should be taken into account. Hence, the atom-field state is given by a density operator which is a solution of the master equation (3.98). Since the dynamics of the atom-field system is ruled by an interplay between the unitary process, leading alone to a coherent superposition state (3.33), and nonunitary leakage of the cavity photons, the density operator of the entire system does not contain, most probably, quantum interference terms and

as a consequence is a statistical mixture. The later happens due to a high sensitivity of the interference terms to the dissipation processes, which, in turn, can be exploit for a monitoring of environmental decoherence.

In order to give a quantitative analysis of the problem we concentrate on an integration of the master equation (3.98). We assume that the atom-field density operator ρ_{at-f} can be expanded in a dressed atomic basis as

$$\rho_{at-f} = |+\rangle\langle+| \otimes \rho_{1f} + |-\rangle\langle-| \otimes \rho_{2f} + |+\rangle\langle-| \otimes \rho_{3f} + |-\rangle\langle+| \otimes \rho_{4f} \quad (3.100)$$

where $|\pm\rangle = (|g\rangle \pm |e\rangle)/\sqrt{2}$ and $\rho_{1f}, \rho_{2f}, \rho_{3f}, \rho_{4f}$ are the weight operators corresponding to the cavity field. The density operators of the field or atom alone can be obtained from ρ_{at-f} by tracing out corresponding degrees of freedom. For instance, the field density operator $\rho_f = \text{Tr}_{at}(\rho_{at-f}) = \rho_{1f} + \rho_{2f}$, so that the operators ρ_{1f} and ρ_{2f} specify completely the cavity field. In contrast, ρ_{3f} and ρ_{4f} are responsible for atom-field entanglement and as a result are sensitive to tracing.

Instead of dealing with the master equation for the atom-field density operator Eq.(3.98) we use an equivalent approach and derive the equations of motion for the weight operators ρ_{if} , $i = 1, 2, 3, 4$. They read

$$\dot{\rho}_{1f} = \frac{\hbar g_{\text{eff}}}{2}([a^\dagger, \rho_{1f}] + [a, \rho_{1f}]) + \mathcal{L}\rho_{1f}, \quad (3.101)$$

$$\dot{\rho}_{2f} = -\frac{\hbar g_{\text{eff}}}{2}([a^\dagger, \rho_{2f}] + [a, \rho_{2f}]) + \mathcal{L}\rho_{2f}, \quad (3.102)$$

$$\dot{\rho}_{3f} = -\frac{\hbar g_{\text{eff}}}{2}(\{a^\dagger, \rho_{3f}\} + \{a, \rho_{3f}\}) + \mathcal{L}\rho_{3f}, \quad (3.103)$$

$$\dot{\rho}_{4f} = \frac{\hbar g_{\text{eff}}}{2}(\{a^\dagger, \rho_{4f}\} + \{a, \rho_{4f}\}) + \mathcal{L}\rho_{4f}. \quad (3.104)$$

The crucial point here, as well as it was in the case of strongly-driven micromaser, is to map the set of operational equations (3.101-3.104) onto an equivalent system of uncoupled differential equation via introducing an operator-function one-to-one correspondence $\chi(\beta)_i = \text{Tr}(\rho_{if}D(\beta))$, $i = 1, 2, 3, 4$. However, unlike in the case of section (3.3), the functions $\chi(\beta)_i$ cannot be interpreted as characteristic functions of the field. The main reason why it is not possible is that the operators ρ_{if} do not possess the whole properties of a density operator. As a consequence, $\chi(\beta)_i$ fulfill only few conditions for a characteristic function. Nevertheless, they are continuous and square-integrable what is enough for our consideration.

Rewriting the equations (3.101-3.104) in terms of χ -functions we arrive at four linear differential equations:

$$\frac{\partial \chi_1}{\partial t} = \frac{i g_{\text{eff}}}{2}(\beta + \beta^*)\chi_1 - \frac{\kappa}{2}|\beta|^2\chi_1 - \frac{\kappa}{2}\left(\beta \frac{\partial}{\partial \beta} + \beta^* \frac{\partial}{\partial \beta^*}\right)\chi_1, \quad (3.105)$$

$$\frac{\partial \chi_2}{\partial t} = -\frac{i g_{\text{eff}}}{2}(\beta + \beta^*)\chi_2 - \frac{\kappa}{2}|\beta|^2\chi_2 - \frac{\kappa}{2}\left(\beta \frac{\partial}{\partial \beta} + \beta^* \frac{\partial}{\partial \beta^*}\right)\chi_2, \quad (3.106)$$

$$\frac{\partial \chi_3}{\partial t} = -ig_{\text{eff}}\left(\frac{\partial}{\partial \beta} - \frac{\partial}{\partial \beta^*}\right)\chi_3 - \frac{\kappa}{2}|\beta|^2\chi_3 - \frac{\kappa}{2}\left(\beta\frac{\partial}{\partial \beta} + \beta^*\frac{\partial}{\partial \beta^*}\right)\chi_3, \quad (3.107)$$

$$\frac{\partial \chi_4}{\partial t} = ig_{\text{eff}}\left(\frac{\partial}{\partial \beta} - \frac{\partial}{\partial \beta^*}\right)\chi_4 - \frac{\kappa}{2}|\beta|^2\chi_4 - \frac{\kappa}{2}\left(\beta\frac{\partial}{\partial \beta} + \beta^*\frac{\partial}{\partial \beta^*}\right)\chi_4. \quad (3.108)$$

Since the equations (3.105-3.108) are uncoupled, we proceed by solving them one by one right from the first one. In order to do so, we alter in the equation (3.105) to Cartesian coordinates, i.e. instead of β and β^* we introduce new coordinates x and y which are connected to the old ones via simple transformations $\beta = x + iy$, $\beta^* = x - iy$. Hence we obtain

$$\frac{\partial \chi_1}{\partial t} = -\frac{\kappa}{2}\left(xG'(x) + x\frac{\partial}{\partial x}\right)\chi_1 - \frac{\kappa}{2}\left(yF'(y) + y\frac{\partial}{\partial y}\right)\chi_1, \quad (3.109)$$

where $G'(x) = x - (2ig_{\text{eff}}/\kappa)$ and $F'(y) = y$. The last equation possesses a simple solution in the following form

$$\chi_1(x, y, t) = \frac{\chi_1^{ss}(x, y)\chi_1^{init}(xe^{-(\kappa t/2)}, ye^{-(\kappa t/2)})}{\chi_1^{ss}(xe^{-(\kappa t/2)}, ye^{-(\kappa t/2)})}, \quad (3.110)$$

here $\chi_1^{ss}(x, y)$ is a steady-state solution (in the limit of $t \rightarrow \infty$) of Eq.(3.109) and $\chi_1^{init}(x, y)$ is an initial χ -function.

We assume that initially the atom and the field were disentangled. Moreover, the cavity field was in vacuum state. Therefore, we may write the initial weight operators as

$$\rho_{1f}(0) = \rho_{2f}(0) = \rho_{3f}(0) = \rho_{4f}(0) = \frac{1}{2}|0\rangle\langle 0|. \quad (3.111)$$

Hence, the initial function $\chi_1^{init}(x, y)$ reads

$$\chi_1^{init}(x, y) = \text{Tr}(\rho_{1f}(0)D(\beta, \beta^*)) = \frac{1}{2}e^{-(|\beta|^2/2)} = \frac{1}{2}e^{-(x^2+y^2)/2}. \quad (3.112)$$

The steady-state solution of Eq.(3.109) can be expressed in terms of functions $G(x) = (x^2/2) - (2ig_{\text{eff}}/\kappa)x$ and $F(y) = y^2/2$ as

$$\chi_1^{ss}(x, y) = e^{-G(x)-F(y)} = e^{-(x^2+y^2)/2}e^{2ig_{\text{eff}}x/\kappa}. \quad (3.113)$$

Taking into account expressions (3.112) and (3.113) we rewrite the general solution of Eq.(3.109) explicitly as

$$\chi_1(x, y, t) = \frac{1}{2} \exp \left\{ -\frac{x^2 + y^2}{2} + \frac{2ig_{\text{eff}}x}{\kappa}(1 - e^{-\kappa t/2}) \right\}. \quad (3.114)$$

It is continuous and square-integrable and consequently possesses a Fourier transform which can be interpreted as the effective Wigner function correspondent to the operator ρ_{1f} . Performing Fourier transformation on the function $\chi_1(x, y, t)$ we obtain

$$W(x, y, t) = \exp \left\{ -2x^2 - 2\left(y + \frac{g_{\text{eff}}}{\kappa}(1 - e^{-\kappa t/2})\right)^2 \right\}. \quad (3.115)$$

The function $W(x, y, t)$ is Gaussian centered at $(x = 0, y = -\frac{g_{\text{eff}}}{\kappa}(1 - e^{-\kappa t/2}))$ and assigns the coherent state $|\alpha(t)\rangle$, where $\alpha(t) = -i\frac{g_{\text{eff}}}{\kappa}(1 - e^{-\kappa t/2})$. Therefore, by virtue of the $\rho_{if} \leftrightarrow \chi_i$ correspondence we may claim that the solution of the equation (3.101) takes form $\rho_{1f}(t) = \frac{1}{2}|\alpha(t)\rangle\langle\alpha(t)|$.

Having at our disposal the solution $\rho_{1f}(t)$ of Eq.(3.101) we can deduce immediately a solution of the equation (3.102). We notice that the equations (3.101) and (3.102) differ from each other only by a sign of the effective coupling constant g_{eff} . Hence, the solution $\rho_{2f}(t)$ of the equation (3.102) can be obtained from $\rho_{1f}(t)$ by inverting the sign of g_{eff} . Consequently, we obtain

$$\rho_{2f}(t) = \frac{1}{2}|-\alpha(t)\rangle\langle-\alpha(t)|; \quad \alpha(t) = -i\frac{g_{\text{eff}}}{\kappa}(1 - e^{-\kappa t/2}). \quad (3.116)$$

Recalling that the density operator of the cavity field is completely determined, at any moment of time, by a sum of the operators $\rho_{1f}(t)$ and $\rho_{2f}(t)$ we conclude that the cavity field is given by a mixture of two coherent field states with opposite phases. In other words, it reads

$$\rho_f(t) = \rho_{1f}(t) + \rho_{2f}(t) = \frac{1}{2}|\alpha(t)\rangle\langle\alpha(t)| + \frac{1}{2}|-\alpha(t)\rangle\langle-\alpha(t)|. \quad (3.117)$$

It is instructive to study a time dependence of the cavity field density operator $\rho_f(t)$. According to Eq.(3.117) for $t = 0$ $\rho_f(0) = |0\rangle\langle 0|$ what agrees with the initial conditions. In the course of time, a mixture of coherent states, which move apart from each other towards their steady state position in phase space, is built. The maximal size of coherent states is reached in the steady-state regime when $t \rightarrow \infty$ and is given by a ration between the effective coupling g_{eff} and cavity decay rate κ .

So far, we have solved the equations of motion for so to say ‘‘diagonal elements’’ of the atom-field density matrix (3.100), namely, for $\rho_{1f}(t)$ and $\rho_{2f}(t)$. They describe perfectly a behaviour of the cavity field alone, however, since our main goal is to study the decoherence in a microscopic-mesoscopic entangled systems we require a knowledge about $\rho_{3f}(t)$ and $\rho_{4f}(t)$ - terms which contain the full information about atom-field entanglement. Their dynamics is described by a pair of operator equations (3.103,3.104) or alternatively by equations (3.107,3.108) for corresponding map functions $\chi_3(\beta, \beta^*, t)$ and $\chi_4(\beta, \beta^*, t)$. In order to solve the equation (3.107) we write it first in a more convenient form:

$$\frac{\partial\chi_3}{\partial t} + \frac{\kappa}{2} \left(\beta + \frac{2ig_{\text{eff}}}{\kappa} \right) \frac{\partial\chi_3}{\partial\beta} + \frac{\kappa}{2} \left(\beta^* - \frac{2ig_{\text{eff}}}{\kappa} \right) \frac{\partial\chi_3}{\partial\beta^*} = -\frac{\kappa}{2}|\beta|^2\chi_3. \quad (3.118)$$

The latter is equivalent to the following system of the linear differential equations of the first order

$$\begin{aligned} \frac{d\beta}{dt} &= \frac{\kappa}{2} \left(\beta + \frac{2ig_{\text{eff}}}{\kappa} \right), \\ \frac{d\beta^*}{dt} &= \frac{\kappa}{2} \left(\beta^* - \frac{2ig_{\text{eff}}}{\kappa} \right), \end{aligned} \quad (3.119)$$

$$\frac{d\chi_3}{dt} = -\frac{\kappa}{2}|\beta|^2\chi_3,$$

with the initial conditions

$$\text{for } t = 0 : \beta(0) = f_1; \beta^*(0) = f_2; \chi_3(\beta(0), \beta^*(0), 0) = \frac{1}{2} \exp\left(-\frac{f_1 f_2}{2}\right), \quad (3.120)$$

which are in agreement with conditions on the cavity field Eq.(3.111).

The system (3.119) together with the initial conditions (3.120) possesses general solution of the form

$$\chi_3(\beta, \beta^*, t) = \frac{1}{2} \exp\left(-\frac{|\beta|^2}{2} + \frac{ig_{\text{eff}}}{\kappa}(\beta^* - \beta)(1 - e^{-\frac{\kappa t}{2}}) - \frac{2g_{\text{eff}}^2}{\kappa}t + \frac{4g_{\text{eff}}^2}{\kappa^2}(1 - e^{-\frac{\kappa t}{2}})\right). \quad (3.121)$$

Before going into details of an analysis of this solution we notice that a solution of the equation (3.108) can be obtained from Eq.(3.121) by inverting a sign of g_{eff} so that it reads

$$\chi_4(\beta, \beta^*, t) = \frac{1}{2} \exp\left(-\frac{|\beta|^2}{2} - \frac{ig_{\text{eff}}}{\kappa}(\beta^* - \beta)(1 - e^{-\frac{\kappa t}{2}}) - \frac{2g_{\text{eff}}^2}{\kappa}t + \frac{4g_{\text{eff}}^2}{\kappa^2}(1 - e^{-\frac{\kappa t}{2}})\right). \quad (3.122)$$

The most striking feature of the solutions (3.121) and (3.122) is their explicit exponential time dependence, namely, factor $e^{-\frac{2g_{\text{eff}}^2}{\kappa}t}$ which is not present in the solutions for χ_1 and χ_2 . This factor leads to a vanishing of the χ_3 and χ_4 for sufficient long times t . Therefore, the final atom-field state in the limit of $t \rightarrow \infty$ is fully characterized by a mixed state of the following form

$$\rho_{at-f}^{ss} = |+\rangle\langle +| \rho_{1f}^{ss} + |-\rangle\langle -| \rho_{2f}^{ss} = \frac{1}{2}|+\rangle\langle +| |\alpha^{ss}\rangle\langle \alpha^{ss}| + \frac{1}{2}|-\rangle\langle -| |-\alpha^{ss}\rangle\langle -\alpha^{ss}|, \quad (3.123)$$

where $\alpha^{ss} = -i\frac{g_{\text{eff}}}{\kappa}$, i.e. it is given by a ratio between coherent pumping and incoherent decay of the cavity field and depending on a mode of operation can be greater or less than one. Hence, as it was expected, the steady-state solution of the master equation (3.98) is a mixed state given by Eq.(3.123) and does not contain terms responsible for atom-field entanglement.

Nevertheless, the atom-field interference terms which are indeed described by χ_3 and χ_4 are present in an intermediate regime. In order to illustrate their behaviour we consider a complex Fourier transform of χ_3 and χ_4 :

$$W_3(u, v, t) = \exp\left(-2\left(u + \frac{ig_{\text{eff}}}{\kappa}(1 - e^{-\frac{\kappa t}{2}})\right)^2 - 2v^2 + \frac{4g_{\text{eff}}^2}{\kappa^2}\left(1 - \frac{\kappa t}{2} - e^{-\frac{\kappa t}{2}}\right)\right) \quad (3.124)$$

$$W_4(u, v, t) = \exp\left(-2\left(u - \frac{ig_{\text{eff}}}{\kappa}(1 - e^{-\frac{\kappa t}{2}})\right)^2 - 2v^2 + \frac{4g_{\text{eff}}^2}{\kappa^2}\left(1 - \frac{\kappa t}{2} - e^{-\frac{\kappa t}{2}}\right)\right) \quad (3.125)$$

where $\xi = u + iv$ and the complex Fourier transform is defined as

$$W_{3,4}(\xi, \xi^*, t) = W_{3,4}(u, v, t) = \frac{1}{\pi} \int d^2\beta e^{\xi\beta^* - \xi^*\beta} \chi_{3,4}(\beta, \beta^*, t) \quad (3.126)$$

In spite of the complexity of the functions $W_3(u, v, t)$ and $W_4(u, v, t)$ their sum is real and reads

$$\begin{aligned} W_3(u, v, t) + W_4(u, v, t) &= 2 \exp\left(-2(u^2 + v^2 - \frac{g_{\text{eff}}^2}{\kappa^2}(1 - e^{-\frac{\kappa t}{2}})^2) + \frac{4g_{\text{eff}}^2}{\kappa^2}(1 - e^{-\frac{\kappa t}{2}})\right) \\ &\quad \times \exp\left(-\frac{2g_{\text{eff}}^2}{\kappa}t\right) \cos\left(4\frac{g}{\kappa}(1 - e^{-\frac{\kappa t}{2}})u\right). \end{aligned} \quad (3.127)$$

This sum represents a cosine-like oscillations along the real axis in phase space with a time-dependent frequency $\omega(t) = 4\frac{g}{\kappa}(1 - e^{-\frac{\kappa t}{2}})$ and exponentially decaying amplitude.

We point out here that according to equations (3.121) and (3.122) functions $\chi_3(t)$ and $\chi_4(t)$ for short evolution times $\kappa t \ll 1$ assign the following field states

$$\rho_{3f}(t) = |\tilde{\alpha}\rangle\langle -\tilde{\alpha}| ; \rho_{4f}(t) = |-\tilde{\alpha}\rangle\langle \tilde{\alpha}| ; \tilde{\alpha} = -\frac{ig_{\text{eff}}t}{2}. \quad (3.128)$$

On the other hand, according to (3.116) the operators $\rho_{1f}(t)$ and $\rho_{2f}(t)$ on the same time scale take form

$$\rho_{1f}(t) = |\tilde{\alpha}\rangle\langle \tilde{\alpha}| ; \rho_{2f}(t) = |-\tilde{\alpha}\rangle\langle -\tilde{\alpha}| ; \tilde{\alpha} = -\frac{ig_{\text{eff}}t}{2}. \quad (3.129)$$

As a consequence, on the short time scale the atom-field density matrix represents a pure ‘‘Schrödinger cat’’ like state:

$$\rho_{at-f}(t) = |\Psi\rangle\langle \Psi| ; |\Psi\rangle = \frac{1}{\sqrt{2}}(|+\rangle|\tilde{\alpha}\rangle + |-\rangle|-\tilde{\alpha}\rangle). \quad (3.130)$$

However, at a later time, decay of the cavity field transforms this pure state to a mixture. This happens because $\rho_{3f}(t)$ and $\rho_{4f}(t)$ do not evolve under decoherence as $|\alpha(t)\rangle\langle -\alpha(t)|$ and $|-\alpha(t)\rangle\langle \alpha(t)|$ but in a slightly different manner what leads at the end to their vanishing on the large time scale. This decoherence induced pure-mixed-state transition has been both theoretically and experimentally studied in the case of high-Q microwave cavities [29]. There are several objective advantages for utilizing a microwave CQED setup for these proposes. First of all, a lifetime of a photon in a microwave resonator is significantly higher then in an optical one. Hence, since most of the schemes for generation of the atom-field ‘‘Schrödinger cat’’ states are multi-step, they can only be implemented in the microwave regime. Nevertheless, there is a serious drawback, it is not possible to measure a microwave cavity field directly. Hence, one uses atoms passing through a cavity in order to determine a state of a cavity field.

Here we present a scheme which combines simultaneously generation of superposition states(see Eq.(3.130)) and monitoring of their decoherence resulting is the state Eq.(3.123). It operates in optical domain and has an important advantage of a single step generation of a required state. Moreover, the information about a cavity field now can be obtained from two channels: 1. from a photodetector measuring an output cavity field 2. from a fluorescence signal of an atom placed inside a cavity playing a

role of a generating medium. The only obstacle which we still need to remove on a way towards direct observation of the cavity field decoherence is expressed by Eq.(3.117). In other words, the “off-diagonal” terms of the atom-field density matrix, namely $\rho_{3f}(t)$ and $\rho_{4f}(t)$ do not directly contribute to a density matrix of the cavity field $\rho_f(t)$. As a consequence, no direct measurement performed on the field can reveal their behaviour. To overcome this difficulty we present the following approach.

Let us consider a situation when an atom and initial vacuum field are subjected to the dynamics governed by the master equation (3.98). After a time τ the atom-field density operator reads

$$\rho_{at-f}(\tau) = |+\rangle\langle+| \otimes \rho_{1f}(\tau) + |-\rangle\langle-| \otimes \rho_{2f}(\tau) + |+\rangle\langle-| \otimes \rho_{3f}(\tau) + |-\rangle\langle+| \otimes \rho_{4f}(\tau), \quad (3.131)$$

where $\rho_{if}(\tau)$, $i = \overline{1,4}$ are the solutions of the system (3.101-3.104). Imagine that at time τ we perform a fast rotation of atomic state by an angle θ so that

$$\begin{aligned} |+\rangle &\rightarrow U^\dagger(\theta)|+\rangle = \sin\theta|+\rangle + \cos\theta|-\rangle \\ |-\rangle &\rightarrow U^\dagger(\theta)|-\rangle = \cos\theta|+\rangle - \sin\theta|-\rangle. \end{aligned}$$

Then the rotated atom-field density operator $\rho_{at-f}^\theta(\tau) = U^\dagger(\theta)\rho_{at-f}(\tau)U(\theta)$ rewritten in the original atomic basis reads

$$\begin{aligned} \rho_{at-f}^\theta(\tau) &= |+\rangle\langle+| \otimes (\rho_{1f}(\tau) \sin^2\theta + \rho_{2f}(\tau) \cos^2\theta + (\rho_{3f}(\tau) + \rho_{4f}(\tau)) \cos\theta \sin\theta) \\ &+ |-\rangle\langle-| \otimes (\rho_{1f}(\tau) \cos^2\theta + \rho_{2f}(\tau) \sin^2\theta - (\rho_{3f}(\tau) + \rho_{4f}(\tau)) \cos\theta \sin\theta) \\ &+ |+\rangle\langle-| \otimes ((\rho_{1f}(\tau) - \rho_{2f}(\tau)) \cos\theta \sin\theta - \rho_{3f}(\tau) \sin^2\theta + \rho_{4f}(\tau) \cos^2\theta) \\ &+ |-\rangle\langle+| \otimes ((\rho_{1f}(\tau) - \rho_{2f}(\tau)) \cos\theta \sin\theta + \rho_{3f}(\tau) \cos^2\theta - \rho_{4f}(\tau) \sin^2\theta). \end{aligned} \quad (3.132)$$

We deduce from Eq.(3.132) that the “diagonal” terms of the rotated density operator $\rho_{at-f}^\theta(\tau)$ in the original $|\pm\rangle$ basis now contain an information about atom-field coherences ρ_{3f} and ρ_{4f} . Therefore, we may develop two strategies how to extract this information experimentally.

The first strategy consists of a measurement of an atomic population in either $|+\rangle$ or $|-\rangle$ state immediately after the performed rotation. Practically, this is equivalent to a measurement of a fluorescence signal from the atom. The probability for, say, detection of the $|+\rangle$ atomic state reads

$$\begin{aligned} P_{|+\rangle\langle+|}(\tau) &= \text{Tr}(|+\rangle\langle+|\rho_{at-f}(\tau)) \\ &= \text{Tr}(\rho_{1f}(\tau)) \sin^2\theta + \text{Tr}(\rho_{2f}(\tau)) \cos^2\theta + \text{Tr}(\rho_{3f}(\tau) + \rho_{4f}(\tau)) \cos\theta \sin\theta \\ &= \frac{1}{2} \left(1 + \sin(2\theta) e^{-\frac{2g_{\text{eff}}^2}{\kappa}\tau + \frac{4g_{\text{eff}}^2}{\kappa^2}(1-e^{-\frac{\kappa\tau}{2}})} \right), \end{aligned} \quad (3.133)$$

where we have employed the following property of the χ -functions: $\text{Tr}(\rho_{if}(\tau)) = \chi_i(0, 0, \tau)$, $i = \overline{1, 4}$. Thus, measuring $P_{|+\rangle\langle+|}$ for different evolution times τ and different rotation angles θ we obtain directly the decoherence rate of the pure atom-field state in an optical cavity.

The second strategy is to perform a joint measurement on an atom and field after the rotation of atomic states. Experimentally this means that we measure, say, a fluorescence signal from the atom and at the same time count the photons leaking out of the cavity. Such an approach, however, does not bring much new information about the intracavity processes, nevertheless, it may help to check a consistency of the measurement itself. The outcome of the joint measurement reads

$$\begin{aligned}
P_{|+\rangle\langle+|}^n(\tau) &= \text{Tr}(|+\rangle\langle+|a^\dagger a \rho_{at-f}(\tau)) \\
&= \text{Tr}(a^\dagger a \rho_{1f}) \sin^2 \theta + \text{Tr}(a^\dagger a \rho_{2f}) \cos^2 \theta + \text{Tr}(a^\dagger a (\rho_{3f} + \rho_{4f})) \cos \theta \sin \theta \\
&= \frac{1}{2} + \frac{g_{\text{eff}}^2}{\kappa^2} (1 - e^{-\frac{\kappa\tau}{2}})^2 \\
&\quad + \frac{1}{2} \sin(2\theta) \left(\frac{1}{2} - \frac{g_{\text{eff}}^2}{\kappa^2} (1 - e^{-\frac{\kappa\tau}{2}})^2 \right) e^{-\frac{2g_{\text{eff}}^2}{\kappa} \tau + \frac{4g_{\text{eff}}^2}{\kappa^2} (1 - e^{-\frac{\kappa\tau}{2}})}. \tag{3.134}
\end{aligned}$$

The crucial step in the last equation is to use a familiar connection between the χ -functions and moments of the field then we may write

$$\text{Tr}(a^\dagger a \rho_{if}(\tau)) = \frac{\partial \chi_i(\beta, \beta^*, \tau)}{\partial \beta \partial (-\beta^*)} \Big|_{\beta=\beta^*=0}, \quad i = \overline{1, 4}. \tag{3.135}$$

Chapter 4

Quantum state engineering in Cavity QED

Quantum state engineering is basically deterministic control over the coherent dynamics of suitable quantum mechanical systems, has become a fascinating perspective of modern physics. Its basic concepts, developed in atomic and molecular physics, has been adopted and further evolved in the light of the perspectives of their applications in the field of quantum computation and communication. For this purpose a number of individual two-state quantum systems (qubits) should be addressed and coupled in a controlled way. Several physical realizations of qubits such as trapped ions, NMR, and quantum optical systems have been considered. In this chapter we discuss the questions of implementation of cavity QED models, introduced in the preceding chapter, for instance, micromaser and one-atom laser in the controlled production of nonclassical states of radiation field as well as atomic qubits. Generation of nonclassical light typically involves active devices and nonlinear optical media, which couple two or more modes of the field through the nonlinear susceptibility of the matter. Since the nonlinear susceptibilities are small, the effective implementation of nonlinear interactions is experimentally challenging, and the resulting processes are generally characterized by a low efficiency. Here, we show how to exploit the micromaser in order to produce high purity Fock states with high efficiency. Moreover, we introduce a scheme for generation of the maximally-entangled states of two atomic qubits in an optical resonator using a no-photon measurement of the cavity field. Finally, we show how the dispersive interaction between an ensemble of atoms, prepared in a ground state, and a cavity field gives a realization of a robust quantum memory.

4.1 Generation of Fock states using the micromaser

We have already mentioned in the preceding chapter that the micromaser offers an unique opportunity for a generation of the cavity field states including pure Fock states and their mixtures with the properties on demand. Since the Fock states are pure quan-

tum feature of a radiation, they are of very importance for a testing the fundamentals of quantum theory, as well as for applications in quantum cryptography and quantum computation [52]. In this section we introduce two elegant schemes suitable for a generation of the pure Fock states, and present the results of their experimental realization. We analyze the latter in the next chapter by applying a novel quantum state tomography technique developed there.

Let us take a closer look at the micromaser field steady-state solution Eq.(3.47). Consider a situation, when the number of thermal photons $\bar{n}_{th} \rightarrow 0$ i.e. when the environment is cooled down to zero temperature. As a consequence, the micromaser steady-state solution (3.47) takes a simpler form

$$\rho_{nn}^{ss} = \rho_{00}^{ss} \frac{(r/\gamma)^n}{n!} \prod_{k=1}^n \left[\sin^2(g\tau\sqrt{k}) \right]. \quad (4.1)$$

Hence, if for some $n = N$, $\sin^2(g\tau\sqrt{N}) = 0$ then according to Eq.(4.1) $\rho_{nn}^{ss} = 0$ for any $n > N$. In this case, we say that the steady-state photon number is “trapped” below $n = N$. Corresponding cavity field state is a statistical mixture of the Fock states up to $n = N$ with different weights.

One of the remarkable trapped states is the trapped vacuum state ($N = 1$) which takes place if $g\tau$ is an integer multiple of π . Physically, the trapped vacuum state means that the atoms perform one or more full Rabi cycles while their passage through the cavity and leave it in the upper state again without contributing to the cavity field, so that the field remains in the initially prepared vacuum state. In order to illustrate that we have plotted on Fig.(4.1) the mean photon number of the steady-state micromaser field as a function of the Rabi angle $g\tau$. Here dips at $g\tau = \pi$ and $g\tau = 2\pi$ indicate trapped vacuum states. Experimentally, states with trapped number up to three have been observed by group in Garching [53].

Despite a theoretical beauty of the idea to generate the Fock states using the trapping conditions one meets a conceptual problem of contaminations of the Fock states built with the trapped numbers N higher than 1. Therefore, a method which allows to design a pure Fock state on demand is desirable. We recall that in the usual micromaser operation atoms enter a cavity in the upper state of the maser transition and undergo the Jaynes-Cummings interaction with the maser field. The interaction of an atom with a field in the state $|n\rangle$ leads to an entangled atom-field state which is a superposition of states $|e\rangle|n\rangle$ and $|g\rangle|n+1\rangle$ with coefficients depending on the interaction time τ and the value of n . Consequently, by measuring an atom in the lower state $|g\rangle$ after the interaction we reduce the field state to $|n+1\rangle$ i.e. we produce a Fock state whose purity can reach unity depending on the parameters. If we do not measure an atom, then, taking into account dissipation processes, the field state represents a statistical mixture of the Fock states $|n\rangle$ and $|n+1\rangle$. Theoretically, starting from an initial vacuum micromaser field, one can build a pure Fock state $|n\rangle$ using n atoms. However a question arises: How to justify that we have prepared a pure Fock state? Since the micromaser field can not be measured directly by means of photodetectors,

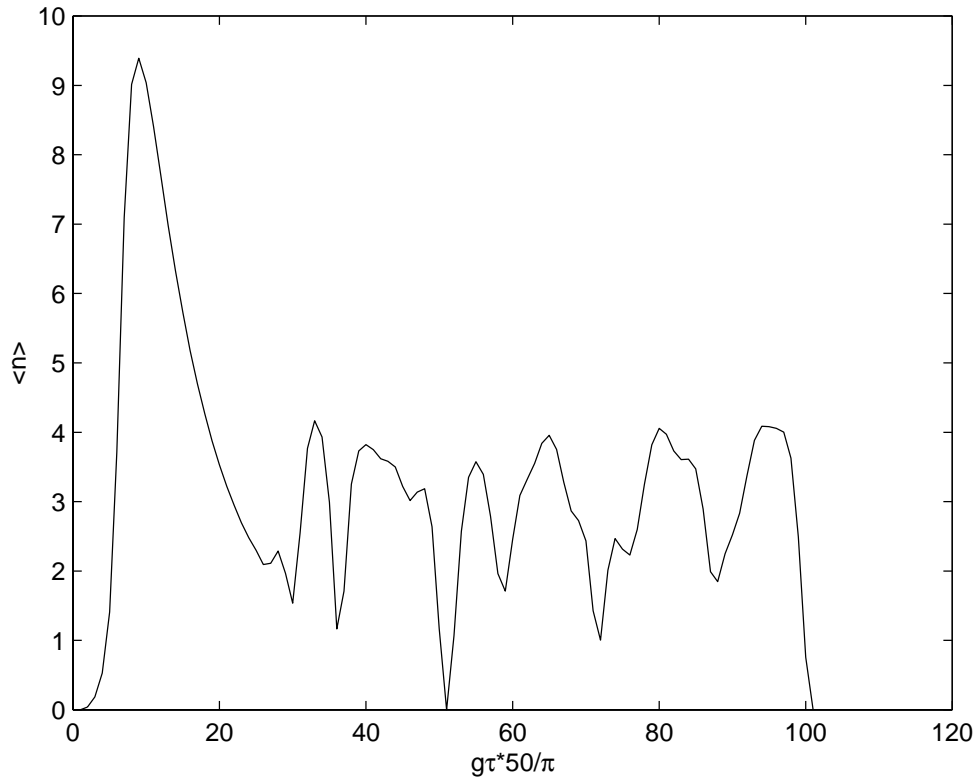


Figure 4.1: Mean photon number of the micromaser steady-state field at zero temperature for $(r/\gamma) = 10$.

the only way to determine it is to measure a levels statistics of a probe atom. Detailed treatment of this problem is given in the next chapter. Here we only mention that the inversion of a probe atom as a function of the interaction time allows one to determine, unambiguously, a state of the cavity field [54, 55, 56]. The above described Fock states generation technique has been successfully realized in experiments [12, 13]. The experimental results from the work of B.Varcoe *et al.*[13] are depicted on the figure (4.2). According to them, highly pure vacuum and one photon states have been produced.

4.2 Generation of maximally-entangled atomic states in optical cavities

Entanglement, first considered by Schrödinger [57], is recognized nowadays as a cornerstone in the fundamentals of quantum physics and as a source of diverse applications in quantum information and computation [52]. In particular, entangled states of discrete systems, such as two or more qubits, play an important role in testing fundamental properties of quantum theory. They allow one, for instance, to prove the nonlocal character of quantum mechanics versus local hidden-variable theories. Maximally-entangled states of two-qubit systems, which are a prerequisite for a two qubit logic operations,

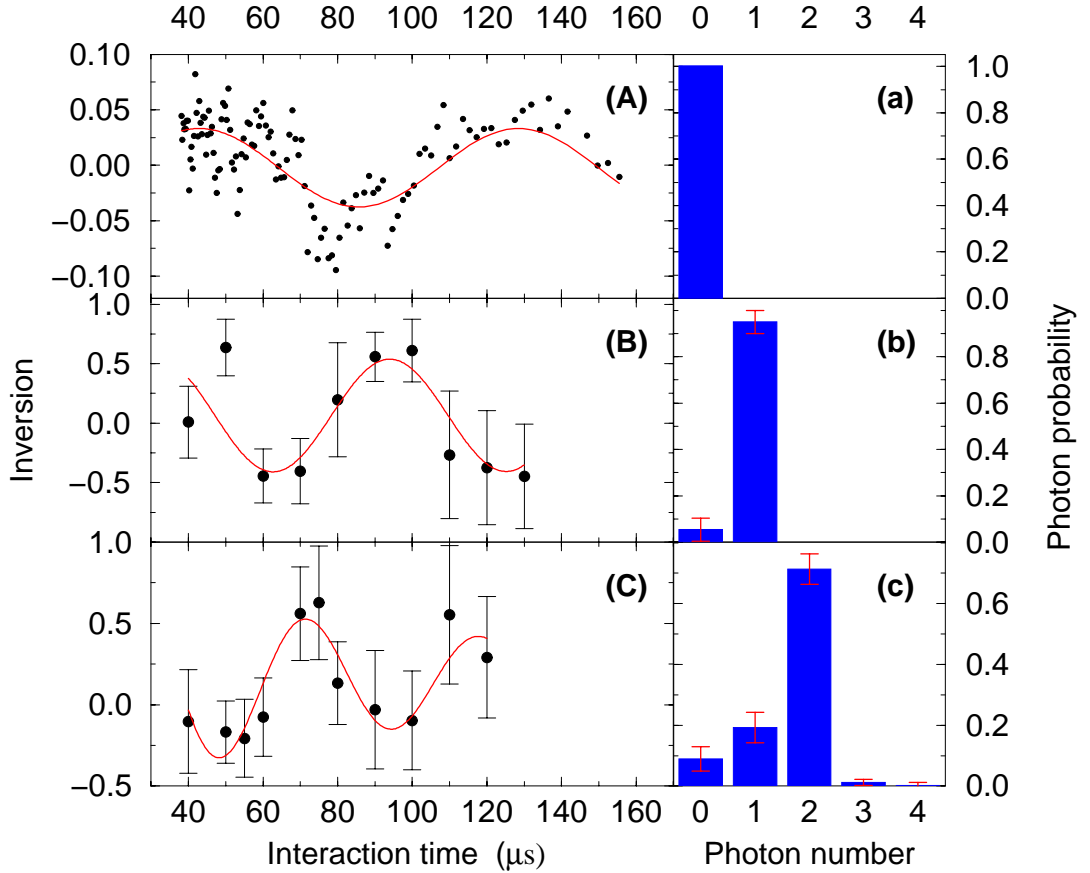


Figure 4.2: Rabi oscillation of the atomic inversion of a probe atom for the Fock states of a cavity field with $n = 0$ (A), $n = 1$ (B), $n = 2$ (C) and corresponding photon distributions of the cavity field (a), (b), (c).

have already been produced experimentally in photonic systems [58] and in the internal degrees of freedom of atoms interacting with a microwave cavity [17, 59]. Nevertheless, neither photonic polarization qubits nor flying atomic qubits in a microwave domain are optimal candidates for a scalable quantum information processing. In the case of trapped ions [60, 61], maximally entangled states have been created through the manipulation of their collective motion, but cavity QED devices are needed for transferring the stored information. Therefore, an optimal realization of a scalable quantum network [62] combines optical cavities with atoms inside playing a role of quantum information processors and photons connecting different nodes of the network [63, 64, 65, 66, 67]. The important step towards practical implementation of such a networking is an ability to generate a maximally-entangled state of two qubits in a node. Despite the diverse and recent theoretical proposals [68, 69, 70] generation of maximally-entangled states of two atoms inside an optical cavity has not yet been accomplished in the lab.

Here, we introduce a scheme [71] that addresses most of the problems of a realistic

4.2 Generation of maximally-entangled atomic states in optical cavities 69

model for entangling two atoms inside an optical cavity: dissipative processes, atomic localization, detection efficiency and purity of the generated entangled state. The proposed protocol allows not only to generate but also to purify the maximally-entangled states of two atoms. The protocol is of a quantum-non-demolition kind, where successive no-photon detection of the cavity field projects and purifies sequentially the desired atomic state. In contrast to recent proposals, our scheme produces atomic Bell states as a steady state of the two-atom-field interaction in correlation with the vacuum field state, which makes our method robust to cavity field decoherence. It combines a reasonably high success probability ($\sim 1/2$) with very high fidelity (~ 1) for a wide range of parameters. The proposed scheme does not rely on a high detection efficiency as long as it is based on discrimination, through projection, between a vacuum field state (zero detector clicks) and orthogonal coherent states (necessarily more than one detector click).

The presented scheme essentially relies on the model of a one-atom laser considered in the section 3.5. It has been shown there that a properly selected external lasers configuration allows to achieve an effective atom-cavity interaction given by the Hamiltonian (3.97) and to monitor a transition from the atom-field entangled state (3.130) to the mixed state (3.123). As a consequence of that consideration, a natural question arises: How much changes the atom-field dynamics if we place simultaneously N identical atoms ($N > 1$) inside the cavity? We assume at first that all atoms have the same coupling strengths¹, the same internal structure and fields applied, depicted on fig.(3.13). Hence, we may write the atom-field Hamiltonian as

$$\begin{aligned}
 \mathcal{H} = & \hbar\omega_e \sum_{j=1}^N |e_j\rangle\langle e_j| + \hbar\omega_c \sum_{j=1}^N |c_j\rangle\langle c_j| + \hbar\omega_f a^\dagger a \\
 & + \hbar g (a^\dagger \sum_{j=1}^N |e_j\rangle\langle c_j| + a \sum_{j=1}^N |c_j\rangle\langle e_j|) + \hbar\Omega (e^{-i(\omega_c-\Delta)t} \sum_{j=1}^N |c_j\rangle\langle g_j| + h.c.) \quad (4.2) \\
 & + \hbar\Omega'_2 (e^{-i(\omega_c-\omega_e-\Delta')t} \sum_{j=1}^N |c_j\rangle\langle e_j| + h.c.) + \hbar\Omega'_1 (e^{-i(\omega_c-\Delta')t} \sum_{j=1}^N |c_j\rangle\langle g_j| + h.c.).
 \end{aligned}$$

Here, as it was in the section 3.5, ω_c and ω_e are the Bohr frequencies associated with the transitions $|c_j\rangle \leftrightarrow |g_j\rangle$ and $|e_j\rangle \leftrightarrow |g_j\rangle$, $j = \overline{1, N}$, respectively, while ω_f is the frequency of the cavity mode and a (a^\dagger) the associated annihilation (creation) operator. As we have mentioned above, we suppose all atoms to couple to the cavity mode with similar strength g , taken as real as all other coupling strengths $\{\Omega, \Omega'_1, \Omega'_2\}$ for the sake of simplicity.

We assume here, just as like in the section 3.5 that the atomic level $|c_j\rangle$, $j = \overline{1, N}$ is corrupted by spontaneous emission, whereas the levels $|e_j\rangle$ and $|g_j\rangle$ are metastable,

¹We will consider later a more realistic situation when the couplings are different.

so that to discard spontaneous emission from our model, as well as to avoid undesired atomic transitions we require again the conditions Eqs.(3.93,3.95) to be fulfilled. Furthermore, we consider the strong-(external)driving regime, where $\Omega_{\text{eff}} \gg g_{\text{eff}}$. In this way, by analogy to a one-atom case we may finally write the effective interaction Hamiltonian between N atoms and the cavity in the interaction picture as

$$\mathcal{H}_{\text{eff}}^{\text{int}} = -\hbar \frac{g_{\text{eff}}}{2} (a^\dagger + a) \sum_{j=1}^N (\sigma_j^\dagger + \sigma_j), \quad (4.3)$$

where $g_{\text{eff}} \equiv \Omega g / \Delta$, $\sigma_j^\dagger = |e_j\rangle\langle g_j|$ and $\sigma_j = |g_j\rangle\langle e_j|$.

A similar Hamiltonian was obtained in [27] for the case of N two-level Rydberg atoms interacting with a microwave cavity and a strong external field, yielding a wide family of multipartite entangled N -atom-cavity states. Here, we have shown that a similar effective Hamiltonian can be realized in the optical domain but, in contrast to the microwave regime, no atom-field entanglement is expected to survive long enough for practical purposes due to the comparatively lower achievable ratios g_{eff}/κ (κ being the cavity decay rate). Nevertheless, it is possible to design strategies for using this faster dissipation process to produce entanglement in the atomic degrees of freedom.

Since from the beginning we have claimed an interest to the generation of the maximally-entangled states of two atoms we proceed our consideration for the case when $N = 2$. Let us assume that at the time $t = 0$ both atoms were prepared in the ground state $|gg\rangle$ and the cavity field in the vacuum $|0\rangle$, so that the initial atom-field state is $|gg\rangle|0\rangle \equiv |g_1\rangle \otimes |g_2\rangle \otimes |0\rangle$. The resulting atom-field state at $t = \tau$ is then a subject of the unitary evolution given by the Hamiltonian (4.3) and reads

$$|\Psi(\tau)\rangle = \frac{1}{2}|++\rangle|2\alpha(\tau)\rangle + \frac{1}{2}|--\rangle|-2\alpha(\tau)\rangle + \frac{1}{\sqrt{2}}|\Psi^+\rangle|0\rangle, \quad (4.4)$$

where

$$\begin{aligned} |++\rangle &\equiv |+_1\rangle|+_2\rangle = \frac{1}{\sqrt{2}}(|g_1\rangle + |e_1\rangle) \times \frac{1}{\sqrt{2}}(|g_2\rangle + |e_2\rangle), \\ |--\rangle &\equiv |-_1\rangle|-_2\rangle = \frac{1}{\sqrt{2}}(|g_1\rangle - |e_1\rangle) \times \frac{1}{\sqrt{2}}(|g_2\rangle - |e_2\rangle), \end{aligned}$$

such that the maximally-entangled atomic state $|\Psi^+\rangle$ reads

$$|\Psi^+\rangle = \frac{1}{\sqrt{2}}(|-_1\rangle|+_2\rangle + |+_1\rangle|-_2\rangle), \quad (4.5)$$

and the amplitude of the coherent states generated is

$$\alpha(\tau) = i \frac{g_{\text{eff}}\tau}{2}. \quad (4.6)$$

We observe that the atomic states $|-_1+_2\rangle$ and $|+_1-_2\rangle$ of Eq. (4.5) are eigenstates of the collective operator $\sigma_x = \sigma_{x,1} + \sigma_{x,2} = \sum_{j=1}^2 (\sigma_j^\dagger + \sigma_j)$ with eigenvalues equal to zero. This

4.2 Generation of maximally-entangled atomic states in optical cavities 71

fact explains, following Eqs. (4.3) and (4.4), the persistent correlation of the vacuum field state with the atomic state $|\Psi^+\rangle$ through the whole unitary evolution. These states are called dark states [21]. Note that the size of the coherent state, estimated by the amplitude α in Eq. (4.6), is proportional to the time τ of the unitary process described by the effective Hamiltonian of Eq. (4.3). If $|\alpha|$ is large enough ($|\alpha| \geq 2$), such that we can consider the states $|\alpha\rangle$, $|0\rangle$ and $|\alpha\rangle$ as mutually orthogonal, then a measurement of the vacuum field in the atom-field state of Eq. (4.4) projects the atomic state onto $|\Psi^+\rangle$ with probability 1/2. In consequence, measuring a zero-photon state leaking the cavity mode, would be enough for producing an atomic $|\Psi^+\rangle$ state with high fidelity. However, one would require (unavailable) detectors with high efficiency and the (already available) strong-coupling regime of optical cavities [23, 22].

The next step is to extend our method to less demanding regimes and more realistic conditions, involving field damping, weak-coupling regime and finite efficiency detection, without increasing the complexity of the experimental requirements. The first complication on the way of the realistic treatment of the problem is to incorporate a cavity field decay into our model. This may be done by writing down the following master equation describing the atom-field dynamics

$$\dot{\rho}_{at-f} = -\frac{i}{\hbar}[\mathcal{H}_{\text{eff}}^{\text{int}}, \rho_{at-f}] + \mathcal{L}\rho_{at-f}, \quad (4.7)$$

where the (field) dissipative term is described by

$$\mathcal{L}\rho_{at-f} = -\frac{\kappa}{2}(a^\dagger a \rho_{at-f} - 2a \rho_{at-f} a^\dagger + \rho_{at-f} a^\dagger a).$$

The master equation (4.7) has a similar to a one-atom laser case structure and therefore can be solved analytically using the same techniques introduced in the section 3.5. Here, we will only sketch a solution method. First of all one should expand the atom-field density operator ρ_{at-f} in the $|\pm\rangle$ basis of both atoms. Then substituting ρ_{at-f} in Eq.(4.7) one obtains a system of 16 operator equations to solve. This system can be solved using a map on χ -functions as it was done in the case of a one-atom laser.

Finally, the steady-state solution of the master equation reads

$$\begin{aligned} \rho_{at-f}^{ss} &= \frac{1}{4}|++\rangle\langle++| \otimes |2\tilde{\alpha}\rangle\langle 2\tilde{\alpha}| + \frac{1}{4}|--\rangle\langle--| \otimes |-2\tilde{\alpha}\rangle\langle -2\tilde{\alpha}| \\ &+ \frac{1}{2}|\Psi^+\rangle\langle\Psi^+| \otimes |0\rangle\langle 0|, \end{aligned} \quad (4.8)$$

with $\tilde{\alpha} = i\frac{g_{\text{eff}}}{\kappa}$. In contrast to the pure state of Eq. (4.4), the steady state of the atom-cavity system is a mixed state with no quantum correlation between the atoms and the field. The remarkable feature of the state in Eq. (4.8) is that the atomic state $|\Psi^+\rangle$ is still correlated with the vacuum of the cavity field. Henceforth, if one performs a first no-photon measurement of the cavity field in the steady state, the projected (normalized) atomic density operator is

$$\rho_{at}^{ss} = \frac{e^{-|2\tilde{\alpha}|^2}}{1 + e^{-|2\tilde{\alpha}|^2}}(|++\rangle\langle++| + |--\rangle\langle--|) + \frac{1}{1 + e^{-|2\tilde{\alpha}|^2}}|\Psi^+\rangle\langle\Psi^+|. \quad (4.9)$$

When $|\tilde{\alpha}| > 1$, in the strong-coupling regime [23, 22], the condition $|2\tilde{\alpha}|^2 \gg 1$ is automatically fulfilled and Eq. (4.9) reduces to the maximally entangled atomic state

$$\rho_{at}^{ss} = |\Psi^+\rangle\langle\Psi^+|. \quad (4.10)$$

with unity fidelity and success probability $1/2$.

If $|\tilde{\alpha}| < 1$, in the weak-coupling regime, the desired atomic state of Eq.(4.10) will be contaminated by other contributions as shown in Eq. (4.9). In this case, we are still able to develop a protocol which purifies the atomic state $|\Psi^+\rangle$ via a successive application of the same scheme. We repeat our procedure second time, shining a similar laser system on our new initial atom-cavity state

$$\rho_{at-f} = \rho_{at}^{ss} \otimes |0\rangle\langle 0| \quad (4.11)$$

until it reaches a new steady state, followed by a measure of a no-photon event with a certain finite probability. By repeating this sequence of steps N times, we arrive at the projected atomic density operator

$$\begin{aligned} \rho_{at}^{ss}(N) &= \frac{e^{-N|2\tilde{\alpha}|^2}}{1 + 2e^{-N|2\tilde{\alpha}|^2}} (|++\rangle\langle++| + |--\rangle\langle--|) \\ &+ \frac{1}{1 + 2e^{-N|2\tilde{\alpha}|^2}} |\Psi^+\rangle\langle\Psi^+|. \end{aligned} \quad (4.12)$$

For a given $|\tilde{\alpha}|$, even in the weak-coupling regime, we can always choose a number of repetitions N such that $e^{-N|2\tilde{\alpha}|^2} = 0$, warranting a highly pure atomic state $|\Psi^+\rangle$. In this case, the fidelity of the state $|\Psi^+\rangle$ is given by

$$F(N) = \langle\Psi^+|\rho_{at}^{ss}(N)|\Psi^+\rangle = \frac{1}{1 + 2e^{-N|2\tilde{\alpha}|^2}}, \quad (4.13)$$

with success probability

$$P_{suc} = \frac{1}{2} \frac{1}{1 + e^{-|2\tilde{\alpha}|^2}} \prod_{m=2}^N \frac{1}{1 + 2e^{-m|2\tilde{\alpha}|^2}}. \quad (4.14)$$

Note that even for $|\tilde{\alpha}| \sim 1$, and $N = 1$ or 2 , the fidelity $F(N) \sim 1$.

The no-photon detection, in competition with the less likely detection of the coherent states $|\pm\tilde{\alpha}\rangle$, assures a minor sensitivity to the low efficiency of the detectors. This is a natural consequence of the fact that if one photon is emitted (but not detected), there is a finite probability of a second photon being emitted, as long as it is one of the two possible coherent states that were selected in the measurement process [72].

So far we have assumed that the atom-field coupling strengths are the same for both atoms. However, in a real experiment a control over a position of the atoms in the cavity is not complete. Therefore, we can not guaranty the equivalence of both couplings. Hence, it is important to estimate the influence of atomic localization on the

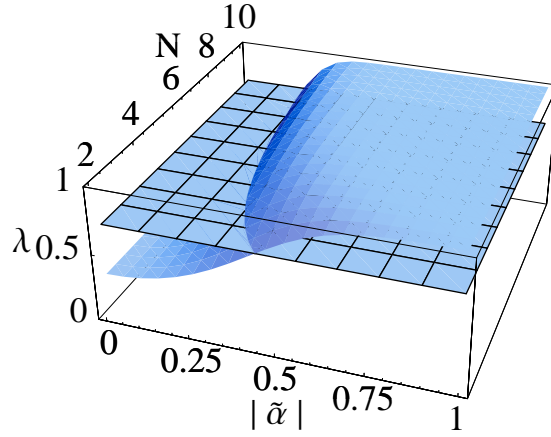


Figure 4.3: Violation of the Bell inequality.

generation of entanglement, as long as our method relies strongly on the production of dark states [21]. The fidelity of the purified dark state in Eq. (4.10) follows $F = 1/1+\epsilon^2$. Here, $\epsilon \equiv \delta g/\kappa$, where δg is the differential variation of the atom-field coupling due to the differential variation in the localization of the two atoms. The parameter ϵ changes very slowly with possible errors in the atomic locations, due to their intrinsic cosine dependence. For realistic parameters, see [73], a maximal localization error of 10% of an optical wavelength yields $\epsilon \approx 0.1$. This implies a fidelity $F > 0.99$, showing the robustness of the proposed scheme.

It was both theoretically [74] and experimentally [75] shown that a family of mixed states, similar to that of Eq. (4.12),

$$\rho = \frac{1-\lambda}{2}(|++\rangle\langle++| + |--\rangle\langle--|) + \lambda|\Psi^+\rangle\langle\Psi^+|, \quad (4.15)$$

violates the Bell inequality if and only if $\lambda > \frac{1}{\sqrt{2}}$. In our case λ is a function of two parameters, $|\tilde{\alpha}|$ and N . In fig.(4.3), we plot the surface $\lambda(|\tilde{\alpha}|, N)$ cut by a plane corresponding to the boundary value $\frac{1}{\sqrt{2}}$. There, we can clearly see that it is possible to cross the threshold parameter $\lambda = 1/\sqrt{2}$ by increasing the number N of repetitions and the amplitude $\tilde{\alpha}$ in the proposed scheme. This transition shows a local parameterized evolution from a mixture (with classical correlations) to a maximally-entangled atomic state (with quantum correlations), as was discussed in [74, 75].

Finally, we illustrate our protocol with a variant for direct generation of another maximally-entangled state of the Bell kind. We assume that in the previous scheme, see fig.(3.13), the coupling strength is $\Omega = 0$ and the detuning frequencies are $\Delta_1 = \Delta_2 = \Delta$. Suppose now that the atoms couple differently to the cavity mode in such a way that the coupling strengths have the same absolute values but the opposite phases ($g_1 = |g|, g_2 = -|g|$). In this case, the adiabatic elimination conditions of Eq. (3.93)

reduce to

$$\left\{ \frac{\Omega'_1}{\Delta}, \frac{\Omega'_2}{\Delta}, \frac{|g|}{\Delta} \right\} \ll 1. \quad (4.16)$$

Therefore, the effective Hamiltonian in the interaction picture, after imposing the strong-(external)driving regime $\Omega_{\text{eff}} \ll |g'_{\text{eff}}|$, with $g'_{\text{eff}} = \Omega'_1 g / \Delta$, reads

$$\tilde{H}_{\text{eff}}^{\text{int}} = \hbar \frac{g'_{\text{eff}}}{2} (a^\dagger + a) \sum_{j=1}^2 (-1)^j (\sigma_j^\dagger + \sigma_j). \quad (4.17)$$

The Hamiltonian of Eq. (4.17) is slightly different from the Hamiltonian of Eq. (4.3) and, when substituted in Eq. (4.7), yields the atom-field steady state

$$\begin{aligned} \rho_{at-f}^{ss} &= \frac{1}{4} | - + \rangle \langle + - | \otimes | 2\beta \rangle \langle 2\beta | + \frac{1}{4} | + - \rangle \langle - + | \otimes | - 2\beta \rangle \langle - 2\beta | \\ &+ \frac{1}{2} | \Phi^+ \rangle \langle \Phi^+ | \otimes | 0 \rangle \langle 0 |, \end{aligned} \quad (4.18)$$

where $|\beta\rangle$ and $| - \beta \rangle$ are coherent states with amplitude $|\beta| = \frac{g'_{\text{eff}}}{\kappa}$ and

$$|\Phi^+\rangle = \frac{1}{\sqrt{2}} (|+1\rangle|+2\rangle + |-1\rangle|-2\rangle)$$

is another maximally-entangled Bell state. Purification of the state $|\Phi^+\rangle$, out of the steady state in Eq. (4.18), can be done by following steps similar to the ones before.

From a practical point of view, the coupling of the atoms to the cavity mode, with a similar or an opposite phase, is a task that could be achieved by using of an ion trap (fixed atoms) or by implementing an optical collimator (falling atoms).

4.3 Multipartite entanglement using atomic coherences

In the preceding section we have studied a problem of generation of entanglement of two qubits represented by two two-level atoms. As we have seen this problem is of great importance for the quantum information processing applications. However, it is also of great experimental complexity to achieve a coupling of two atoms(ions) to a cavity. Nevertheless, experiments involving macroscopic atomic ensembles coupled to optical cavities have become a routine [76, 77, 78]. The atomic ensembles, on one hand, due to a lack of precise experimental control over them, can not be used as quantum processing devices but, on the other hand, they are ideal for an implementation of the quantum memory devices [79, 80] and quantum repeaters [81] recognized as a necessary ingredient for quantum information communication [82].

The question of storage and retrieval of light pulses has been extensively studied both theoretically and experimentally [83, 79, 80, 84, 78, 85, 86, 87, 88, 77]. The light

pulses can be stored in atomic coherences and later the atomic coherence can be converted back into the original light pulses [83, 88]. The original work has been extended to storage of pulses of moderate powers [89, 90]. Hence, a natural question arises: can one store and retrieve the quantum state of the field? This is the question to be addressed in this section. It is shown how coherently prepared atomic systems interacting with far-detuned elliptical fields can serve the purpose. It is also demonstrated how the atomic coherences can be used for generating a variety of nonclassical states, including multiatom entangled states.

4.3.1 Model

The model consists of N identical two-level atoms, with hyperfine structure splitting as depicted in fig.(4.4), coupled to two mutually orthogonal modes of a quantized electromagnetic field described by creation (annihilation) operators a_-^\dagger, a_+^\dagger (a_-, a_+) with the ground and excited-state coupling strengths Ω_+ and Ω_- , respectively. The Hamiltonian for the atom-field system reads

$$\begin{aligned} \mathcal{H} = & \hbar \frac{\omega_1}{2} \sum_{j=1}^N (|e_-\rangle\langle e_-| - |g_+\rangle\langle g_+|)_j + \hbar \frac{\omega_2}{2} \sum_{j=1}^N (|e_+\rangle\langle e_+| - |g_-\rangle\langle g_-|)_j \\ & + \hbar \omega_f (a_+^\dagger a_+ + a_-^\dagger a_-) + \hbar (\Omega_- a_- \sum_{j=1}^N |e_-\rangle\langle g_+|_j + h.c.) \\ & + \hbar (\Omega_+ a_+ \sum_{j=1}^N |e_+\rangle\langle g_-|_j + h.c.), \end{aligned} \quad (4.19)$$

where ω_1 and ω_2 are the frequencies of the transitions $|g_+\rangle \leftrightarrow |e_-\rangle$ and $|g_-\rangle \leftrightarrow |e_+\rangle$, respectively, and ω_f is the field frequency.

We consider a case when the cavity modes frequency ω_f is far detuned from a resonance with atomic transition frequencies ω_1 and ω_2 . In other words we require that the conditions $\omega_1 - \omega_f = \omega_2 - \omega_f = \Delta \gg \{|\Omega_+|, |\Omega_-|\}$ are fulfilled. Using a standard adiabatic elimination technique [50] we expand the Hamiltonian Eq.(4.19) up to the second order in $|\Omega_+|/\Delta$ and $|\Omega_-|/\Delta$ obtaining the following effective Hamiltonian

$$\begin{aligned} \mathcal{H}_1 = & \hbar \frac{|\Omega_-|^2}{\Delta} a_-^\dagger a_- \sum_{j=1}^N (|e_-\rangle\langle e_-| - |g_+\rangle\langle g_+|)_j \\ & + \hbar \frac{|\Omega_+|^2}{\Delta} a_+^\dagger a_+ \sum_{j=1}^N (|e_+\rangle\langle e_+| - |g_-\rangle\langle g_-|)_j \\ & + \frac{2\hbar}{\Delta} (|\Omega_-|^2 \sum_{j=1}^N |e_-\rangle\langle e_-|_j + |\Omega_+|^2 \sum_{j=1}^N |e_+\rangle\langle e_+|_j). \end{aligned} \quad (4.20)$$

The effective Hamiltonian Eq.(4.20), in contrast to the original Eq.(4.19), does not couple ground atomic states $\{|g_{-}\rangle_j, |g_{+}\rangle_j\}$, $j = 1, N$ to the excited ones. Therefore, if one starts from the initial atomic ground state, the only relevant contribution to the atom-field dynamics from the Hamiltonian Eq.(4.20) is

$$\mathcal{H}' = -\hbar \frac{|\Omega_{-}|^2}{\Delta} a_{-}^{\dagger} a_{-} \sum_{j=1}^N (|g_{+}\rangle\langle g_{+}|)_j - \hbar \frac{|\Omega_{+}|^2}{\Delta} a_{+}^{\dagger} a_{+} \sum_{j=1}^N (|g_{-}\rangle\langle g_{-}|)_j. \quad (4.21)$$

Let us analyze the Hamiltonian Eq.(4.21) in more details. We can rewrite it in more transparent way by introducing the collective atomic operator

$$\hat{R}_z = \frac{1}{2} \sum_{j=1}^N (|g_{+}\rangle\langle g_{+}| - |g_{-}\rangle\langle g_{-}|)_j. \quad (4.22)$$

As a consequence, one can express the operators $\sum_{j=1}^N (|g_{+}\rangle\langle g_{+}|)_j$ and $\sum_{j=1}^N (|g_{-}\rangle\langle g_{-}|)_j$ in terms of \hat{R}_z as follows:

$$\frac{1}{2} \pm \hat{R}_z = \sum_{j=1}^N (|g_{\pm}\rangle\langle g_{\pm}|)_j. \quad (4.23)$$

For the sake of simplicity hereafter we suppose that the two field modes have identical coupling strengths, i.e. $|\Omega_{+}| = |\Omega_{-}| = \Omega$. Finally, the effective Hamiltonian Eq.(4.21) will read

$$\mathcal{H}' = \frac{\hbar\Omega^2}{\Delta} \hat{R}_z (a_{+}^{\dagger} a_{+} - a_{-}^{\dagger} a_{-}). \quad (4.24)$$

Apart from the \hat{R}_z operator, we construct the lowering \hat{R}_{-} and raising \hat{R}_{+} operators,

$$\hat{R}_{-} = \sum_{j=1}^N (|g_{-}\rangle\langle g_{+}|)_j, \quad (4.25)$$

$$\hat{R}_{+} = \sum_{j=1}^N (|g_{+}\rangle\langle g_{-}|)_j. \quad (4.26)$$

The operators \hat{R}_{\pm} and \hat{R}_z fulfill the following commutation relations:

$$[\hat{R}_{-}, \hat{R}_{+}] = -2\hat{R}_z, [\hat{R}_z, \hat{R}_{\pm}] = \pm\hat{R}_{\pm}, \quad (4.27)$$

and therefore describe an effective spin $J = \frac{N}{2}$ system, where N is the number of atoms in the sample. As next step we define the eigenvectors of the z component of the total spin operator \hat{R}_z as follows:

$$\hat{R}_z |m\rangle = \hbar m |m\rangle, J = \frac{N}{2}, m = -J, -J + 1, \dots, J - 1, J. \quad (4.28)$$

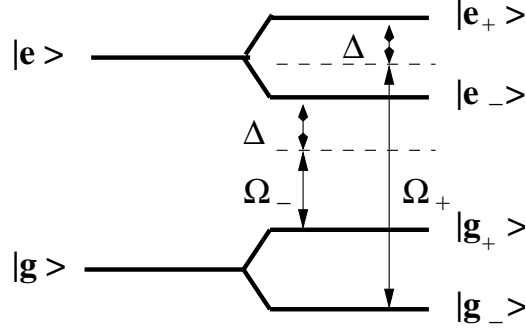


Figure 4.4: Internal atomic structure

Action of the lowering (raising) operators \hat{R}_- (\hat{R}_+) on the eigenvectors of \hat{R}_z can be calculated in a straightforward manner:

$$\hat{R}_-|m\rangle = \hbar\sqrt{(J+m)(J-m+1)}|m-1\rangle, \quad (4.29)$$

$$\hat{R}_+|m\rangle = \hbar\sqrt{(J-m)(J+m+1)}|m+1\rangle. \quad (4.30)$$

The set of eigenvectors $|m\rangle, m = \overline{-J, J}$ of the operator \hat{R}_z is trivially connected to the previously introduced set $\{|g_-\rangle_j, |g_+\rangle_j\}, j = \overline{1, N}$, which denotes the hyperfine structure of the ground states of atoms. For example $| -J \rangle = \prod_{k=1}^N |g_-\rangle_k$, and consequently we will call the state $| -J \rangle$ the ground state.

Returning back to the Hamiltonian (4.24) we introduce, following Schwinger, a set of field operators

$$\hat{N}_- = a_-^\dagger a_+, \hat{N}_+ = a_+^\dagger a_-, \hat{N}_z = a_+^\dagger a_+ - a_-^\dagger a_- \quad (4.31)$$

and compare the algebraic properties of the two sets of operators, $\hat{N}_z, \hat{N}_-, \hat{N}_+$ and $\hat{R}_z, \hat{R}_-, \hat{R}_+$. Operators \hat{N}_z, \hat{N}_- and \hat{N}_+ satisfy the same commutation relations as in Eq.(4.27), i.e.

$$[\hat{N}_-, \hat{N}_+] = -2\hat{N}_z, [\hat{N}_z, \hat{N}_\pm] = \pm\hat{N}_\pm. \quad (4.32)$$

Therefore, coming back to the Hamiltonian Eq.(4.24), one can say that there is effectively a spin-spin interaction along the z-axis, where one of the spins is the collective spin of the atomic sample and the other one is some effective spin which corresponds to two orthogonally polarized modes of the cavity field. As a result, the Hamiltonian Eq.(4.24) is very suitable for spin quantum nondemolition measurement (QND) as well as being a good candidate for the generation of spin-squeezed atomic samples [91, 81, 76, 92].

4.3.2 Mesoscopic superposition of atomic states

Having at our disposal the effective atom-field interaction Hamiltonian (4.24) we demonstrate how to create mesoscopic superposition of atomic states [57] employing

atomic coherent states. Let us define an atomic coherent state $|\theta, \phi\rangle$ as [93]

$$|\theta, \phi\rangle = R_{\theta, \phi} | -J \rangle = \sum_{m=-J}^J \binom{2J}{J+m}^{\frac{1}{2}} \left[\cos\left(\frac{\theta}{2}\right) \right]^{J-m} \left[\sin\left(\frac{\theta}{2}\right) e^{-i\phi} \right]^{J+m} |m\rangle. \quad (4.33)$$

Here $R_{\theta, \phi}$ is the rotation operator which rotates the initial ground state $| -J \rangle$ by an angle θ around an axis $\hat{m} = (\sin(\phi), -\cos(\phi), 0)$. From the practical point of view the coherent atomic state in Eq.(4.33) can be prepared in a number of ways; for example, by applying a homogeneous magnetic field along the \hat{m} axis to the ground state of the atomic sample $| -J \rangle$. The other interesting and popular possibility is to use short pulses and Raman transitions, a technique that has been extensively used by, for example, Wineland and co-workers [94].

We consider interaction of the coherently prepared atomic sample with an elliptically polarized photon which we represent by the state $|\psi_f\rangle = \alpha|1_+, 0_-\rangle + \beta|0_+, 1_-\rangle$, ($|\alpha|^2 + |\beta|^2 = 1$). Note that $\alpha = 0$ or $\beta = 0$ corresponds to a circularly polarized field. A calculation by means of the interaction Hamiltonian Eq.(4.24) leads to the following atom-field state

$$\begin{aligned} |\Psi_{at-f}\rangle &= \exp(-i\phi_0 t \hat{N}_z \hat{R}_z) |\theta, \phi\rangle |\psi_f\rangle \\ &= \alpha |\theta, \phi + \phi_0 t\rangle |1_+, 0_-\rangle e^{i\phi_0 t J} + \beta |\theta, \phi - \phi_0 t\rangle |0_+, 1_-\rangle e^{-i\phi_0 t J}. \end{aligned} \quad (4.34)$$

Here $\phi_0 = \Omega^2/\Delta$ and t is the interaction time. The atom-field state Eq.(4.34) describes a situation when atoms and the cavity field get entangled. Detection of the field polarization in the direction of, say, x leads to an atomic state

$$|\Psi\rangle_{cat} = \alpha e^{i\phi_0 t J} |\theta, \phi + \phi_0 t\rangle + \beta e^{-i\phi_0 t J} |\theta, \phi - \phi_0 t\rangle. \quad (4.35)$$

This corresponds to a mesoscopic superposition of coherent states for the atomic system. This is the case as long as the two coherent states in the above equation are not orthogonal, i.e.

$$\langle \theta, \phi + \phi_0 t | \theta, \phi - \phi_0 t \rangle = \exp(2iJ\phi_0 t) [\cos(\phi_0 t) - i \cos(\theta) \sin(\phi_0 t)]^{2J}. \quad (4.36)$$

is not zero. From Eq.(4.36) follows that for a particular choice of parameters (for example, $\phi_0 t = \frac{\pi}{2}$ and $\theta = \frac{\pi}{2}$, $\forall \phi$) the overlap between coherent atomic states is zero and hence, the atom-field state in Eq.(4.34) becomes a mixed state. From the practical point of view the hyperfine splitting states are extremely robust to decoherence. We have thus shown how the dispersive interactions on ground-state atoms can produce long-lived mesoscopic superpositions. It is worth mentioning that dispersive interaction has been already considered in the context of two-level atoms to produce both atomic and field cat states [95, 29, 96, 97, 98]. Moreover it has been experimentally realized by Haroche and co-workers [29] for a case of one two-level Rydberg atom interacting with a microwave cavity field. Here we use ground-state coherence to demonstrate the

same result. Consider, for example, a single atom $J = 1/2$ interacting with a field in coherent state $|\alpha, \beta\rangle$. Obviously, the state of the combined system at time t will be

$$\begin{aligned} |\psi(t)\rangle &\equiv \exp(-i\phi_0 t \hat{N}_z \hat{R}_z) |\alpha, \beta\rangle |\theta, \phi\rangle \\ &= \cos\frac{\theta}{2} |g_-\rangle |\alpha e^{i\phi_0 t/2}, \beta e^{-i\phi_0 t/2}\rangle + e^{-i\phi} \sin\frac{\theta}{2} |g_+\rangle |\alpha e^{-i\phi_0 t/2}, \beta e^{i\phi_0 t/2}\rangle. \end{aligned} \quad (4.37)$$

Clearly, measurement of the atomic population in a state different from $|g_{\pm}\rangle$ produces a ‘‘Schrödinger cat’’ state of the radiation field.

There is another one important consequence from Eq.(4.34). It is clear from Eq.(4.34) that the probability of detecting the field state unchanged after the coupling to atoms strongly depends on the atom-field interaction time. If we choose $\phi_0 t = \pi$ and make the number of atoms in the sample N even, the cavity field after interaction is in the same state as the initial cavity field. This is reminiscent of the trapping states in a micromaser [53] where for certain field states the atoms leave the cavity in the original states. To verify the above statement we consider the evolution operator $\exp(-i\pi \hat{N}_z \hat{R}_z)$ for $\phi_0 t = \pi$. Since \hat{N}_z has the eigenvalues ± 1 and for even N , \hat{R}_z has an integer eigenvalue and the above evolution operator is the same for the two eigenvalues of \hat{N}_z . Thus the field would revert to the original state. For odd N , the eigenvalues of $\left(\frac{N}{2} + \hat{R}_z\right)$ are integers and then the two evolution operators $\exp(\mp i\pi \hat{R}_z)$ will differ by an overall phase factor π ($e^{2i\pi N/2}$). In this case the state of the output field will be $\alpha|1_+, 0_-\rangle - \beta|0_+, 1_-\rangle$.

4.3.3 Generation of the multiatom entangled states

We return now back to the question announced at the beginning of this section, namely, how to create a multiatom entangled state using the interaction (4.24) and atomic coherences (4.33).

Let us have a closer look at the atomic coherent state of Eq.(4.33). We notice that it can be written as a product of single atom coherent states over all atoms, i.e.

$$\begin{aligned} |\theta, \phi\rangle &= \left| \prod_{j=1}^N |\theta, \phi\rangle_j \right. \\ |\theta, \phi\rangle_j &= \sin(\theta/2) e^{-i\phi} |g_+\rangle_j + \cos(\theta/2) |g_-\rangle_j, \end{aligned} \quad (4.38)$$

and hence the mesoscopic superposition Eq.(4.35) can be expressed as

$$|\Psi\rangle_{cat} = \alpha e^{i\phi_0 t J} \prod_{j=1}^N |\theta, \phi + \phi_0 t\rangle_j + \beta e^{-i\phi_0 t J} \prod_{j=1}^N |\theta, \phi - \phi_0 t\rangle_j. \quad (4.39)$$

The latter is a multi-atom entangled state involving N parties. We further note that individual coherent states $|\theta, \phi + \phi_0 t\rangle_j$ and $|\theta, \phi - \phi_0 t\rangle_j$ become orthogonal, i.e. $\langle \theta, \phi -$

$\phi_0 t |\theta, \phi + \phi_0 t\rangle = 0$ if $\phi_0 t = \pi/2$, $\theta = \pi/2$. In this case Eq.(4.39) becomes an example of GHZ states [99]. Therefore, depending on the choice of the atom-field interaction time one can switch from an entangled atomic state Eq.(4.39) to the maximally-entangled atomic GHZ state.

It is only left to demonstrate how our system can be used to store the quantum state of the field via atomic coherence. This is the quantum counterpart of holography in which the object information is stored in a hologram using a reference field. The hologram when irradiated by a coherent field, recovers the information on the object. Clearly Eq.(4.34) already shows how the information about the field state is stored in atomic ground-state coherence. Note that this is long-lived storage since we use the ground states of the atomic systems. It is now shown how this quantum hologram can be read to retrieve the information on the field. One possibility is to measure the atomic population in the state $|g_-\rangle$. This is easily done by applying a laser pulse polarized appropriately so as to move the population from $|g_-\rangle$ (and not from $|g_+\rangle$) to an excited state and to measure the subsequent fluorescence. This measurement will project the state Eq.(4.34) on to a state of the field given by

$$|\psi_f\rangle_{-J} \rightarrow \left(\cos \frac{\theta}{2}\right)^{2J} (\alpha |1_+, 0_-\rangle e^{i\phi_0 t J} + \beta |0_+, 1_-\rangle e^{-i\phi_0 t J}). \quad (4.40)$$

Thus the stored state of the field is recovered apart from a relative phase factor $2J\phi_0 t$. Note that this phase factor is known a priori from the preparation process of the hologram.

Chapter 5

Quantum state reconstruction in Cavity QED

To produce a required quantum state is only half the work. It is equally important to justify whether the correct state has been prepared. This problem can be formulated even more generally. Given a particular quantum mechanical system, how to determine its state? On the other hand, in the chapter 2, it has been shown that any quantum state can be equivalently described in terms of a quasidistribution function in associated quantum phase space. Hence, a suitable question can be asked: is it possible to measure experimentally a quasidistribution function of a given quantum state? In principle, we are free to use any of quasidistribution functions however, from the mathematical point of view, only the Wigner function is a well-behaved mathematical object. The Q- and P-quasidistributions, in general, can not express an arbitrary state in terms of continuous function. Furthermore, following the approach advocated by Lamb [100], we would like to have an operational definition of the Wigner function, that is, definition which is based on an experimental setup [101, 102, 103, 104, 105]. In other words, we ought to know, at least in principle, which apparatus is necessary for the task of a direct measurement of the Wigner function of a quantum system.

In this chapter we address the question of the operational definition of the Wigner function for a simple, but rather instructive quantum system, namely, a particle in an arbitrary symmetrical potential. Depending on the form of the potential this system may model a wide spectrum of quantum problems ranging from a hydrogen atom to the Jaynes-Cummings model. At first, we give an introduction to the pioneer results in the field of operational definition of the Wigner function. Then we discuss a question of the reconstruction of the Wigner function of a micromaser field and introduce its novel operational definition in terms of the Fresnel transform of an atomic inversion. Finally, we consider general integral transform for the definition of the Wigner function of a particle in a symmetrical potential.

5.1 Operational definition of the quantum quasidistribution functions

This section is aimed at introducing a procedure of determination of the Wigner function which would correspond to a realistic physical measurement. As a model quantum system, the Wigner function of which we want to specify, we take a free particle in one dimension. This is of course the simplest case, nevertheless, it allows to present an operational definition of the Wigner function pioneered by Wódkiewicz [106] and Royer [107].

We start by reminding the original definition of the Wigner function Eq.(2.26) introduced in the chapter 2 for a case of a pure state of the free particle, i.e. when $\rho = |\phi\rangle\langle\phi|$:

$$W(q, p) = \int_{-\infty}^{+\infty} dx e^{-(i/\hbar)px} \phi^*(q + \frac{1}{2}x) \phi(q - \frac{1}{2}x). \quad (5.1)$$

On the other hand, following Wódkiewicz, we would like to measure the probability of finding our particle in a well defined state $|\psi\rangle$. This probability is equal to $\text{Tr}(\rho P)$, where ρ is the density operator of the particle and $P = |\psi\rangle\langle\psi|$ is a projection operator on the state $|\psi\rangle$. The state of the particle ρ is unknown, however, varying the state $|\psi\rangle$ we, in principle, can determine it by recording the probabilities $\text{Tr}(\rho|\psi\rangle\langle\psi|)$. At the same time, to vary the state $|\psi\rangle$ means to displace it in a controlled manner simultaneously in a coordinate and momentum and as the result to explore the whole space, determining a position and momentum of the particle. The mathematical notion of the displacement operator $D(p, q)$ in the coordinate q and momentum p has been introduced in Eq.(2.35). Therefore, we can write the probability to measure the state of the particle in $D^{-1}(p, q)|\psi\rangle\langle\psi|D(p, q)$ as

$$P(q, p) = \text{Tr}(\rho D^{-1}(p, q)|\psi\rangle\langle\psi|D(p, q)). \quad (5.2)$$

Assuming that the particle has been initially prepared in the pure state, say, $\rho = |\phi\rangle\langle\phi|$ and evaluating the trace in the coordinate representation we obtain

$$P(q, p) = \left| \int dx e^{-(i/\hbar)px} \psi^*(x + q) \phi(x) \right|^2. \quad (5.3)$$

The latter can be further rewritten as

$$P(q, p) = \int dx \int dp' W_\psi(q + x, p + p') W_\phi(x, p'), \quad (5.4)$$

where according to Eq.(5.1) we have defined the Wigner function for the displaced state $|\psi\rangle$ as W_ψ and the Wigner function for the original state of the particle $|\phi\rangle$ as W_ϕ .

Hence, we can interpret Eq.(5.4) as an operational definition of the Wigner function of the unknown pure state ρ in terms of probability distribution function $P(q, p)$.

On the other hand, the $P(q, p)$ itself is an overlap between the detected (W_ϕ) and “filtering” (W_ψ) Wigner functions. The notion of necessity of a filtering device for a direct measurement of the Wigner function was emphasized in [106]. It has been also shown there that the projector $P = |\psi\rangle\langle\psi|$ can be interpreted as such a filter.

One of the possible physical realization of this operational scheme relies on a measurement of the coordinate and momentum of the free particle. One can, in principle, measure them by applying an interaction potential centered at the position q of the kind $U_q(x)$. By changing the q and measuring the amplitude of the scattered wave packet of the particle one gets the probability distribution $P(q, p)$ which defines the original Wigner function of the particle.

Theoretically, the presented operational definition can be generalized to a case of a particle(particles) in an arbitrary potential(potentials). However, in practice, there are cases when a system of interest cannot be accessed for a direct measurement. For instance, a single mode of the microwave cavity does not allow any direct observation. In this situation an interaction with a well-accessible supplementary system should be employed in order to deduced an information on the system of interest. As a consequence, an optimal operational definition based on the information from the ancilla is required. Such a definition will of course depend on the type of system-ancilla interaction which in its turn must satisfy possible theoretical and experimental requirements. For example, it should be relatively fast in order to avoid possible effects of decoherence due to a weak coupling with the environment. This is the case of the next section where we derive an operational definition of the Wigner function of harmonic oscillator, which models a single mode of a micromaser field as well as a motion of an ion in an ion trap, is optimized with respect to decoherence and based on a Fresnel transform of the population of a two-level ancilla atom.

5.2 Fresnel representation of the Wigner function

Many methods to reconstruct the Wigner function [4] of a cavity field or the motional state of a harmonic oscillator have been proposed [106, 107, 108, 109]. In particular, the Wigner function of a cavity field can be expressed in terms of the measured atomic inversion [55, 54]. This operational scheme [110] lives off the dispersive interaction between the atom and the field. Since this scheme requires long interaction times, and as a result it is less robust to decoherence, an operational definition of the Wigner function based on a resonant interaction is desirable. The method of nonlinear homodyning [111] and quantum state endoscopy [112] fulfill this need, but require rather complicated reconstruction schemes.

In contrast, the Fresnel representation proposed here is rather elementary. It is based on the resonant interaction of an atom with a single mode of the electromagnetic field and unlike the earlier works it is the atomic dynamics that performs the major part of the reconstruction. It expresses the value of the Wigner function at a phase space point α as a weighted time integral of the measured atomic dynamics caused by

the state displaced by α . The weight function is the Fresnel phase factor. Since this method can be applied to a cavity field as well as a trapped ion [113] we use a harmonic oscillator as a model system. However, we will show that this approach can easily be generalized to non-harmonic oscillators.

Our definition relies on controlled displacements [113, 114] of the quantum state of interest and the observation of Rabi oscillations of a two-level atom(ancilla) interacting resonantly with this field. The measurement scheme can be sketched as follows:

1. The two-level atom(ancilla) is prepared in the upper state $|e\rangle$. The state of interest is displaced into the fixed point α of phase space.
2. The ancilla interacts resonantly with the displaced cavity field for the time τ . The interaction is described by the Jaynes-Cummings model Eq.(3.20).
3. The state of the ancilla is recorded immediately after the interaction.

According to Eq.(3.24),

$$P_g(\tau; \alpha) = \frac{1}{2} - \frac{1}{2} \sum_{n=0}^{\infty} P_n(\alpha) \cos(2\sqrt{n+1}\tau) \quad (5.5)$$

is the probability [115, 116] of finding the atom in the ground state $|g\rangle$ as a function of dimensionless interaction time τ and complex-valued displacement α . Here $P_n(\alpha) \equiv \langle n | \hat{D}(\alpha) \hat{\rho} \hat{D}^\dagger(\alpha) | n \rangle$ denotes the occupation statistics of the state $\hat{\rho}$ displaced by the displacement operator $\hat{D}(\alpha)$.

On the other hand, the Wigner function $W(\alpha)$ of the original state $\hat{\rho}$ is determined [2] by the alternating sum Eq.(2.45)

$$W(\alpha) \equiv \frac{2}{\pi} \sum_{n=0}^{\infty} (-1)^n P_n(-\alpha) \quad (5.6)$$

of the probabilities P_n . Hence, we can find the Wigner function from the atomic dynamics when we measure the probabilities P_g for different interaction times and solve Eq. (5.5) for the occupation probability $P_n(\alpha)$. However, this method has two important disadvantages. First of all it relies on the inversion of a system of linear equation where one must invert the matrix built of $\cos(2\sqrt{n+1}\tau)$ which in general is not numerically stable since its determinant is close to zero. This numerical problem can be overcome by implementing the singular value decomposition method rather than a direct inversion scheme. Secondly, it operates with quite big arrays of data which require high operational time.

However, there is no need to evaluate the probabilities P_n explicitly. In the spirit of Wódkiewicz, we can obtain the Wigner function directly from the atomic dynamics P_g without ever calculating P_n , making use of the integral relation

$$\frac{2}{\pi\sqrt{i}} \int_0^\infty d\tau \exp(i\tau^2/\pi) \cos(2\sqrt{n}\tau) = (-1)^n. \quad (5.7)$$

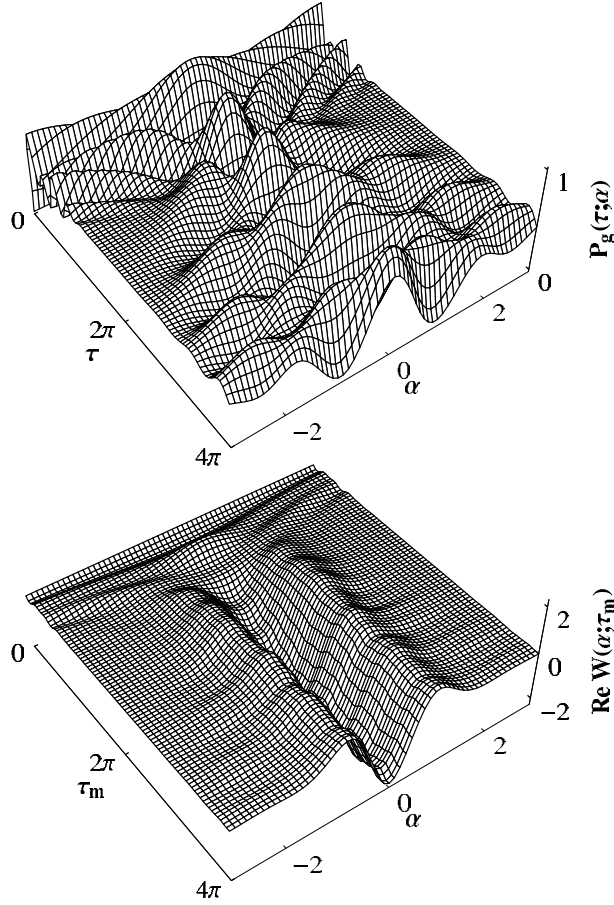


Figure 5.1: Fresnel representation of Wigner function illustrated by the first excited energy eigenstate of a harmonic oscillator. The atomic dynamics $P_g(\tau; \alpha)$, Eq. (5.5), as a function of interaction time τ and real-valued displacement α (top) serves as input to the truncated Fresnel representation, Eq. (5.9). For a finite measurement time τ_m the so-obtained function $W(\alpha; \tau_m)$ is complex-valued. The real part of $W(\alpha; \tau_m)$ (bottom) approaches the correct Wigner function, $W_{|1\rangle}$, already for moderate measurement times.

When we multiply $P_g - 1/2$ from Eq. (5.5) by $2/(\pi\sqrt{i}) \exp[i\tau^2/\pi]$ and integrate over τ , Eq. (5.7) yields

$$\frac{2}{\pi\sqrt{i}} \int_0^\infty d\tau e^{i\tau^2/\pi} \left[P_g(\tau; -\alpha) - \frac{1}{2} \right] = \frac{1}{2} \sum_{n=0}^{\infty} (-1)^n P_n(-\alpha). \quad (5.8)$$

We recall the connection, Eq. (5.6), between $W(\alpha)$ and $P_n(\alpha)$ and find the Wigner

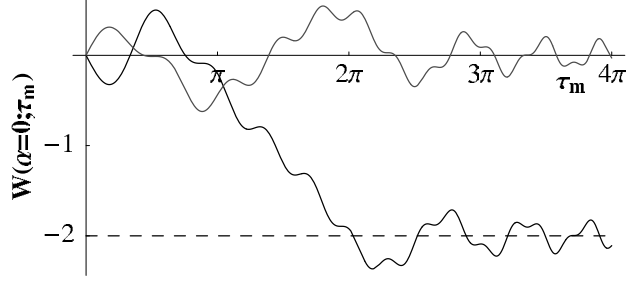


Figure 5.2: Asymptotic approach of the truncated Fresnel representation for the first excited state. Real part (black line) and imaginary part (gray line) of $W(\alpha = 0; \tau_m)$ oscillate around their asymptotic values -2 and 0 , respectively, with slowly decreasing amplitudes. The asymptotic values emerge already after a measurement time of the order of 2π .

function $W(\alpha) \equiv \lim_{\tau_m \rightarrow \infty} W(\alpha; \tau_m)$ in terms of the truncated Fresnel transform ¹

$$W(\alpha; \tau_m) \equiv 4 \int_0^{\tau_m} \frac{2 d\tau}{\pi \sqrt{i}} e^{i\tau^2/\pi} \left[P_g(\tau; -\alpha) - \frac{1}{2} \right] \quad (5.9)$$

of the Rabi oscillations.

Hence, the Wigner function at the phase space point α is determined by a weighted time integral of the atomic dynamics due to the initial state displaced by $-\alpha$. The weight function is the Fresnel phase factor $\exp(i\tau^2/\pi)$.

It is instructive to compare the Fresnel representation, Eq. (5.9), to the Fourier method used in [113]. The latter relies on the analysis of the Fourier transform of the Rabi oscillations P_g and thus needs the full functional dependence on frequency. In contrast, the Fresnel representation gives the Wigner function as a single integral of P_g without the need to analyze an intermediate function.

At the first glance, the Fresnel representation seems to suffer from three disadvantages:

1. It contains the complete time evolution of P_g , that is, from $\tau = 0$ to $\tau = \infty$. However, any experiment can only record the dynamics for a finite measurement time τ_m .
2. It can take on complex values. However, the Wigner function is always real.
3. It relies on a continuous time evolution. However, the experiment can only provide a discrete sampling.

¹The usual notation for the Fresnel transform $\mathcal{F}_s[f]$ of a function $f(t)$ is $\mathcal{F}_s[f](\zeta) \equiv \int_0^\infty dt \exp[i(\zeta - t)^2] f(t)$. Hence, the Wigner function is the Fresnel transform of the Rabi oscillations at one single point $\zeta = 0$.

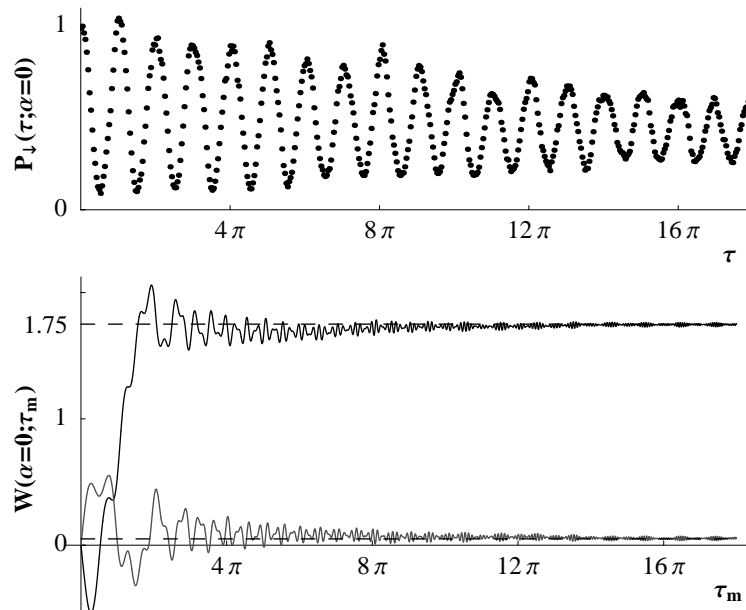


Figure 5.3: Wigner function at the origin of phase space obtained from experimental Rabi oscillations (top) of a stored ion [117] using the truncated Fresnel representation, Eq. (5.9): Approach (bottom) of real (black line) and imaginary parts (gray line) of $W(\alpha = 0; \tau_m)$ towards their asymptotic values (dashed line) yielding $W_{|0\rangle}(0) = 1.75 + i0.05$. The ion was prepared initially in the atomic and vibrational ground state.

We address each of these problems separately and first demonstrate that the phase factor $\exp(i\tau^2/\pi)$ makes the integral insensitive to the long time behavior of P_g . For this purpose we show in Fig.(5.1) the Fresnel reconstruction for the first excited energy eigenstate of a harmonic oscillator. The corresponding Wigner function [4] $W_{|1\rangle}(\alpha) = -2(1 - 4|\alpha|^2) \exp(-2|\alpha|^2)$ is rotationally symmetric. Therefore, it is sufficient to depict $W_{|1\rangle}$ along the real axis.

The top of Fig.(5.1) displays the atomic dynamics P_g as a function of interaction time τ and real-valued displacement α . Sinusoidal Rabi oscillations appear along $\alpha = 0$. Moreover, for appropriately large displacements we find collapses and revivals. In the bottom part we present the real part of $W(\alpha; \tau_m)$. The time axis corresponds to the upper limit τ_m of the truncated Fresnel representation, that is the measurement time. For very short times the function has no similarity with the correct Wigner function, $W_{|1\rangle}$. However, for longer measurement times the curves approach the exact Wigner function.

In order to study the asymptotic behavior in more detail we show in Fig. 5.2 a cut of the truncated Fresnel representation along $\alpha = 0$. Here we depict both, real and imaginary part of $W(\alpha; \tau_m)$. We note that after $\tau_m \approx 2\pi$ the real part, indicated by the black line, begins to oscillate around the correct value $W_{|1\rangle}(\alpha = 0) = -2$ with

decreasing amplitude. In a similar way, the imaginary part, denoted by the gray line, approaches its asymptotic value zero. Unfortunately, this convergence is slow. This feature is a consequence of the familiar Cornu spiral [4], also used by R. P. Feynman and J. A. Wheeler to add up scattered waves — a precursor of the path integral [118]. Despite the slow asymptotic the knowledge of the Rabi oscillations up to a measurement time of a least $\tau_m \cong 2\pi$ is sufficient to obtain the asymptotic Wigner function.

The upper part of Fig.(5.3) shows measured Rabi oscillations of an ion due to its center-of-mass motion² [117]. Due to the high sampling frequency we can directly interpolate the measured data to evaluate the Wigner function. In the bottom part we display the approaches of the real part (black line) and imaginary part (gray line) of the truncated Fresnel integral towards their asymptotic values (dashed lines). For the ion in the motional ground state with Wigner function [4] $W_{|0\rangle}(\alpha) = 2 \exp(-2|\alpha|^2)$ we find the asymptotic value $W_{|0\rangle}(0) = +1.75 + i 0.05$ whereas the ideal value is $W_{|0\rangle}(0) = 2$. The presence of an imaginary part in the estimated Wigner function does not represent a fundamental drawback, as long as it comes from a complex integral of realistic data that ideally should produce a real value.

It is quite remarkable that the method works so well considering the fact that in the particular experiment [117] the atomic dynamics is governed by the non-linear Jaynes-Cummings model [119]. In this case the relation between the atomic population and the photon statistics is not of the form of Eq. (5.5). However, for low excitations the deviations from the familiar Jaynes-Cummings model are small as shown in Fig. 1(b) of Ref. [117]. Therefore, superpositions of low excitations can be successfully reconstructed.

The inset of Fig.(5.4) shows Rabi oscillations of an atom due to a cavity field [13]. Since in this case only a few data points are available we have to employ a discrete version of the Fresnel representation. The data [13] consist of a finite set of M interaction times τ_j and measured probabilities $P_g(\tau_j; -\alpha)$. We now choose kernel coefficients f_j such that

$$\sum_{j=1}^M \cos(2\sqrt{n+1}\tau_j) f_j = (-1)^{n+1}, \quad (5.10)$$

multiply Eq. (5.5) evaluated at discrete times τ_j by f_j , and sum over j . With the help of Eq. (5.10) we then arrive at the discrete representation

$$W(\alpha) = 4 \sum_{j=1}^M f_j \left[P_g(\tau_j; -\alpha) - \frac{1}{2} \right] \quad (5.11)$$

of the Wigner function.

Since the photon number n runs from zero to infinity, Eq. (5.10) describes a system of infinitely many equations for M unknown coefficients f_j . When we consider the truncated system of $N > M$ equations we find the solutions $f_j^{(N)}$ of this overdetermined

²For the anti-Jaynes-Cummings model [117], the minus sign in Eq. (5.5) is replaced by a plus sign and the Fresnel representation, Eq. (5.9) assumes an overall minus sign.

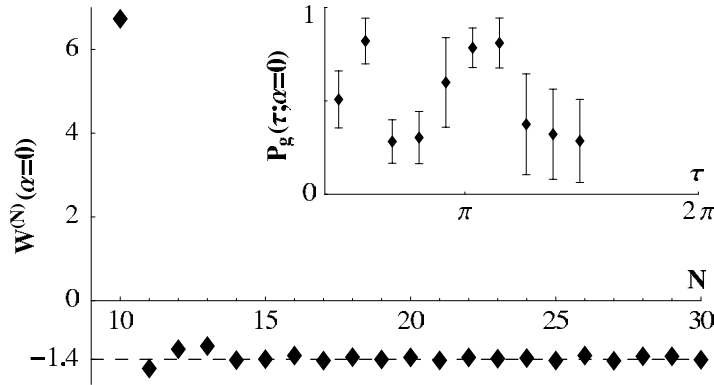


Figure 5.4: Dependence of the Wigner function $W^{(N)}(\alpha = 0)$ at the origin of phase space on the cutoff N of the overdetermined system, Eq. (5.10). The values scatter around $W_{|1\rangle}(0) = -1.4$. The Rabi oscillations [13] (inset) result from a cavity field prepared in a one-photon number state.

system by minimizing the sum of quadratic deviations. Substitution of the so-calculated coefficients $f_j^{(N)}$ into Eq. (5.11) results in the Wigner function $W^{(N)}(\alpha)$.

Figure (5.4) displays the dependence of $W^{(N)}(\alpha = 0)$ on the cutoff N . The values scatter around $W_{|1\rangle}(0) = -1.4$ indicated by the dashed line. We recall that the ideal value of the Wigner function corresponding to a one-photon number state is $W_{|1\rangle}(0) = -2$. For $N = M = 10$ the method is extremely sensitive to uncertainties in the measured data resulting in a large deviation from -1.4.

The error bars δP_j translate into a standard deviation $\delta W = 4 \left[\sum_j f_j^2 \delta P_j^2 \right]^{1/2}$ of the Wigner function. According to Eq. (5.10) the coefficients f_j are solely determined by the set of τ_j and can take almost any values. Obviously large values give rise to a large error in the Wigner function, unless the corresponding uncertainties δP_j are small and compensate this effect.

For the experiment of Ref. [13] performed for a different purpose and therefore not taking advantage of this feature, we find $\delta W \approx 4.3$. However, a future experiment can either choose the interaction times τ_j such as to minimize the f_j or increase the accuracy of the measurement of P_g at times where f_j is large.

Finally, let us consider a more general situation. Imagine that instead of the Fresnel factor $\exp(i\tau^2/\pi)$ in Eq.(5.7) one uses the modified factor, say, $\exp((i - \varepsilon)\beta\tau^2)$ where ε is a positive real, i.e. $\varepsilon \geq 0$ and $\beta = (1/\pi m)$, m is rational. Then the integral relation Eq.(5.7) with the new kernel reads

$$\frac{2}{\pi} \sqrt{\frac{1+i\varepsilon}{im}} \int_0^\infty d\tau \exp((i - \varepsilon)\tau^2/m\pi) \cos(2\sqrt{n}\tau) = \exp\left(-\frac{i\pi nm}{1+i\varepsilon}\right), \quad (5.12)$$

If we impose the condition $\frac{m}{1+i\varepsilon} = 1 + 0i$ then the integral transform Eq.(5.12) recovers $(-1)^n$ in the left hand side and consequently becomes equivalent to the Fresnel

transform Eq.(5.7). However the transformation Eq.(5.12) is richer than the Fresnel transform since it has two parameters to vary. So far we did not specify the parameter ε . Let us consider a case when ε is small, i.e. we assume that $\varepsilon^2 = 0$. This implies that Eq.(5.12) can be rewritten as

$$\frac{2}{\pi} \sqrt{\frac{1+i\varepsilon}{im}} \int_0^\infty d\tau \exp((i-\varepsilon)\tau^2/m\pi) \cos(2\sqrt{n}\tau) = \exp(-i\pi nm(1-i\varepsilon)). \quad (5.13)$$

In order to understand the importance of the latter transformation we differentiate both parts of the Eq.(5.13) with respect to ε in the vicinity of $\varepsilon = 0$. The result reads

$$\int_0^\infty d\tau \left(\sqrt{\frac{i}{m}} - \sqrt{\frac{1}{im} \frac{\tau^2}{m\pi}} \right) \exp(i\tau^2/m\pi) \cos(2\sqrt{n}\tau) = -\pi nm \exp(-i\pi nm). \quad (5.14)$$

The next step is to apply the integral kernel $(\sqrt{\frac{i}{m}} - \sqrt{\frac{1}{im} \frac{\tau^2}{m\pi}}) \exp(i\tau^2/m\pi)$ from Eq.(5.14) to the both parts of Eq.(5.5) and integrate them from 0 to ∞ . Fixing the second free parameter m by setting it to be an even integer we arrive at

$$\begin{aligned} \int_0^\infty d\tau \left(\sqrt{\frac{i}{m}} - \sqrt{\frac{1}{im} \frac{\tau^2}{m\pi}} \right) \exp(i\tau^2/m\pi) \cos(2\sqrt{n}\tau) P_g(\tau; -\alpha) &= -\pi m \sum_{n=0}^{\infty} n P_n(-\alpha) \\ &= -\pi m \langle n \rangle. \end{aligned} \quad (5.15)$$

Hence we have obtained an operational definition of the mean value of the number of excitations of the harmonic oscillator. The value of higher moments, i.e. $\langle n^2 \rangle$ and so on, can be obtained again from the $P_g(\tau; -\alpha)$ by integrating Eq.(5.5) with the kernel stemming from the second and so on derivative of the integral relation Eq.(5.13) at the point $\varepsilon = 0$. Therefore we have obtained a powerful tool for studying the statistics of the system of interest without ever inverting the equation (5.5).

It is needless to say that all remarks concerning the Fresnel representation of the Wigner function are also valid for the integral representation Eq.(5.15). There is however an important difference between them. In contrast to the Fresnel kernel the integral kernel of the representation (5.15) contains the square of the integration parameter τ what influences of course the convergence of the integral in Eq.(5.15). As a consequence, one requires longer integration times, when compared with the Fresnel transform, in order to reach its asymptotic value.

5.3 Integral representation of the Wigner function: General case

The Fresnel representation, Eq. (5.9), of the Wigner function as well as the discrete version, Eq. (5.11), rely on the resonant Jaynes-Cummings model. However, the technique to obtain the Wigner function directly by an appropriate integral transform of the

time dependence of a measurable quantity is much more general. Indeed, our method even allows us to obtain the Wigner function of a wave packet $|\psi(0)\rangle = \sum_n \psi_n |\phi_n\rangle$ consisting of a superposition of energy eigenstates $|\phi_n\rangle$ with energy $E_n \equiv \hbar\omega_n$ of a potential $V \equiv V(\vec{r})$. Here, we do not restrict ourselves to a harmonic oscillator potential. Our only assumption is that V is symmetric with respect to the origin. In this case, the representation Eq. (5.6) of the Wigner function still holds true. Moreover, we recall that the autocorrelation function $\mathcal{C}(t) \equiv \langle \psi(0) | \psi(t) \rangle = \sum_n |\psi_n|^2 \exp(-i\omega_n t)$ is measured routinely in wave packet experiments, e.g. [120, 121].

When we apply the displacement \hat{D} to the initial state $\rho \equiv |\psi(0)\rangle\langle\psi(0)|$, the autocorrelation function $\mathcal{C}(t; \alpha) = \sum_n P_n(\alpha) \exp(-i\omega_n t)$ is similar to Eq. (5.5) with $P_n(\alpha) \equiv \langle \phi_n | \hat{D}(\alpha) \hat{\rho} \hat{D}^\dagger(\alpha) | \phi_n \rangle$. We multiply both sides of the equation for \mathcal{C} by

$$f(t) \equiv \frac{1}{2\pi} \int_{-\infty}^{\infty} d\omega e^{i\omega t} \cos[n(\omega)\pi] \quad (5.16)$$

and integrate over t . Here $n(\omega)$ is an arbitrary and continuous function such that $n(\omega_n) = n$.

When we make use of the symmetry relations $f(-t) = f^*(t)$ and $\mathcal{C}(-t) = \mathcal{C}^*(t)$, we find the Wigner representation

$$W(\alpha) = 4 \operatorname{Re} \left[\int_0^{\infty} dt f(t) \mathcal{C}(t; -\alpha) \right] \quad (5.17)$$

of the initial wave packet in terms of the measured autocorrelation function \mathcal{C} and the integral kernel f .

Equation (5.17) is the generalization of the Fresnel representation, Eq. (5.9), to a quantum system with arbitrary discrete spectrum. For wave packets in a harmonic oscillator or in a box with energy spectra $\omega_n \equiv 2\pi n/T_{cl}$ or $\omega_n \equiv 2\pi n^2/T_r$, respectively, the integral kernels from Eq. (5.16) are delta functions at half of the classical period T_{cl} , or half of the revival time T_r . For these potentials, the time evolution itself creates the function $(-1)^n$, that is the parity operator. For a spectrum $\omega_n \equiv \sqrt{n+1} 2\Omega$, Eq. (5.16) predicts a quadratic Fresnel-like phase.

Complications arise for spectra with degeneracies, such as the hydrogen atom. Nevertheless, we can reconstruct Rydberg wave packets measuring the autocorrelation function at half of the revival time.

Chapter 6

Outlook

The ongoing research in the field of cavity QED is traditionally based on the exploiting of the Jaynes-Cummings model in a combination with various effects of decoherence of an atom and a field. This leads to rather complicated master equations describing an entire atom-field system which can only be treated numerically. In contrast in this thesis we have demonstrated that the adding of a classical strong-driving field to the standard Jaynes-Cummings based approach surprisingly allows to solve the correspondent master equations analytically. With this we have entered a new soluble regime of cavity QED.

There are however several open questions for further investigations. The model of SDM as well as the model of a one-atom laser are derived in such a way that the effects of atomic spontaneous emission are either irrelevant due to physical reasons (SDM) or eliminated (one-atom laser). Taking into account spontaneous emission in the case of SDM will lead to a soluble model of the strongly-driven micromaser operating in optical domain (strongly-driven microlaser [122]). On the other hand consideration of the effects of spontaneous emission in the model of N -atom laser will not change a solubility property of the model but at the same time will simplify the proposed setup for its implementation.

The traditional models of a one-atom laser are aimed at describing the generation properties of a single atom placed inside an optical cavity and pumped by a coherent field. Their main concern is the state of a generated output cavity field which in contrast to the macroscopic lasers can be purely nonclassical. As distinct, in this work we have presented the model of a one-atom laser which do not possess a nonclassical output field state but nevertheless generates a mesoscopic atom-field superposition state which unfortunately due to its high sensitivity to the decoherence effects evaluates to a mixed atom-field steady state. We have briefly suggested how to use this distinct feature of our model in order to measure a decoherence rate. This questions deserves a more careful study since it has never been investigated in past neither in an experiment with the optical cavities nor in theory.

Following the modern quantum information trends in cavity QED we have studied the questions of the generation of maximally-entangled states of two atomic qubits.

We have chosen as a basis the model of two-atom laser. Having at our disposal its steady-state analytical solution we have shown that the maximally-entangled state of two atoms is always correlated to the vacuum cavity field and therefore a no-photon measurement of the cavity field leads to the generation of a maximally-entangled atomic state. Since this approach neglects the effects of a low single photon detection efficiency of the standard schemes it allows generation of maximally-entangled states of high fidelity even in the low coupling limit of the atom-field interaction. However there is still a question to answer whether it is possible to employ the model of N -atom laser for the production of multipartite atomic entangled states. On the other hand, we have demonstrated how the dispersive interaction between atoms prepared in the ground state and two orthogonal modes of a cavity can serve this propose.

The last but not least topic addressed in this thesis is the quantum state reconstruction in cavity QED. Despite the extensive research over the last two decades the question of optimal operational schemes for the reconstruction of the Wigner function of a given state is pertinent. Here we have been able to introduce a simple scheme for the reconstruction of the micromaser field using the Fresnel transform of the atomic inversion of a probe atom. It turned out that such an integral transform based scheme can reconstruct the Wigner function of a particle in an arbitrary symmetric potential. Therefore this scheme in principle can be used for the Wigner function reconstruction of a wave packet or even for cold atoms placed inside an optical lattice.

Bibliography

- [1] E. Wigner. On the quantum correction for thermodynamic equilibrium. *Phys. Rev.*, 40:749–759, 1932.
- [2] K. E. Cahill and R. J. Glauber. Ordered expansions in boson amplitude operators. *Phys. Rev.*, 177:1857–1881, 1969.
- [3] K. E. Cahill and R. J. Glauber. Density operators and quasiprobability distributions. *Phys. Rev.*, 177:1882–1902, 1969.
- [4] W.P. Schleich. *Quantum optics in phase space*. Wiley-VCH, 2001.
- [5] R. J. Glauber. Coherent and incoherent states of the radiation field. *Phys. Rev.*, 131:2766–2788, 1963.
- [6] E. M. Purcell. Spontaneous emission probabilities at radio frequencies. *Phys. Rev.*, 69:681, 1946.
- [7] H. B. G. Casimir and D. Polder. Spontaneous emission probabilities at radio frequencies. *Phys. Rev.*, 73:360–372, 1948.
- [8] G. Feher, J. P. Gordon, E. Buehler, E. A. Gere, and C. D. Thurmond. Spontaneous emission of radiation from an electron spin system. *Phys. Rev.*, 109:221–222, 1958.
- [9] K.H. Drexhage, H. Kuhn, and F.D. Schafer. *Ber. Bunsen Ges. Phys.*, 72:329, 1968.
- [10] D. Meschede, H. Walther, and G. Müller. One-atom maser. *Phys. Rev. Lett.*, 54:551–554, 1985.
- [11] S. Haroche and J.M. Raimond. Radiative properties of rydberg states in resonant cavities. In D. Bates and B. Bederson, editors, *Advances in Atomic and Molecular Physics*, volume 20, pages 350–412. Academic, New York, 1985.
- [12] G. Nogues, A. Rauschenbeutel, S. Osnaghi, M. Brune, J. M. Raimond, and S. Haroche. Seeing a single photon without destroying it. *Nature (London)*, 400:239–242, 1999.

- [13] B. T. H. Varcoe, S. Brattke, M. Weidinger, and H. Walther. Preparing pure photon number states of the radiation field. *Nature (London)*, 403:743–746, 2000.
- [14] M.O. Scully, B.-G. Englert, and H. Walther. Quantum optical tests of complementarity. *Nature (London)*, 351:111–116, 1991.
- [15] J.M. Raimond, M. Brune, and S. Haroche. Manipulating quantum entanglement with atoms and photons in a cavity. *Rev. Mod. Phys.*, 73:565–582, 2001.
- [16] A. Rauschenbeutel, G. Nogues, S. Osnaghi, P. Bertet, M. Brune, J. M. Raimond, and S. Haroche. Coherent operation of a tunable quantum phase gate in cavity qed. *Phys. Rev. Lett.*, 83:5166–5169, 1999.
- [17] B.-G. Englert, M. Löffler, O. Benson, B. Varcoe, M. Weidinger, and H. Walther. Entangled atoms in micromaser physics. *Fortschr. Phys.*, 46:897–926, 1998.
- [18] M. G. Raizen, R. J. Thompson, R. J. Brecha, H. J. Kimble, and H. J. Carmichael. Normal-mode splitting and linewidth averaging for two-state atoms in an optical cavity. *Phys. Rev. Lett.*, 63:240–243, 1989.
- [19] A. Kuhn, M. Hennrich, and G. Rempe. Deterministic single-photon source for distributed quantum networking. *Phys. Rev. Lett.*, 89:067901, 2002.
- [20] A. Kuzmich, W. P. Bowen, A. D. Boozer, A. Boca, C. W. Chou, L.-M. Duan, and H. J. Kimble. Experimental realization of a one-atom laser in the regime of strong coupling. *Nature (London)*, 423:731–734, 2003.
- [21] T. Pellizzari, S. A. Gardiner, J. I. Cirac, and P. Zoller. Decoherence, continuous observation, and quantum computing: A cavity qed model. *Phys. Rev. Lett.*, 75:3788–3791, 1995.
- [22] C. J. Hood, T. W. Lynn, A. C. Doherty, A. S. Parkins, and H. J. Kimble. The atom-cavity microscope: Single atoms bound in orbit by single photons. *Science*, 287:1477–1453, 2000.
- [23] P. W. H. Pinkse, T. Fischer, P. Maunz, and G. Rempe. Trapping an atom with single photons. *Nature (London)*, 404:365–368, 2000.
- [24] E. T. Jaynes and F. W. Cummings. Comparison of quantum and semiclassical radiation theories with application to the beam maser. *Proc. IEEE*, 51:89, 1963.
- [25] B. W. Shore and P. L. Knight. The jaynes-cummings model. *J. Mod. Opt.*, 40:1195–1238, 1993.
- [26] C. Cohen-Tannoudji, J. Dupont-Roc, and G. Grynberg. *Photons and Atoms: Introduction to Quantum Electrodynamics*. Wiley, 1989.

- [27] E. Solano, G. S. Agarwal, and H. Walther. Strong-driving-assisted multipartite entanglement in cavity qed. *Phys. Rev. Lett.*, 90:0279031–0279034, 2003.
- [28] P. M. Alsing, D. A. Cardimona, and H. J. Carmichael. Suppression of fluorescence in a lossless cavity. *Phys. Rev. A*, 45:1793–1803, 1992.
- [29] M. Brune, E. Hagley, J. Dreyer, X. Maître, A. Maali, C. Wunderlich, J.M. Raimond, and S. Haroche. Observing the progressive decoherence of the "meter" in a quantum measurement. *Phys. Rev. Lett.*, 77:4887–4890, 1996.
- [30] J. A. C. Gallas, G. Leuchs, H. Walther, and H. Figger. Rydberg atoms: High resolution spectroscopy and radiation interaction - rydberg molecules. In D. Bates and B. Bederson, editors, *Advances in Atomic and Molecular Physics*, volume 20, pages 414–466. Academic, New York, 1985.
- [31] P. Filipowicz, J. Javanainen, and P. Meystre. Theory of a microscopic maser. *Phys. Rev. A*, 34:3077–3087, 1986.
- [32] L.A. Lugiato, M.O. Scully, and H. Walther. Connection between microscopic and macroscopic maser theory. *Phys. Rev. A*, 36:740–743, 1987.
- [33] H.J. Carmichael. *Statistical Methods in Quantum Optics 1 Master Equations and Fokker-Planck Equations*. Springer, 1999.
- [34] P. Lougovski, F. Casagrande, A. Lulli, B.-G. Englert, E. Solano, and H. Walther. Solvable model of a strongly driven micromaser. *Phys. Rev. A*, 69:0238121–0238129, 2004.
- [35] E. Solano, R. L. de Matos Filho, and N. Zagury. Mesoscopic superpositions of vibronic collective states of n trapped ions. *Phys. Rev. Lett.*, 87:060402, 2001.
- [36] G. S. Agarwal, W. Lange, and H. Walther. Intense-field renormalization of cavity-induced spontaneous emission. *Phys. Rev. A*, 48:4555–4568, 1993.
- [37] W. Lange and H. Walther. Observation of dynamic suppression of spontaneous emission in a strongly driven cavity. *Phys. Rev. A*, 48:4551–4554, 1993.
- [38] M.O. Scully and M.S. Zubairy. *Quantum optics*. Cambridge University Press, 1997.
- [39] H.-J. Briegel, B.-G. Englert, N. Sterpi, and H. Walther. One-atom maser: Statistics of detector clicks. *Phys. Rev. A*, 49:2962–2985, 1996.
- [40] J. Dalibard, Y. Castin, and K. Mølmer. Wave-function approach to dissipative processes in quantum optics. *Phys. Rev. Lett.*, 68:580–583, 1992.
- [41] F. Casagrande, A. Lulli, and V. Santagostino. Coherently driven and coherently pumped micromaser. *Phys. Rev. A*, 65:023809, 2002.

- [42] F. Casagrande, A. Ferraro, A. Lulli, R. Bonifacio, E. Solano, and H. Walther. How to measure the phase diffusion dynamics in the micromaser. *Phys. Rev. Lett.*, 90:183601, 2003.
- [43] D.T. Pegg and S.M. Barnett. Phase properties of the quantized single-mode electromagnetic field. *Phys. Rev. A*, 39:1665–1675, 1989.
- [44] W. E. Lamb. Theory of an optical maser. *Phys. Rev.*, 134:A1429, 1964.
- [45] Y. Mu and C.M. Savage. One-atom lasers. *Phys. Rev. A*, 46:5944–5954, 1992.
- [46] C. Ginzel, H.-J. Briegel, U. Martini, B.-G. Englert, and A. Schenzle. Quantum optical master equations: The one-atom laser. *Phys. Rev. A*, 48:732–738, 1993.
- [47] T. Pellizzari and H. Ritsch. Preparation of stationary fock states in a one-atom laser. *Phys. Rev. Lett.*, 72:3973–3976, 1994.
- [48] M. Löffler, G.M. Meyer, and H. Walther. Spectral properties of the one-atom laser. *Phys. Rev. A*, 56:3923–3930, 1997.
- [49] P. Maunz, T. Puppe, P.W.H. Pinkse I. Schuster, N. Syanssen, and G. Rempe. Cavity cooling of a single atom. *Nature (London)*, 428:50–52, 2004.
- [50] A.B. Klimov, L.L. Sanchez-Soto, A. Navarro, and E.C. Yustas. Effective hamiltonians in quantum optics: a systematic approach. *J. Mod. Opt.*, 49:2211–2226, 2002.
- [51] A. Biswas and G.S. Agarwal. Quantum logic gates using stark shifted raman transitions in a cavity. *Los Alamos preprint server*, quant-ph:0401099, 2004.
- [52] M.A. Nielsen and I.L. Chuang. *Quantum computation and quantum information*. Cambridge, 2000.
- [53] M. Weidinger, B. T. H. Varcoe, R. Heerlein, and H. Walther. Trapping states in the micromaser. *Phys. Rev. Lett.*, 82:3795–3798, 1999.
- [54] B.-G. Englert, N. Sterpi, and H. Walther. Parity states in the one-atom maser. *Opt. Comm.*, 100:526–535, 1993.
- [55] L. G. Lutterbach and L. Davidovich. Method for direct measurement of the wigner function in cavity qed and ion traps. *Phys. Rev. Lett.*, 78:2547–2550, 1997.
- [56] P. Lougovski, E. Solano, Z. M. Zhang, H. Walther, H. Mack, and W. P. Schleich. Fresnel representation of the wigner function: An operational approach. *Phys. Rev. Lett.*, 91:010401–010404, 2003.

- [57] E. Schrödinger. Die gegenwärtige situation in der quantenmechanik. *Naturwissenschaften*, 23:807–812, 823–828, 844–849, 1935.
- [58] P. G. Kwiat, K. Mattle, H. Weinfurter, and A. Zeilinger. New high-intensity source of polarization-entangled photon pairs. *Phys. Rev. Lett.*, 75:4337–4341, 1995.
- [59] E. Hagley, X. Maître, G. Nogues, C. Wunderlich, M. Brune, J. M. Raimond, and S. Haroche. Generation of einstein-podolsky-rosen pairs of atoms. *Phys. Rev. Lett.*, 79:1–5, 1997.
- [60] Q. A. Turchette, C. S. Wood, B. E. King, C. J. Myatt, D. Leibfried, W. M. Itano, C. Monroe, and D. J. Wineland. Deterministic entanglement of two trapped ions. *Phys. Rev. Lett.*, 81:3631–3634, 1998.
- [61] F. Schmidt-Kaler, H. Häffner, M. Riebe, S. Gulde, G. P. T. Lancaster, T. Deuschle, Ch. Becher, Ch. F. Roos, J. Eschner, and R. Blatt. Realization of the cirac-zoller controlled-not quantum gate. *Nature (London)*, 422:408–411, 2003.
- [62] J. I. Cirac, P. Zoller, H. J. Kimble, and H. Mabuchi. Quantum state transfer and entanglement distribution among distant nodes in a quantum network. *Phys. Rev. Lett.*, 78:3221–3224, 1997.
- [63] Xun-Li Feng, Zhi-Ming Zhang, Xiang-Dong Li, Shang-Qing Gong, and Zhi-Zhan Xu. Entangling distant atoms by interference of polarized photons. *Phys. Rev. Lett.*, 90:217902, 2003.
- [64] K. Mølmer. Entanglement of distant atoms by a continuous supply of quantum correlated photons. *Opt. Comm.*, 179:429–437, 2000.
- [65] L.-M. Duan and H. J. Kimble. Efficient engineering of multiatom entanglement through single-photon detections. *Phys. Rev. Lett.*, 90:253601, 2003.
- [66] D. E. Browne, M. B. Plenio, and S. F. Huelga. Robust creation of entanglement between ions in spatially separate cavities. *Phys. Rev. Lett.*, 91:067901, 2003.
- [67] B. Kraus and J. I. Cirac. Discrete entanglement distribution with squeezed light. *Phys. Rev. Lett.*, 92:013602, 2004.
- [68] A. Beige, D. Braun, B. Tregenna, and P. L. Knight. Quantum computing using dissipation to remain in a decoherence-free subspace. *Phys. Rev. Lett.*, 85:1762–1765, 2000.
- [69] A. S. Sørensen and K. Mølmer. Probabilistic generation of entanglement in optical cavities. *Phys. Rev. Lett.*, 90:127903, 2003.

- [70] C. Marr, A. Beige, and G. Rempe. Entangled-state preparation via dissipation-assisted adiabatic passages. *Phys. Rev. A*, 68:033817, 2003.
- [71] P. Lougovski, E. Solano, and H. Walther. Generation and purification of maximally-entangled atomic states in optical cavities. *Los Alamos preprint server*, quant-ph:0308059, 2003.
- [72] M. B. Plenio, S. F. Huelga, A. Beige, and P. L. Knight. Cavity-loss-induced generation of entangled atoms. *Phys. Rev. A*, 59:2468–2475, 1999.
- [73] G. R. Guthöhrlein, M. Keller, K. Hayasaka, W. Lange, and H. Walther. A single ion as a nanoscopic probe of an optical field. *Nature (London)*, 414:49–51, 2001.
- [74] N. Gisin. Hidden quantum nonlocality revealed by local filters. *Phys. Lett. A*, 210:151–156, 1996.
- [75] P. G. Kwiat, S. Barraza-Lopez, A. Stefanov, and N. Gisin. Experimental entanglement distillation and 'hidden' non-locality. *Nature (London)*, 409:1014–1017, 2001.
- [76] A. Kuzmich, L. Mandel, and N. P. Bigelow. Generation of spin squeezing via continuous quantum nondemolition measurement. *Phys. Rev. Lett.*, 85:1594–1597, 2000.
- [77] C. H. van der Wal, M. D. Eisaman, A. André, R. L. Walsworth, D. F. Phillips, A. S. Zibrov, and M. D. Lukin. Atomic memory for correlated photon states. *Science*, 301:196–200, 2003.
- [78] C. Liu, Z. Dutton, C.H. Behroozi, and L.V. Hau. Observation of coherent optical information storage in an atomic medium using halted light pulses. *Nature (London)*, 409:490, 2001.
- [79] M. Fleischhauer and M.D. Lukin. Quantum memory for photons: Dark-state polaritons. *Phys. Rev. A*, 65:022314, 2002.
- [80] D.F. Phillips, A. Fleischhauer, A. Mair, R.L. Walsworth, and M.D. Lukin. Storage of light in atomic vapor. *Phys. Rev. Lett.*, 86:783–786, 2001.
- [81] A. Kuzmich and E. S. Polzik. Atomic quantum state teleportation and swapping. *Phys. Rev. Lett.*, 85:5639–5642, 2000.
- [82] L.M. Duan, M.D. Lukin, J.I. Cirac, and P. Zoller. Long-distance quantum communication with atomic ensembles and linear optics. *Nature (London)*, 414:413–418, 2001.
- [83] M. Fleischhauer and M.D. Lukin. Dark-state polaritons in electromagnetically induced transparency. *Phys. Rev. Lett.*, 84:5094–5097, 2000.

- [84] J. R. Czesznegi and R. Grobe. Recall and creation of spatial excitation distributions in dielectric media. *Phys. Rev. Lett.*, 79:3162–3165, 1997.
- [85] A.S. Zibrov, A.B. Matsko, O. Kocharovskaya, Y.V. Rostovtsev, G.R. Welch, and M.O. Scully. Transporting and time reversing light via atomic coherence. *Phys. Rev. Lett.*, 88:103601, 2002.
- [86] A.B. Matsko, Y.V. Rostovtsev, O. Kocharovskaya, A.S. Zibrov, and M.O. Scully. Nonadiabatic approach to quantum optical information storage. *Phys. Rev. A*, 64:043809, 2001.
- [87] A. Kuzmich, W. P. Bowen, A. D. Boozer, A. Boca, C. W. Chou, L.-M. Duan, and H. J. Kimble. Generation of nonclassical photon pairs for scalable quantum communication with atomic ensembles. *Nature (London)*, 423:731–734, 2003.
- [88] M. G. Payne and L. Deng. Quantum entanglement of fock states with perfectly efficient ultraslow single-probe photon four-wave mixing. *Phys. Rev. Lett.*, 91:123602, 2003.
- [89] T. N. Dey and G. S. Agarwal. Storage and retrieval of light pulses at moderate powers. *Phys. Rev. A*, 67:033813, 2003.
- [90] V. G. Arkhipkin and I. V. Timofeev. Electromagnetically induced transparency; writing, storing, and reading short optical pulses. *JETP Lett.*, 76:66, 2002.
- [91] L. M. Duan, J. I. Cirac, P. Zoller, and E. S. Polzik. Quantum communication between atomic ensembles using coherent light. *Phys. Rev. Lett.*, 85:5643–5646, 2000.
- [92] S. Massar and E. S. Polzik. Generating a superposition of spin states in an atomic ensemble. *Phys. Rev. Lett.*, 91:060401, 2003.
- [93] F.T. Arecchi, E. Courtens, R. Gilmore, and H. Thomas. Atomic coherent states in quantum optics. *Phys. Rev. A*, 6:2211–2237, 1972.
- [94] C. Monroe, D. M. Meekhof, B. E. King, and D. J. Wineland. A “schrödinger cat” superposition state of an atom. *Science*, 272:1131–1136, 1996.
- [95] G. S. Agarwal, R. R. Puri, and R. P. Singh. Atomic schrödinger cat states. *Phys. Rev. A*, 56:2249–2254, 1997.
- [96] S. B. Zeng. One-step synthesis of multiatom Greenberger-Horne-Zeilinger states. *Phys. Rev. Lett.*, 87:230404, 2001.
- [97] C. C. Gerry and R. Grobe. Cavity-qed state reduction method to produce atomic schrödinger-cat states. *Phys. Rev. A*, 57:2247–, 1998.

- [98] C. C. Gerry. Proposal for a mesoscopic cavity qed realization of the greenberger-horne-zeilinger state. *Phys. Rev. A*, 54:2529, 1996.
- [99] D. M. Greenberger, M. A. Horne, and A. Zeilinger. Multiparticle interferometry and the superposition principle. *Physics Today*, 46:22, 1993.
- [100] Jr. W. E. Lamb. An operational interpretation of nonrelativistic quantum mechanics. *Physics Today*, 22:23, 1969.
- [101] D. T. Smithey, M. Beck, M. G. Raymer, and A. Faridani. Measurement of the wigner distribution and the density matrix of a light mode using optical homodyne tomography: Application to squeezed states and the vacuum. *Phys. Rev. Lett.*, 70:1244–1247, 1993.
- [102] Ch. Kurtsiefer, T. Pfau, and J. Mlynek. Measurement of the wigner function of an ensemble of helium atoms. *Nature (London)*, 386:150–153, 1997.
- [103] G. Breitenbach, S. Schiller, and J. Mlynek. Measurement of the quantum states of squeezed light. *Nature (London)*, 387:471–475, 1997.
- [104] K. Banaszek, C. Radzewicz, and K. Wódkiewicz. Direct measurement of the wigner function by photon counting. *Phys. Rev. A*, 60:674–677, 1999.
- [105] A. I. Lvovsky, H. Hansen, T. Aichele, O. Benson, J. Mlynek, and S. Schiller. Quantum state reconstruction of the single-photon fock state. *Phys. Rev. Lett.*, 87:050402, 2001.
- [106] K. Wódkiewicz. Operational approach to phase-space measurements in quantum mechanics. *Phys. Rev. Lett.*, 52:1064–1067, 1984.
- [107] A. Royer. Measurement of the wigner function. *Phys. Rev. Lett.*, 55:2745–2748, 1985.
- [108] K. Banaszek and K. Wódkiewicz. Direct probing of quantum phase space by photon counting. *Phys. Rev. Lett.*, 76:4344–4347, 1996.
- [109] S. Wallentowitz and W. Vogel. Unbalanced homodyning for quantum state measurements. *Phys. Rev. A*, 53:4528–, 1996.
- [110] G. Nogues, A. Rauschenbeutel, S. Osnaghi, P. Bertet, M. Brune, J. M. Raimond, S. Haroche, L. G. Lutterbach, and L. Davidovich. Measurement of a negative value for the wigner function of radiation. *Phys. Rev. A*, 62:054101, 2000.
- [111] M. Wilkens and P. Meystre. Nonlinear atomic homodyne detection: A technique to detect macroscopic superpositions in a micromaser. *Phys. Rev. A*, 43:3832–3835, 1991.

- [112] P. J. Bardroff, E. Mayr, W. P. Schleich, P. Domokos, M. Brune, J. M. Raimond, and S. Haroche. Simulation of quantum-state endoscopy. *Phys. Rev. A*, 53:2736–2741, 1996.
- [113] D. Leibfried, D. M. Meekhof, B. E. King, C. Monroe, W. M. Itano, and D. J. Wineland. Experimental determination of the motional quantum state of a trapped atom. *Phys. Rev. Lett.*, 77:4281–4285, 1996.
- [114] M. Brune, F. Schmidt-Kaler, A. Maali, J. Dreyer, E. Hagley, J. M. Raimond, and S. Haroche. Quantum rabi oscillation: A direct test of field quantization in a cavity. *Phys. Rev. Lett.*, 76:1800–1803, 1996.
- [115] C. T. Bodendorf, G. Antesberger, M. S. Kim, and H. Walther. Quantum-state reconstruction in the one-atom maser. *Phys. Rev. A*, 57:1371–1378, 1998.
- [116] M. S. Kim, G. Antesberger, C. T. Bodendorf, and H. Walther. Scheme for direct observation of the wigner characteristic function in cavity qed. *Phys. Rev. A*, 58:R65–R68, 1998.
- [117] D. M. Meekhof, C. Monroe, B. E. King, W. M. Itano, and D. J. Wineland. Generation of nonclassical motional states of a trapped atom. *Phys. Rev. Lett.*, 76:1796–1799, 1996.
- [118] J. A. Wheeler. The young feynman. *Physics Today*, 42:24–28, 1989.
- [119] W. Vogel and R. L. de Matos Filho. Nonlinear jaynes-cummings dynamics of a trapped ion. *Phys. Rev. A*, 52:4214–4217, 1995.
- [120] J. A. Yeazell, G. Raithel, L. Marmet, H. Held, and H. Walther. Observation of wave packet motion along quasi-landau orbits. *Phys. Rev. Lett.*, 70:2884–2887, 1993.
- [121] L. Marmet, H. Held, G. Raithel, J. A. Yeazell, and H. Walther. Observation of quasi-landau wave packets. *Phys. Rev. Lett.*, 72:3779–3782, 1994.
- [122] K. An, J.J. Childs, R.R. Desari, and M. Feld. Microlaser: A laser with one atom in an optical resonator. *Phys. Rev. Lett.*, 73:3375–3378, 1994.

Lebenslauf

Name: Pavel Lougovski
Geboren: 06.05.1980 in Minsk (Weißrussland)
Familienstand: ledig

Studium:

1986 - 1994 Grundschule 98 Minsk
1994 - 1996 Lyzeum der weißrussischen staatlichen Universität (Minsk)
Juni 1996 Abschluß
1996 - 2001 Studium der Physik an der weißrussischen staatlichen Universität (Minsk)
Dezember 2000 Diplomarbeit am Institut der Physik
- Juni 2001 der nationalen Akademie der Wissenschaften, Minsk
Juni 2001 Diplom mit Auszeichnung in Physik
seit Doktorarbeit am Max-Planck-Institut für Quantenoptik, Garching
Oktober 2001 und an der Ludwig-Maximilians-Universität München

Auszeichnung:

September 1999 Träger des Francisk Skorina's Stipendiums der nationalen Akademie
- Juni 2001 der Wissenschaften, Minsk

Sprachkenntnisse:

Deutsch, Englisch, Russisch, Weißrussisch (Muttersprache)

Computerkenntnisse:

UNIX, Windows, Matlab, Mathematica, Pascal

Hobbys:

Klavier, Wandern, Fußball spielen, Lesen

Danksagung

Zum Schluss möchte ich die Gelegenheit nutzen und mich bei allen herzlich bedanken, die zum Gelingen dieser Arbeit beigetragen haben.

Zuallererst gilt mein ganz besonderer Dank Prof. Herbert Walther für die engagierte Betreuung und die Möglichkeit meine Promotion in der faszinierenden Forschungsatmosphäre seiner Gruppe am Max-Planck-Institut für Quantenoptik durchzuführen. Seine Begeisterungsfähigkeit und seine Unterstützung haben mich fortwährend motiviert und mir viel geholfen.

Prof. Wolfgang P. Schleich danke ich insbesondere für die angenehme Zusammenarbeit, die einen großen Teil dieser Arbeit geworden ist. Die zahlreichen Diskussionen mit ihm waren eine große Freude und Bereicherung.

Ich möchte mich bei Prof. Girish S. Agarwal für die fruchtbare Kollaboration während seines Besuches im Sommer 2003 ganz herzlich bedanken.

Den Salsameister, Profifußballer und nebenberuflich guten Theoretiker Dr. Enrique Solano möchte ich hier ebenfalls hervorheben. Diese Arbeit ist ein Resultat unserer wunderbaren Zusammenarbeit, die wir während der letzten Jahre hatten.

Dem ganzen experimentellen Micromaserteam; Dr. Thomas Becker, Dr. Mikhail Gorodetsky, Dr. Gabriele Marchi, Mikhail Klembovsky, Pierre Thoumany und nicht zuletzt Linas Urbonas sei gedankt für die vielen wissenschaftlichen Diskussionen, manchmal auch in einer informellen Umgebung, über die Micromaserphysik.

Besonderer Dank gebührt Dr. Giovanna Morigi, Dr. Geza Giedke, Dr. Juan Jose Garcia Ripoll, Dr. Jiannis Pachos, Dr. Almut Beige, Dr. Gombojav Ariunbold, Dr. Wolfgang Lange, Dr. Sascha Nevsky, Thomas Baier, Matthias Keller, Fabrizio Lindner, Christian Schwedes, Birgit Lange, Volker Ludsteck, Gernot Stania für die Hilfsbereitschaft und freundliche Unterstützung. Nok Tsao und Michael Schätzel danke ich für die angenehme Gesellschaft.

Dr. Mohamed Bourennane, Manfred Eibl, Nikolai Kiesel, Pavel Trojek und Christian Schmid möchte ich für die angenehme Nachbarschaft und hilfreichen Tipps ganz herzlich danken.

Schließlich danke ich meinen Eltern und meinem Bruder Sascha, die mich immer unterstützt und ermutigt haben, für ihre Liebe und fürs Begleiten während aller Höhen und Tiefen dieser Arbeit.

